UNIVERSITAT POLITÈCNICA DE CATALUNYA BARCELONATECH

Politecnico di Torino

ETSECCPB - Escola Tècnica Superior d'Enginyeria de Camins, Canals i Ports de Barcelona

DISEG - Dipartimento di Ingegneria Strutturale, Edile e Geotecnica Department d'Enginyeria Civil i Ambiental

Civil Engineering - Structures

Master Degree Thesis

Investigation of the dynamic properties of masonry arch bridges via 3D finite element modelling

Supervisors
Prof. Luca PELÀ
Prof. Semih GÖNEN
Prof. Pietro CORNETTI
Prof. Gianfranco PIANA

Candidate
Francesco PINO

Dedicato alla mia dolce Mamma e al mio caro Papà,

in memoria dell'esperienza Erasmus, nella vibrante città di Barcellona.

Abstract

Masonry arch bridges hold a crucial role in global road and railway networks, constituting a significant portion of these infrastructures. In Europe alone, masonry arch bridges represent over 40% of railway bridges and 25% of road bridges. The dynamic behavior of these bridges is heavily influenced by their geometrical and material properties, as well as boundary conditions. Despite their importance, there is a lack of comprehensive understanding regarding how the geometric characteristics of masonry arch bridges impact their modal frequencies and mode shapes.

This study explored the **correlation between the geometrical characteristics of masonry arch bridges and their dynamic behavior**, specifically focusing on modal frequencies and mode shapes. The study commenced with an investigation into the **historical empirical rules utilized** in the construction of masonry arch bridges. This investigation provided a foundational understanding of traditional design principles and their influence on bridge dynamics. Subsequently, **critical geometrical parameters** were identified, including arch span, thickness and rise, bridge width, pier thickness, width and height, backing height, and arch slenderness. These critical geometrical parameters are then considered as random variables to carry out a **parametric modal analysis using 3D solid element finite element (FE) models** to capture the dynamic properties of single-span masonry arch bridges with different geometrical properties.

The core of the research involved the creation with **STKO Software** of 3D FE models for modal analysis. These models allowed for the detailed examination of the dynamic behavior of masonry arch bridges under various conditions. A total of **75 FE models were generated**, and **75 Monte Carlo simulations were conducted** to extract the modal frequencies of the prominent modes of the bridge. The modal analysis provided insights into the natural frequencies and mode shapes, highlighting the impact of different geometrical configurations on the dynamic response of the bridges.

The study's findings revealed that the **natural frequencies of masonry arch bridges are highly dependent on the span of the arch**. It was observed that the frequencies decrease monotonically as the span increases, indicating a clear inverse relationship. Additionally, the thickness of the arch and its rise also significantly influence the modal frequencies, with thicker and higher arches generally exhibiting higher natural frequencies. The width of the bridge and the dimensions of the piers (thickness, width, and height) were found to have a notable impact as well, with wider bridges and

larger piers contributing to a more complex dynamic behavior. The backing height and arch slenderness were also critical, affecting both the frequencies and the mode shapes of the bridges. However, it was found that not all of the critical geometrical parameters are effective on the modal frequencies. A new parameter, **arch slenderness**, has been proposed and is observed to be affecting the modal properties significantly.

The results of the modal analyses were systematically compiled into a comprehensive database. From this database, **empirical equations** were developed to predict the natural frequencies of masonry arch bridges based on their geometric characteristics. These equations serve as valuable tools for engineers and researchers, enabling quick and reliable predictions of dynamic behavior without the need for extensive computational analyses.

Overall, this study significantly advances the understanding of the relationship between the geometric characteristics of masonry arch bridges and their dynamic behavior. The development of empirical equations for predicting natural frequencies represents a key contribution to the field. By bridging the gap between historical construction practices and modern engineering analysis, this research supports the preservation and improvement of an essential component of global infrastructure.

Acknowledgements

Contents

List of Figures

16

List of Tables

Terminology

Figure 1.   Elements of stone arch (vault) bridges [16].

Action ISO 2394:2015: Assembly of concentrated or distributed forces acting on a structure (direct actions), displacements or thermal effects imposed to the structure, or constrained in it or environmental influences that may cause changes with time in the material properties or in the dimensions of a structure.

Abutment CIRIA C656: A body, usually formed of masonry, which provides resistance to horizontal and vertical forces from the arch ring and surrounding backfill.

Assessment The evaluation of a bridge's structural capacity and performance, often using one of a variety of predefined methodologies and, in some cases, specialized software.

19

Arch CIRIA C656: A structure curved in a vertical plane spanning an obstruction and capable of supporting vertical loads, and transferring these loads to the abutments or piers.

Arch barrel CIRIA C656: The load bearing part of an arch consisting of a single thickness of voussior stones or multiple rings of brickwork spanning between abutments and/or piers.

Arch ring A curved course of masonry, or series of masonry courses, which supports loads principally in compression.

Backfill (fill/infill) CIRIA C656: Material (usually low-quality fill) used to give support behind a structure. For a masonry arch bridge, backfill material is placed in the spandrels between the arch barrel and the road surface and retained laterally by the spandrel walls and/or wingwalls. It normally consists of granular material, e.g., gravel or building debris, which may have been excavated for the foundations or is waste from the construction.

Backing CIRIA C800: Concrete or masonry infill material used to provide additional horizontal support to the arch barrel.

Brick A kiln fired block of clay usually rectangular in shape used in masonry construction.

Bridge A Structure that is constructed to span a physical obstacle (such as a body of water,valley, road, or rail) without blocking the way underneath. It is constructed to provide passage over the obstacle, which is typically something that would be difficult or impossible to cross otherwise.

Centring A temporary structure upon which the units of an arch or vault are positioned during construction. On historical masonry arch bridges is typically made of timber.

Circular arch An arch with an intrados of constant radius.

Crown The centre and highest point on an arch barrel.

Deep arch An arch with a rise to span ratio equal to or greater than 0.5.

Extrados CIRIA C656: In an arch or vault is the top surface of the arch barrel i.e., the outer (convex) curve of an arch.

Failure ISO 13824:2020: State which does not meet the required performance objectives due to structural damage and/or loss of function.

Fill Material, usually low strength, placed above the extrados and retained between the spandrel walls which support the railway.

Foundation The part of the masonry arch below ground level, that transfers and distributes the load from the abutment or piers into the surrounding ground.

Haunch CIRIA C656: The lower section of the arch barrel towards the springing.

Intrados CIRIA C656: In an arch or vault is the inner surface of the arch barrel i.e., the inner (concave) curve of the barrel.

Key parameter A crucial characteristic, requirement, or design basis that, if changed would drastically impact the structural performance, integrity, or ability of a masonry arch bridge to fulfil its mission requirements.

Keystone CIRIA C656: The highest and last-placed stones in an arch. In the arch barrel of a bridge there are a series of keystones at the crown, across its width, which are often left projecting on side elevations.

Masonry An assemblage of structural units usually laid in-situ in which the structural units, usually clay bricks, concrete blocks or stones, are bonded and solidly put together with mortar.

Mortar A mix of inorganic binders (lime or cement), sand aggregate and water forming the joint between stone or bricks in masonry, and which may be bedding mortar providing structural load transfer or pointing mortar for the outer finish of the masonry.

Parapet CIRIA C656: Usually a vertical continuation of the spandrel wall; an upward extension of a spandrel wall above road surface level to protect those on and below the bridge.

Pier CIRIA 656: An intermediate support between two adjoining arch spans.

Ring CIRIA C656: A layer of transverse single masonry elements that form slender units which make up an arch barrel. In brickwork, multiple adjacent rings are commonly used to produce a multi-ring arch.

Rise CIRIA 656: The vertical height from the springing point of an arch to the crown of the intrados.

Segmental arch A circular arch with a rise to span ratio less than 0.5.

Semi-circular arch An arch with an intrados of constant radius forming an arc of 180 degrees (rise/span ratio = 0.5).

Shallow arch CIRIA 656: Arch with a rise to span ratio less than 0.25.

Skewback CIRIA 656: The inclined masonry surface located at the extremity of an arch barrel which transmits the thrust to an abutment or pier.

Span CIRIA C656: The distance between the supports of an individual arch along its longitudinal axis.

Spandrel area CIRIA C656: The area overlying the arch barrel under the road surface (or equivalent), occupied by the spandrel walls, fill material or voids, and occasionally hidden elements such as internal spandrel walls.

Spandrel wall CIRIA C656: Masonry wall that sits on the edge of the arch barrel and that limits the extent of, and retains, the backfill. Sometimes "internal" spandrel walls may be present at other locations on the arch.

Springing CIRIA C656: Plane from which an arch spring, i.e. the junction between the vertical face of the abutment and the arch barrel.

Thrust line The locus (set of all points whose location satisfies one or more specified conditions) of the locations of the compressive force centroid within the arch. Specifically, it is the point on a specific section where, if all the stresses are transferred there, there is no bending moment but only axial force.

Voussoir CIRIA C656: Wedged shaped blocks usually brick/stone forming an arch.

Width The transverse dimension between edges of the arch barrel perpendicular to the spandrel walls.

Wing Wall CIRIA C656: A wall at the abutment of a bridge, which extends beyond the bridge to retain the earth behind the abutment.

Chapter 1

Introduction

1.1 Background and motivation

Masonry arch bridges are crucial components of road and railway networks globally, making up over 40% of railway bridges and 25% of road bridges in Europe alone. These structures, often centuries old, continue to be vital links in modern transportation systems. Understanding their dynamic behavior, including modal frequencies and mode shapes, is essential for assessing structural health, designing resilient new bridges, and developing effective maintenance strategies.

The dynamic properties of masonry arch bridges are pivotal because they determine how these structures respond to dynamic loads such as traffic, wind, and seismic events. Modal frequencies and mode shapes play a key role in predicting and analyzing these responses, ensuring the safety and longevity of these historic bridges.

Despite their importance, there is a **lack of comprehensive knowledge on how the geometric characteristics of masonry arch bridges influence their dynamic properties**. Previous studies have mostly focused on static load-bearing capacity or material degradation, neglecting the intricate relationship between geometric parameters—such as arch span, thickness, rise, bridge width, and pier dimensions—and dynamic behavior. This knowledge gap limits our ability to predict and optimize bridge performance under dynamic loads.

Traditional empirical rules and historical design principles do not provide the detailed insights needed for modern engineering analysis. Thus, a systematic and quantitative approach is necessary to understand the dynamic behavior of these bridges. **This study aims to fill this gap by investigating the correlation between the geometrical characteristics of masonry arch bridges and their dynamic behavior using advanced finite element (FE) modeling techniques**.

To achieve this, the study includes the automization of generating finite element models. Because several models needed to be generated, an automatic procedure was devised, and a Python code was developed for this purpose. This approach ensures efficient and consistent model creation, allowing for a thorough examination of the dynamic behavior under various geometric configurations.

By creating a comprehensive database and developing empirical equations to predict natural frequencies, this research will offer practical tools for engineers and researchers. These tools will enable quick and reliable assessments of dynamic behavior, aiding in the preservation and improvement of these critical structures. Ultimately, this study supports efforts to maintain, rehabilitate, and design masonry arch bridges, ensuring their resilience and continued service in modern infrastructure.

1.2   Objectives

1.2.1   General Objectives

The primary objective of this study is to **investigate the dynamic behavior of masonry arch bridges** through the use of 3D solid element finite element (FE) models. The research aims to bridge the knowledge gap regarding the influence of geometric characteristics on the modal frequencies and mode shapes of these structures, ultimately contributing to improved assessment, design, and preservation practices for masonry arch bridges.

1.2.2   Specific Objectives

To achieve the primary objective, the study will focus on the following specific objectives:

- **Identification of Critical Geometrical Parameters**: Determine key geometric parameters such as arch span, thickness, rise, bridge width, pier thickness, width and height, backing height, and arch slenderness that significantly influence the dynamic behavior of masonry arch bridges.

- **Historical Analysis**: Investigate and document historical empirical rules and construction practices used in the design of masonry arch bridges to provide context and foundational knowledge.

- **Automization of Model Generation**: Devise an automatic procedure to generate finite element models and develop a Python code for this purpose, enabling the creation of several models efficiently.

- **Finite Element Model Development**: Create detailed 3D solid element FE models of masonry arch bridges to simulate their dynamic behavior under various conditions.

- **Modal Analysis**: Conduct comprehensive modal analyses using the FE models to capture the modal frequencies and mode shapes of these structures.

- **Database Development**: Compile the results of the modal analyses into a comprehensive database that includes various geometric configurations and their corresponding dynamic properties.

- **Empirical Equation Formulation**: Develop empirical equations based on the database to predict the natural frequencies of masonry arch bridges, facilitating quick and reliable dynamic assessments.

- **Sensitivity Analysis**: Perform sensitivity analyses to understand the relative impact of different geometric parameters on the dynamic behavior of masonry arch bridges.

1.3   Methodology

The **methodology** of this study involves several key tasks designed to systematically explore and understand the dynamic behavior of masonry arch bridges. The approach combines historical analysis, geometric parameterization, advanced modeling, and empirical validation to achieve comprehensive insights.

- **Historical Investigation**: We began by investigating the historical empirical rules used in the construction of masonry arch bridges. This step was crucial for understanding the foundational design principles that have guided the construction of these bridges over centuries. By analyzing historical documents and construction records, we identified traditional methods and materials, providing a contextual background for our study.

- **Identification and Parameterization of Geometrical Aspects**: The next step involved identifying and parameterizing the critical geometrical aspects of masonry arch bridges. Key parameters such as arch span, thickness, rise, bridge width, pier thickness, width and height, backing height, and arch slenderness were systematically defined. This parameterization allowed for a structured approach to model various geometric configurations and their impact on dynamic behavior.

- **Development of a Parametric Geometric Model**: A custom Python code was developed to generate the parametric geometric model of the bridge. This code facilitated the creation of accurate and versatile models by allowing easy adjustments to the geometric parameters. The parametric model served as a foundation for generating the detailed finite element models used in subsequent analyses.

- **Finite Element Model Creation and Modal Analysis**: Using the parametric geometric models, detailed 3D finite element (FE) models were created using STKO (Scientific ToolKit for OpenSees). STKO provided the necessary tools for performing high-fidelity modal analyses, capturing the dynamic properties of the bridges under various conditions. These models were essential for understanding how different geometric configurations affect the modal frequencies and mode shapes.

- **Database and Empirical Equations Development**: The results of the modal analyses were compiled into a comprehensive database. From this data, empirical equations were developed to predict the natural frequencies of masonry arch bridges based on the identified geometrical parameters.

This methodology integrates historical context, geometric analysis, advanced modeling, and empirical validation to offer a robust framework for understanding and predicting the dynamic behavior of masonry arch bridges. The combination of custom Python code for geometric modeling and STKO for finite element analysis ensures accurate and efficient exploration of the key factors influencing bridge dynamics.

1.4   Outline of the Thesis

The **structure** of this thesis is organized as follows:

- **Chapter 1: Introduction** - Provides an overview of the background, motivation, objectives, and methodology of the study.

- **Chapter 2: State of the Art** - Reviews the current literature and previous research on the dynamic behavior of masonry arch bridges, including methodologies and findings related to modal analysis.

- **Chapter 3: Empirical Rules and Geometrical Parameters** - Examines historical empirical rules and identifies the critical geometrical parameters influencing the dynamic behavior of masonry arch bridges.

- **Chapter 4: Design of the Model** - Details the process of parametrizing the geometrical characteristics and creating 3D FE models for the study.

- **Chapter 5: Eigenvalue Sensitivity Analysis of Single Span Bridges** - Discusses the influence of different parameters on the dynamic properties of the bridge.

- **Chapter 6: Conclusions** - Summarizes the findings, discusses their implications, and provides recommendations for future research and practical applications.

Chapter 2

State of the Art

2.1 Historical review

The utilization of arches and vaults to traverse horizontal expanses traces back thousands of years. The origins of arches can be traced to underground tombs in Mesopotamia around 3000 BC [19], where the Sumerians pioneered their construction techniques. This architectural innovation transcended civilizations, with the Egyptians and Greeks also adept in vault and arch structures [28]. However, it was the Etruscans who are credited as the first to utilize wedge stones to construct masonry arches, paving the way for the advancements later perfected by the Romans [28]. With the Roman Empire's ascent, arch construction flourished, not only enhancing architectural grandeur but also serving essential infrastructural needs, particularly in bridge construction (Figure 2.1).

The subsequent decline of the Roman Empire, circa the 5th century, heralded a period of deterioration for road networks and bridges across Europe. However, as societal and economic shifts unfolded in the following centuries, spurred by increased trade and urbanization, the demand for robust transportation infrastructure resurged. This resurgence saw a revival in the construction of **masonry arch bridges**, marking a renaissance in architectural and engineering achievements.

Fast forward to the modern era, and the legacy of these ancient structures endures. Roman bridges, characterized by their sturdy construction and distinctive arches, still stand as testaments to ancient engineering prowess. Meanwhile, medieval bridges (Figure 2.2), with their adaptability and larger spans, continue to serve as vital arteries in contemporary transportation networks.

Figure 2.1.   Roman bridge of Alcántara, Spain.

Figure 2.2.   Medieval bridge of Besalù, Spain.

Yet, the passage of time has not been kind to these venerable structures. Decades of wear and tear, compounded by shifting traffic patterns and environmental stressors, have taken their toll. Many bridges now face structural integrity issues, necessitating comprehensive assessments and rehabilitation efforts to ensure their continued viability

[9].

In recent years, advancements in structural analysis and assessment techniques have provided invaluable insights into the behavior of masonry arch bridges. From numerical modeling to experimental investigations, researchers have delved deep into understanding the intricacies of these ancient marvels. However, challenges remain, as ongoing efforts are needed to address the complex interplay of factors influencing the long-term durability and safety of these structures.

In essence, masonry arch bridges stand as enduring symbols of human ingenuity and resilience, bridging the gap between ancient heritage and modern infrastructure needs. Their preservation not only honors the past but also ensures a legacy of connectivity and cultural heritage for generations to come.

2.2 Construction materials of masonry arches

The structural system of stone masonry arch bridges is essentially made up of two types of materials: **masonry** and **filling material**. These are heterogeneous, anisotropic materials, in certain cases containing discontinuities, with complex behavior, generally with reduced tensile strength.

2.2.1 Masonry

Masonry, encompassing brickwork, stonework, or concrete blockwork, is a construction material composed of masonry units separated by mortar joints (Figure 2.3).

Figure 2.3. Brickwork arch bridges featuring various stone masonry elements: (a) skewback and (b) quoins [12].

In masonry arch bridges, various masonry materials can be employed, such as brickwork for the arch barrel and stone masonry for spandrel walls and abutments. The

visible exterior may differ from internal components, with options including stone masonry throughout or a combination of materials [12].

Composite masonry properties stem from both the masonry units (Table 2.1) and mortar (Table 2.2) used, with mortar content ranging from zero in well-dressed stone masonry to around 40% in random rubble masonry.

Table 2.1.   Masonry unit types [12].

Masonry Unit	Description
Clay brick	Wide range of mechanical properties, from locally sourced soft red bricks with a compressive strength of less than $10N/mm^2$, to engineering bricks with a compressive strength of $150N/mm^2$. Solid rather than frogged or perforated bricks were usually employes, often fired locally.
Stone	Wide range of mechanical properties, with compressive strengths ranging from less than 10 to in excess of $300N/mm^2$ (granite). Properties sometimes anisotropic, with weathering and mechanical resistance dependent upon orientation.
Concrete	Pragmatic alternative to stone. Typical compressive strengths range from 10 to $50N/mm^2$.

Table 2.2.   Mortar types [12].

Mortar Type	Description
Lime	Lime mortars comprise lime and sand. They are slow setting and relatively weak (compressive strength typically about 0.5 to $1.0N/mm^2$) but more forgiving than modern Portland cement mortars due to their ability to accommodate movement.
Hydraulic lime	Hydraulic lime mortars (sometimes referred to as 'Roman cements') use a hydraulic binder that sets in the presence of water. These mortars are slow setting but have higher strength than traditional lime mortars.
Portland cement	Portland cement mortars have been in use since the mid-19th century and typically comprise cement, lime and sand. However, modern Portland cement produces stronger/stiffer mortars than were possible in the 19th century, with compressive strengths of in excess of $10N/mm^2$ possible.

While masonry exhibits **strength in compression**, it is **weak in tension**, with properties influenced by the orientation of bed-joints. Compressive strength can be determined through standards or tests, with saturation potentially reducing strength.

Masonry is quasi-brittle, prone to degradation under persistent gravity loading or repeated short-term vehicle loading, leading to microcrack propagation and potential abrupt failure (Figure 2.4). Weathering further contributes to degradation, affecting structural integrity over time (Figure 2.5).

Figure 2.4. Brickwork test specimen under high pre-compression showing failure due to formation of tensile cracks [12].

Construction quality in older masonry structures can vary greatly, with facing materials often masking lower-quality interior components. Consequently, surface quality may not accurately reflect overall structural integrity, especially in piers where low-quality infill material may compromise shear and compressive capacity.

Given the age and uncertain loading history of most masonry arch bridges, tensile strength is typically neglected for assessment purposes, although constituent masonry units are assumed to possess sufficient strength. Similarly, unit-mortar shear-bond strength is often disregarded unless evidence suggests otherwise.

2.2.2   Backfill

The **material used to fill a masonry arch bridge** may be granular and/or cohesive in nature and is often heterogeneous. The top layer of material is usually very highly compacted because of repeated loadings from vehicles. The properties of the fill will be strongly influenced by the presence of water, and by seasonal variations. It may experience a full range of moisture conditions from a high suction unsaturated state to fully flooded conditions and a corresponding range of strengths. In general, the

Figure 2.5.   Degradation of bridge parapet, likely due to freeze-thaw action [12].

strength of waterlogged backfill will be significantly lower than the strength of the same material in a dry state, which can adversely affect bridge load carrying capacity. The backfill types likely to be encountered in a masonry arch bridge are listed in Table 2.3 and shown in Figure 2.6.

Table 2.3.   Backfill types [12].

Infill	Description
Granular	Sand, gravel and cobbles are granular materials that get their shear strength from inter-particle friction, which partly depends on the density achieved. Shear strength is reduced by the presence of water (due to pore water pressures reducing the normal stresses).
Clay	Clay is a fine-grained soil material that possesses cohesive strength. This strength is very dependent on the moisture content.
Other	Locally sourced cohesive-frictional materials (eg Essex 'hoggin") were commonly used as backfill around retaining walls and masonry bridges. The properties of these materials are often highly dependent on moisture content.

Figure 2.6.   Backfill materials taken from bridge trial pits: a) granular, b) cohesive, c) other (cohesive-frictional) [12].

2.2.3   Other elements

As well as masonry and backfill, other elements may be present which contribute to the performance of a bridge (Table 2.4).

Table 2.4.   Other elements [12].

Element	Description
Metallic elements	These include tie bars and pattress plates, strapping, curved beam under-ringing, stitches (eg connecting rings in a multi-ring brickwork arch) and reinforcement provided as part of a proprietary strengthening technique. (Note that metallic elements such as stitches may have insufficient stiffness to contribute significantly to overall performance.)
Waterproofing materials	These include traditional puddled clay and tar, injected polyurethane materials and modern polymer sheeting designed to keep the primary elements of the structure dry. (Note that waterproofing a structure from below (eg for a tenanted arch) may lead to the original structure become saturated, potentially accelerating degradation.)
Piled foundations	May be formed from timber, or, if installed more recently, steel or concrete.
Mass concrete	Mass concrete was often used for 'backing' material but is now sometimes used to replace backfill. (In some cases mass concrete has been used to form complete arch bridge structures, but such structures are beyond the scope of this guidance.)
Shotcrete	Shotcrete, sprayed concrete, has sometimes been applied to exposed surfaces of masonry arch bridges in poor condition. (Note that a shotcrete liner will waterproof a structure from below, leading to the issue mentioned under 'waterproofing materials. The liner may also peel away from the masonry and has generally been found not to be an effective or long-lasting solution.)
Grout	Cementitious grout has often been used to fill voids in the masonry and/or to strengthen backfill. (Note that grout may not always have migrated to the desired location, and unanticipated filling of a void on one side of a bridge only may destabilise the structure.)
Reinforced	These include reinforced concrete saddles and near-surface concrete slabs or 'U' decks.

2.3   Elements of a masonry arch bridge

The principle components of a masonry arch are shown in Figures 2.7 [16] and 2.8 [12]; they are analyzed in the following paragraphs.
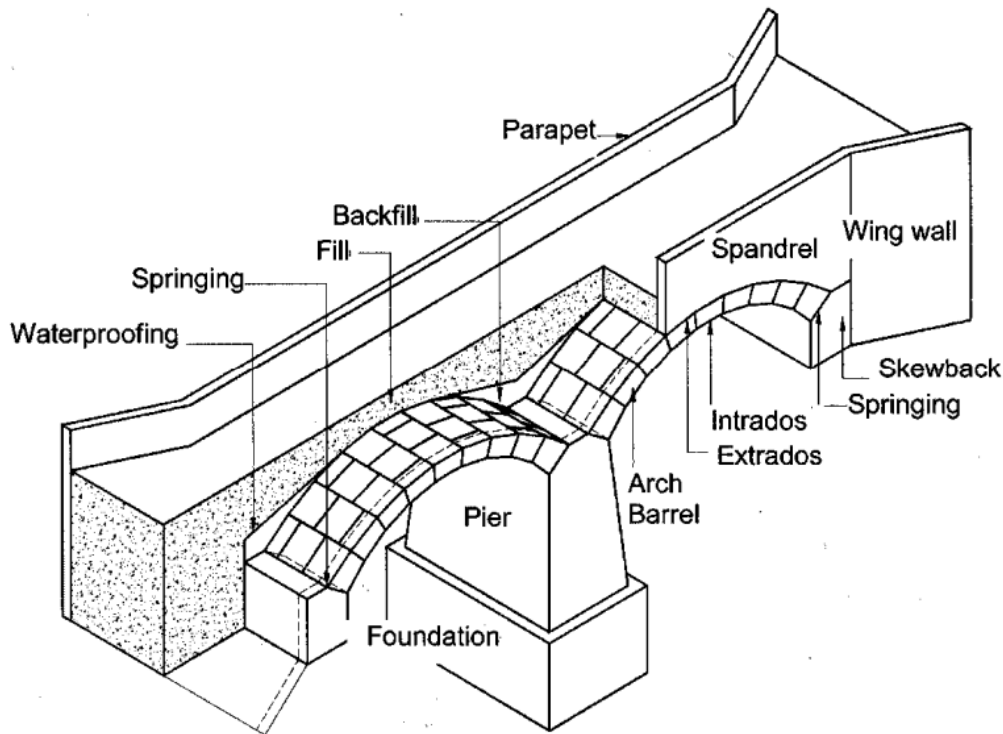
Figure 2.7.   Elements of stone arch (vault) bridges [16].

2.3.1   Arch barrel

The central component of an arch bridge is the **arch barrel**, which can be crafted from either meticulously hewn stone or bricks. In instances where bricks are employed, the barrel typically comprises multiple layers or rings, each intricately bonded together. However, compared to their stone counterparts, brick rings inherently possess less robustness, necessitating thicker dimensions for equivalent spans and rises [16].

Across the width of the arch barrel, localized reductions in thickness may occur beneath the external spandrel walls. The overall shape of the barrel is typically influenced by clearance requirements and economic considerations prevailing at the time of construction. Consequently, bridges along the same route often feature arch barrels with nearly identical or closely resembling geometries [16].
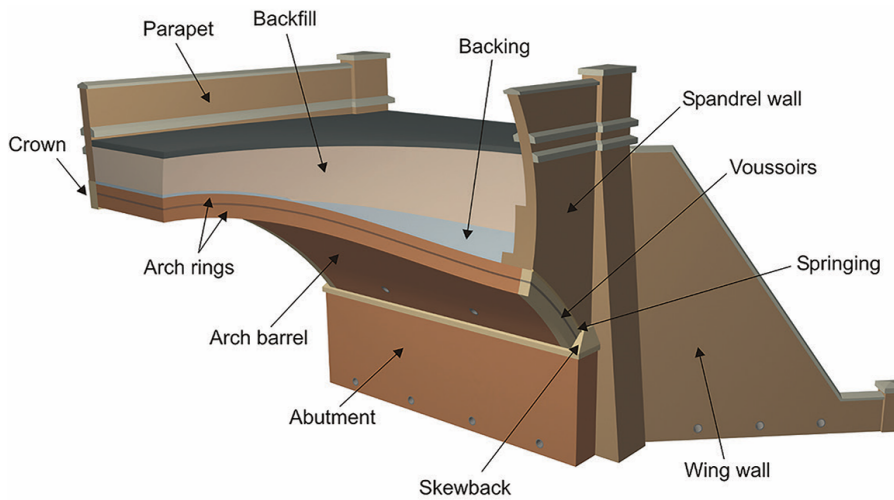
Figure 2.8.   Elements of a masonry arch bridge [12].

2.3.2   Abutment and pier

The **abutment** serves as a crucial element in counteracting both the vertical and horizontal forces exerted by the arch. Despite its robust construction aimed at withstanding the thrust from the arch barrel, the abutment undergoes imperceptible movement towards the supported embankments. Typically, this movement remains minimal, measuring less than 0.5 mm for spans up to 8 meters.

The **piers** primarily bear vertical loads, with minimal horizontal load transmission, as any horizontal loads stemming from dead weight are effectively balanced. While the horizontal load has negligible impact on the behavior of shorter piers, it may become significant for slender, elongated piers.

2.3.3   Spandrel walls

The **spandrel walls**, positioned at the periphery of the arch barrel, serve to confine the fill material. Typically, these walls are constructed as extensions of the edge voussoirs. However, they are usually erected on top of the arch without any form of key. Additionally, walls situated above the sleeper's bottom level are referred to as parapets.

2.3.4   Fill

The main function of the compacted **fill** within the spandrel is to establish a level surface. Additionally, the fill serves to disperse the live load across a broader section of the arch, enhancing stability. Moreover, it offers a counteraction to the movement of the arch barrel, further bolstering the arch's stability. Typically, local materials are employed for the fill, aligning with common industry practice.

2.3.5   Backing and haunching

Extra masonry featuring a horizontal upper surface is referred to as **backing**, while masonry with a sloping surface is termed **haunching**. While this additional masonry may consist of rough or formally bonded materials, it is typically not visible at the face of the arch barrel. Its primary function is to create a pathway for the thrust, ensuring substantial distribution before it reaches the soil fill behind the abutment. Additionally, it enhances the capacity and durability of the structure.

2.3.6   Wing walls

Wing walls, whether extending the line of the spandrel walls or angled differently, serve to enclose the fill behind the abutment. Additionally, they enhance the stability of the abutment, albeit to a lesser extent as the angle increases. When founded at the base of an embankment, wing walls enable the arch to achieve stability before the embankment's construction. However, if founded within the embankment, the typical lack of compaction of the fill makes settlement of the structure inevitable.

2.3.7   Track system

The **track system** plays a crucial role in distributing the load from the wheel-rail contact to the base of the sleepers. The effectiveness of this distribution depends on the relative stiffness of the different track components. As the load passes through the sleepers and into the ballast, it is further distributed to the supporting arch.

2.4   Types of arches

Regarding the arch typology, according to the classification identified by Proske & Van Gelder in 2009, the most common types of arch to be found in masonry arch bridges are those shown in Figure 2.9.

2.4.1   Shape and thickness of arches

Theoretical derivations can establish the ideal **shape** of an arch under a fixed load. However, the actual shape of an arch must balance structural integrity with practical considerations such as ease of construction, inspection, and maintenance. The parabolic shape closely approximates the ideal shape. In the context of Indian Railways, the prevalent arch design is the segmental arch, where the arch barrel forms a segment of a circle. This design facilitates straightforward construction and measurement.

The **thickness** of the arch barrel can be achieved through layers of individual pieces, particularly in brick masonry arches. These layers may be separate or interlocked. While interlocking enhances stability by preventing sliding between layers, separate layers are more commonly employed due to construction convenience. Stone arches typically feature a single thickness of stone. The type of arch construction shows

Figure 2.9.   Types of arch geometries [28].

certain regional consistencies around Europe, for example arch bridges in Britain are generally built without headers, while in Southern Europe arches with interlocking headers are more common [3].

Various configurations illustrating these principles are here reported and depicted in Figure 2.10 [12]:

- **Multi-ring (stretcher)**: Adjacent rings of brickwork connected only by circumferential mortar joints, leading to the potential for delamination. Rings may slide relative to each other, thereby reducing ultimate load carrying capacity. A physical gap may also open up between the separated rings.

- **Intermediate (some header-bonded rings)**: Thicker, bonded arch rings connected by circumferential mortar joints with the potential for delamination.

- **Bonded (header)**: Adjacent rings of brickwork connected by brick headers, reducing the likelihood of delamination, although this may occasionally still occur.

2.5   Force flow in arch bridges

2.5.1   Force flow and load paths

More than any other structural form, comprehending the behavior of arch bridges hinges on visualizing the **flow of force**. Force is naturally drawn to stiffness, favoring
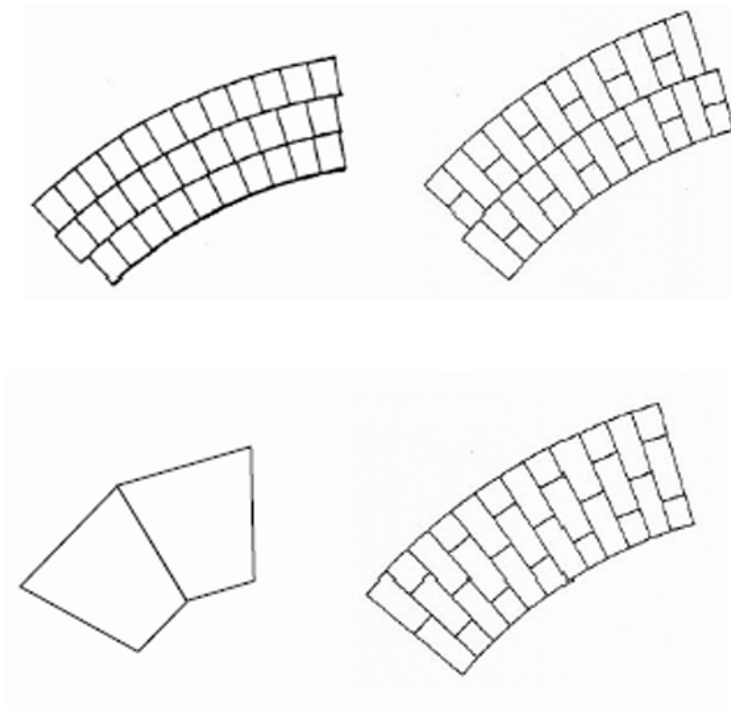
Figure 2.10.   Brick layers layout: (a) multi-ring; (b) intermediate; (c) single stone; (d) bonded [12].

stiff load paths over more flexible ones. However, if the stiff paths fail, the more flexible ones will come into play. It's important to recognize that within an arch system, there can be significant differences in stiffness, despite the overall stiffness of the structure.

Before a structure collapses, it will utilize all available **load paths**. When there are few and similar paths, this is relatively easy to envision. However, when there are numerous and varied paths, conceptualizing becomes more challenging. It's exceptionally rare for the forces in an arch to be so high that crushing failure occurs before the formation of a mechanism.

In the case of larger arches, excessive deflection may occur before reaching the ultimate load, in which case deflection becomes significant. Shear issues are extremely uncommon in arch bridges.

2.5.2   Line of thrust

Since Robert Hooke's observations in 1695, the concept of a line of thrust has been fundamental in understanding arch behavior. Hooke likened an arch to an inverted hanging chain, emphasizing that stability hinges on force equilibrium rather than material strength.

Consider an arch composed of unbonded blocks (Figure 2.11).
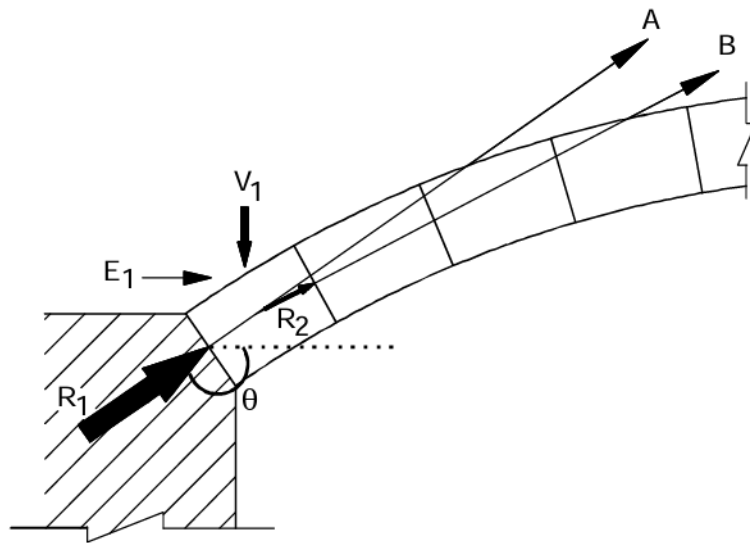
Figure 2.11.   Force flow in an arch [16].

Thrust R_1 from the abutment, dead load V_1, and earth pressure E_1 act on the first block. The resultant force R_2 changes magnitude and direction as it passes through subsequent blocks, defining the line of thrust. As long as this line remains within the middle half of the arch ring, stability is maintained.

The initial angle θ between R_1 and the springing is crucial; for a semicircular arch, $\theta = 90°$. Minimum stability thickness for a semicircular arch is 12% of the radius, reducing to 3% for a 120° arch.

A thin bare arch having only self weight is shown in Figure 2.12, where the red line shows the line of the thrust.

Figure 2.12.   A Bare arch, where the red line shows the line of thrust [16].

A concentrated live load disrupts reactions. If the arch's weight is insignificant compared to the live load, two direct forces support it (Figure 2.13). With adequate self-weight, forces follow a curve towards the abutments (Figure 2.14), further curving for distributed live loads (Figure 2.15).

40
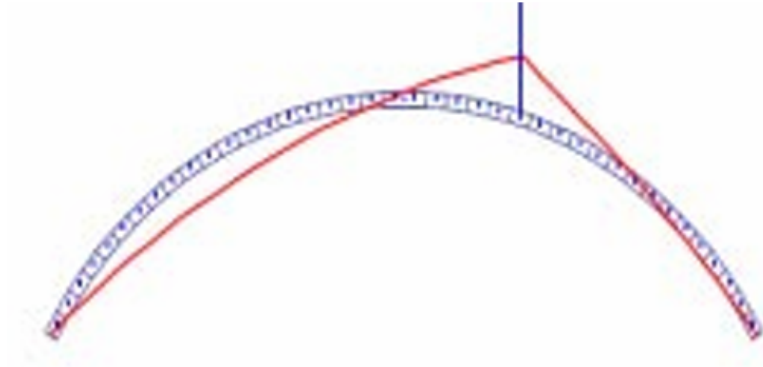
Figure 2.13.   A Thin arch with concentrated load, where the red line shows the line of thrust [16].
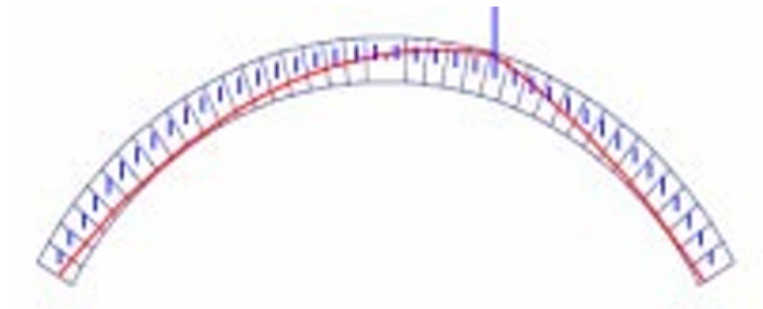
Figure 2.14.   A Thick arch with concentrated load, where the red line shows the line of thrust [16].
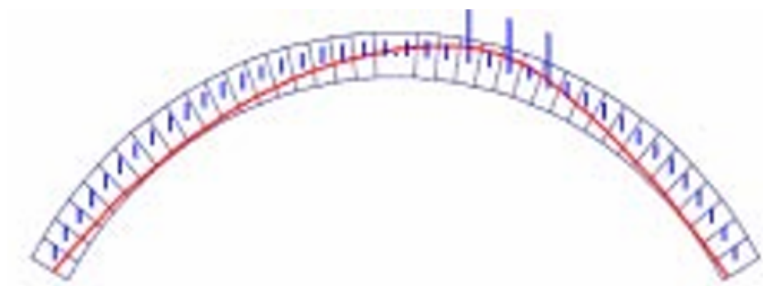
Figure 2.15.   A Thick arch with distributed load, where the red line shows the line of thrust [16].

Strength considerations are paramount. While old mortar offers some tensile strength,

it may fail if thrust deviates significantly from the arch center. However, minimal strength can maintain ring integrity and prevent crack propagation.

Zones prone to cracking under thrust are depicted in Figure 2.16, with multiple cracks forming where thrust nears the arch boundary. Compressive stress becomes concerning if thrust approaches the arch edge, potentially causing localized rotation.
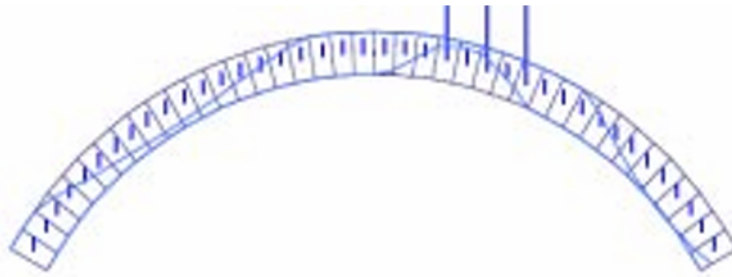
Figure 2.16. Areas which will cracks due to loads as shown in Figure 2.15 [16].

Shear strength, particularly tangential to brick rings, is crucial. Despite independent layers in brick rings, thrust transmission occurs over considerable lengths, minimizing shear stress on mortar beds.

Understanding arch behavior necessitates balancing force equilibrium and strength considerations, ensuring stability and structural integrity.

2.6   Effect of various parameters

2.6.1   Effect of fill

The presence of **soil fill** over an arch significantly impacts its behavior in several ways.

One notable effect is the substantial alteration of the scale and distribution of dead load. Additionally, it's important to note that the soil exerts not only vertical pressure but also generates a horizontal force component (as depicted in Figure 2.17).

Another significant effect of the fill could be observed in cases of arch distortion under load. Typically, such distortion occurs at a specific point (referred to as point B in Figure 2.17), causing upward and inward movement towards the near springing at the opposite side (point C in Figure 2.17). Although these movements may be minimal, they lead to a reduction in soil pressure on the falling side and an increase on the rising side, resulting in the fill generating forces that resist this movement.

Moreover, there will be a distribution of load through the fill in the transverse direction.
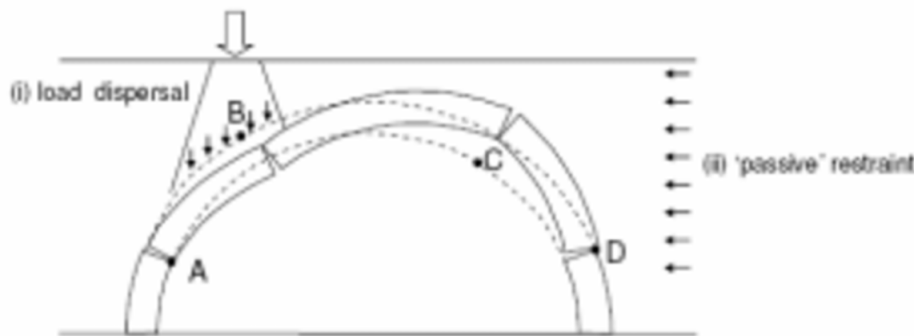
Figure 2.17. Effect of fill [16].

2.6.2 Effect of arch width

The **arch** itself demonstrates an inherent capability to distribute the effect of a load. When a live load is imposed on its surface, the line of thrust may locally deviate and flatten away from the load, as depicted in Figure 2.14. However, in the case of a wide arch, this scenario offers an incomplete understanding.

While the live load component of thrust initially concentrates at the point of application of the load, it does not maintain this concentration all the way to the abutments. In masonry walls, it's often assumed that a concentrated load distributes at a 1:1 ratio on each side of the line of application. In essence, an arch can be viewed as a wall rolled over. Although there are no specific tests or analytical results to validate this behavior, it is evident that the effect of the applied load cannot remain concentrated throughout the entirety of the structure to the abutments.

2.6.3 Effect of arch edges

The **edges** of an arch can either be free or fixed, with fixed edges being more common in railway bridges. The significance of the arch edges becomes apparent when the width is less than about four times the span. If the edges are prevented from moving vertically (as rotation fixity is not feasible), the flow of force near the edges will be altered.

Referring to Figure 2.17, it becomes evident that the arch would need to bow upwards on the right and downwards on the left. Additionally, it would sway sideways at the crown, applying a significant force to the stiff flat masonry panel. This sideways movement at the crown is resisted primarily by the thrust around the arch and horizontal or inclined force from the spandrel.

Spandrel walls are typically not bonded to the arch edge, limiting the resistance they provide to movement. Movement away from the spandrel encounters negligible resistance. The upward movement at the right of Figure 2.17 will also be resisted, causing the arch to bow upwards across its width and transferring force back into the

swaying element. As a result, all movements are resisted to some extent.

This resistance to movement significantly increases the stiffness of the arch relative to the soil. Consequently, the distribution of live load is reduced, and the modification of soil pressures towards active and passive states is constrained. Until cracks form in the arch, most of the stabilizing force comes from the spandrels. However, since cracks sometimes occur under the spandrel walls, it is necessary to assume that the soil ultimately bears the load, as it may be required to do so in extreme cases.

2.6.4   Effect of skew

Skew arches present significant complexity in their structural behavior. The discussions so far have assumed that the abutments can be treated as fixed, but in the case of a skew bridge, this assumption may not hold true. Nevertheless, starting with the assumption of rigid abutments provides a useful basis for discussion.

Force always seeks the path of least resistance to the foundations. When forces are applied near the center of a skew arch, they flow by the shortest (normal) route to the abutment. However, near the edges, this direct path becomes impractical, and the arch forces must span on the skew (Figure 2.18).
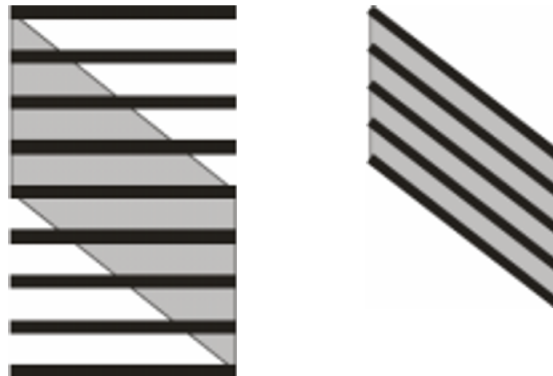
Figure 2.18.   Square and skew load paths [16].

Horizontal forces exerted on arch abutments typically exceed the vertical forces. An arch can twist with relatively little resistance, so even slight settlement or tilting of one end of an abutment can have minimal impact. However, if the abutment tilts back slightly, especially at the obtuse, heavily loaded corner compared to the acute angle, the arch force will begin to span on the skew.

For instance, in a skew arch with a 10-meter span, 2.5-meter rise, and 45° skew, a differential movement of just 1mm at the springing is adequate to ensure that the thrust operates on the skew rather than on the square line.

2.6.5 Effect of abutments

The required actions of **abutments** can vary significantly depending on the characteristics of the arch they support.

For abutments supporting shallow, large-span arches, the primary requirement is to distribute the thrust over as large a contact area as possible. This prevents the abutment from being pushed back into the surrounding ground.

In contrast, for tall abutments carrying high-rise arches, the thrust at the top may be primarily vertical, requiring the wall to act as a retaining wall with some support from the arch itself.

Live loads further modify these actions as they move across the bridge. When a load approaches an arch, it compresses the soil and generates horizontal pressure, pushing the abutment forward and shortening the span. The farther abutment typically experiences less movement, causing the crown of the arch to rise.

When a load is near the center of the span, the thrust in the arch increases, causing both abutments to move back. As the load leaves the bridge, the increased pressure it generates pushes the farther abutment into the span, shortening the span further.

While these movements may be small, they are easily measurable and contribute to the dynamic behavior of the bridge structure.

2.6.6 Effect of piers

Piers serve the purpose of supporting the two adjacent spans of an arch bridge. However, they offer limited resistance to horizontal movement. The thrust generated by the arch is transferred from span to span, and if a live load distributes across the width of the arch as it approaches the springing, the full width of an adjacent span is utilized to resist the toppling of the pier. Additionally, the stiff spandrel walls also play a role in providing support and stability.

2.6.7 Effect of backing or haunching

An arch with an included angle greater than 60 degrees often has solid masonry extending above the extrados at the springing. This extension, when brought to a horizontal top, is termed as **backing**, as illustrated in Figure 2.19. Alternatively, if the extension has an inclined top tangential to the arch ring, it is referred to as **haunching**. Haunching is more commonly observed on shallower arches or on single spans and end spans of viaducts. Many railway viaducts feature a solid layer with internal walls above. Regardless of the specific design, these extensions significantly enhance the stiffness and load capacity of the structure without increasing its overall depth (Figure 2.20). In fact, with firm haunching or backing, it may even be possible to reduce the ring thickness.

Figure 2.19. Backing [16].

Figure 2.20. Backing and spandrel walls [31].

2.6.8 Effect of ring thickning

Stone rings in arch bridges typically exhibit greater thickness at the springing compared to the crown. This is frequently accomplished by selecting deeper stones near the springing. Similarly, in brick rings, an equivalent effect is achieved by incorporating additional rings of brick within the main arch. However, these additional brick

rings are seldom visible at the exposed edge, as they are typically located between the spandrel walls.

2.6.9 Effect of internal spandrel walls

Internal spandrel walls are typically positioned above a solid backing block, which may or may not correspond to the rail positions in a railway viaduct. These walls add further stiffness and strength to the structure and can also reduce weight if the void between them is left unfilled. In order to maintain flexibility in the arch ring, most engineers truncate the internal spandrel walls at around the 1/4 or 1/3 span position. However, there are viaducts where the internal spandrel walls extend completely over the crown. The deck of the viaduct may be constructed from stone slabs or brick jack arches. Figure 2.21 illustrates exposed spandrel walls in a viaduct after the destruction of a pier, with the tension in the railway tracks supporting the remaining deck. Despite the arches collapsing beneath the spandrels, the vertical end is still clearly visible.

Figure 2.21. Internal spandrel walls [16].

2.6.10 Effect of decentering of the arches

In engineering practice, linear elastic models are commonly utilized, particularly within the ultimate limit state framework, where internal forces are typically computed by combining the effects of various loads linearly. This approach assumes that stress states in linear elastic structures remain constant throughout construction, leading to the belief that removing temporary scaffolding doesn't significantly impact structural analysis.

However, masonry arches are inherently nonlinear structures, even in their elastic phase. Consequently, the **removal of provisional scaffolding** becomes crucial for assessing stress distribution within the arch and other bridge components. Unlike linear models, limit analysis, the predominant method for analyzing masonry arches, considers the collapse load as a function of the actual stress state during construction, thus highlighting the importance of the building sequence in determining load-carrying capacity.

The impact of arch decentering on stress distribution remains somewhat unclear, with only initial insights available for discussion:

- the significant displacements observed during decentering cannot solely be attributed to arch elastic deformation. Factors such as the deformation of fresh mortar joints and the compaction of residual voids in the joints can play a significant role. This observation suggests that despite technical challenges, arch joints are typically found to be well-filled.

- the subsequent increase in displacement post-decentering may result from short-term creep response of the mortar. This phenomenon could lead to stress redistribution within the arch, potentially mitigating the effects of construction phases.

- foundation settlement, particularly at abutments and piers, appears to be the most probable cause for these displacements. Bridge piers often support centerings entirely or partially during construction, transferring a significant portion of dead loads to the foundations. However, at decentering, the load added to the foundations is limited or absent, making it unlikely that foundation settlement is a direct result of increased loads during decentering.

2.6.11 Effect of strength of material

The impact of **material strength** on an arch depends largely on how the arch ultimately fails. Typically, a masonry arch will not fail due to the crushing of masonry, but rather due to the development of tension and the subsequent formation of a collapse mechanism. Therefore, while the strength of the masonry is important to a certain extent, it may not be the primary factor determining the failure of the arch. In cases where existing arches appear to have poor-quality brick or masonry, it cannot be automatically assumed that they have significantly less strength. Instead, a thorough analysis is essential to accurately assess their structural integrity and potential failure modes.

2.7 Modes of failure of masonry arch bridges

The findings from both real-scale and model-scale experimental tests have contributed to identifying the potential **failure mechanisms** for masonry arch bridges [22] [15] [26].

These failure mechanisms include (Figure 2.22):

(a) Four-hinge mechanism   (b) Sliding

(c) Ring separation   (d) Abutment movement
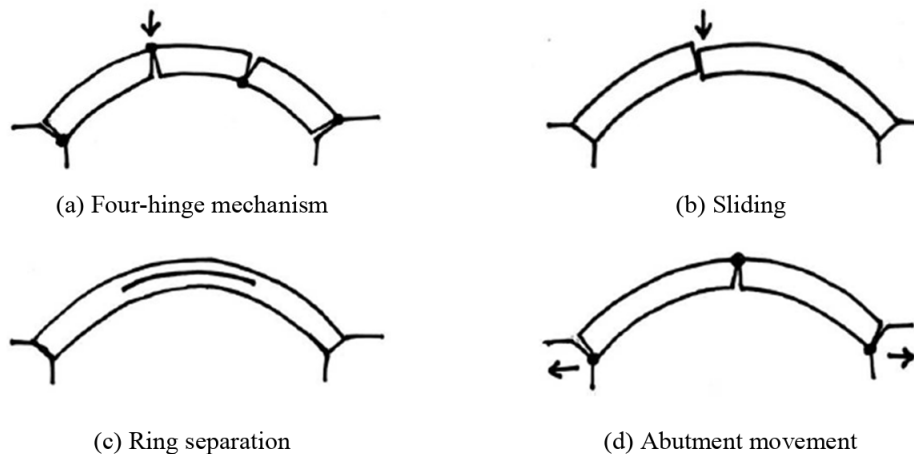
Figure 2.22.   Failure modes for masonry arches [22].

1. **Four-hinge mechanism**: the most common failure mode, characterized by the development of radial fracture lines in the arch barrel. Typically, four radial cracks (hinges) lead to the transformation of the arch into a mechanism, ultimately causing the bridge to collapse. In single-ring arches, a large crack in one mortar bed joint serves as a hinge, while in multi-ring brickwork arches, a group of radial cracks may form a diffused hinge [11].

2. **Shear sliding**: local failure mode characterized by the development of a sliding crack along the arch, typically near areas of concentrated load application.

3. **Ring separation**: commonly observed in brick-masonry multi-ring arches, especially those built using the stretcher method. This occurs when circumferential mortar joints connecting adjacent rings become weak surfaces.

4. **Failure due to movements at the abutments**: when relative movements occur at the abutments, such as settlements, failure may happen after the development of three hinges at the springings and around the crown of the arch.

5. **Material failure (e.g., crushing)**: arises when internal stresses in the arch exceed the compressive strength of the masonry.

6. **Snap-through buckling**: particularly relevant for shallow arches, where buckling may occur before the formation of four hinges or material failure [32].

For square arches, these failure modes are typically observed at the point of collapse. However, skew arches present more complex three-dimensional failure modes associated with the arrangement of mortar bed and perpendicular joints [14].

2.8 Dynamic properties of structures

Masonry arch bridges are impressive historical structures that have stood the test of time, often lasting for centuries. Understanding the dynamic properties of these bridges is essential, not only for preserving these historical landmarks but also for ensuring their safety and functionality today. The dynamic properties of masonry arch bridges are crucial because, according to the modal theory, the bridge's response under dynamic actions is determined by the combination of modal responses. This means that knowing the modal frequencies and mode shapes allows engineers to predict how the bridge will behave under various dynamic loads, such as traffic, wind, and seismic activity. Additionally, modal properties are used for several other applications, such as finite element model updating and damage detection in structures. By accurately determining these properties, engineers can update numerical models to reflect the current condition of the bridge, identify potential damage, and make informed decisions about maintenance and rehabilitation efforts.

2.8.1 Overview of Dynamic Properties

The dynamic properties of a structure describe how it responds to dynamic loads, such as vibrations from traffic, wind, earthquakes, and other transient forces. The key dynamic properties include natural frequencies, mode shapes, and damping ratios. These properties help determine how a structure will react to different types of dynamic excitation.

- **Natural Frequencies**: The natural frequency of a structure is the rate at which it vibrates when disturbed, measured in Hertz (Hz). For bridges, these frequencies provide insights into the stiffness and mass distribution of the structure. The natural frequency f is related to the period T (the time it takes to complete one vibration cycle) by the equation $f = 1/T$. Lower natural frequencies indicate a more flexible structure, while higher frequencies indicate a stiffer structure.

- **Mode Shapes**: Mode shapes describe the deformation patterns of a structure at different natural frequencies. Each mode shape corresponds to a particular natural frequency and shows how different parts of the structure move relative to each other. Understanding mode shapes is crucial for identifying potential points of weakness or failure under dynamic loads.

- **Damping Ratios**: Damping ratios measure how quickly a vibrating structure dissipates energy. This property is crucial for determining how quickly vibrations subside and how well the structure can resist dynamic loads. Damping is typically expressed as a percentage of critical damping, which is the minimum damping that prevents oscillations.

Resonance occurs when the frequency of an external force matches a structure's natural frequency, causing large amplitude vibrations. This can lead to significant structural damage or failure. For example, if the frequency of traffic-induced vibrations

matches the natural frequency of a bridge, resonance can occur, resulting in excessive oscillations.

2.8.2   Dynamic Properties of Masonry Arch Bridges

Masonry arch bridges are unique because they are primarily made of stone or brick without reinforcing steel. This construction method leads to distinctive dynamic behavior compared to modern bridges.

- **Material Characteristics**: The main materials used in masonry arch bridges, stone and brick, have high compressive strength but low tensile strength. This affects the bridge's natural frequencies, often resulting in lower frequencies compared to steel or concrete bridges.

- **Structural Geometry**: The curved shape of arch bridges helps them carry loads primarily through compression. However, this shape also affects their dynamic response. Factors like the span length, rise of the arch, and thickness of the arch ring significantly influence the bridge's natural frequencies and mode shapes.

- **Mass Distribution**: Masonry arch bridges usually have a substantial mass because of their thick, heavy construction materials. This significant mass contributes to lower natural frequencies and influences the bridge's overall dynamic response to loads such as traffic and earthquakes.

2.8.3   Analysis and Assessments

Evaluating the dynamic properties of masonry arch bridges involves both experimental and analytical methods.

- **Experimental Methods**: Modal testing, where the bridge is subjected to controlled vibrations, helps determine its natural frequencies and mode shapes. Instruments like accelerometers are placed at various points on the bridge to measure its response.

- **Analytical Methods**: Finite Element Analysis (FEA) is often used to model the bridge's dynamic behavior. This involves creating a detailed computer model of the bridge and simulating its response to dynamic loads. Parametric studies can then be conducted to understand how variations in bridge geometry and material properties affect its dynamic response

2.8.4   Preservation and Rehabilitation

Understanding the dynamic properties of masonry arch bridges is crucial for their preservation and rehabilitation. Identifying the natural frequencies and mode shapes helps engineers diagnose potential issues such as structural weaknesses or damage. For

example, changes in natural frequencies over time can indicate the presence of cracks or material degradation.

Rehabilitation efforts might include strengthening the bridge to improve its dynamic response. Techniques such as adding reinforcing materials, modern grouting methods, or even introducing damping devices can enhance the bridge's ability to withstand dynamic loads. However, these interventions must be carefully designed to respect the historical and aesthetic value of the structure.

Chapter 3

Empirical rules and geometrical parameters

3.1 Relevant geometrical parameters

When designing an arch bridge, several key parameters must be carefully considered to ensure structural integrity and functionality. These main parameters include (Figure 3.1):

- **Span of the arch** s: determines the distance between the supports;

- **Rise of the arch** r: defines the vertical curvature of the arch;

- **Thickness of the arch** t: influences its strength and stability;

- **Height** H**, thickness** T **and width** W **of the piers**: play crucial roles in supporting the arch and distributing loads.

- **Backing height** h_b: to provide additional weight and stability to the structure.

   Together, these parameters form the foundation for the design and construction of a robust and durable arch bridge. The goal of this Chapter is to make a comparison of the geometric characteristics of the bridges featured with the empirical rules practiced by ancient builders.

3.2 Historical empirical construction rules

3.2.1 Span of the arch

Considering the **span** s, arch bridges can be classified in the following way [25]:

- short span bridge: $0.0m < s \leq 7.5m$;

- medium span bridge: $7.5m < s \leq 15.0m$;
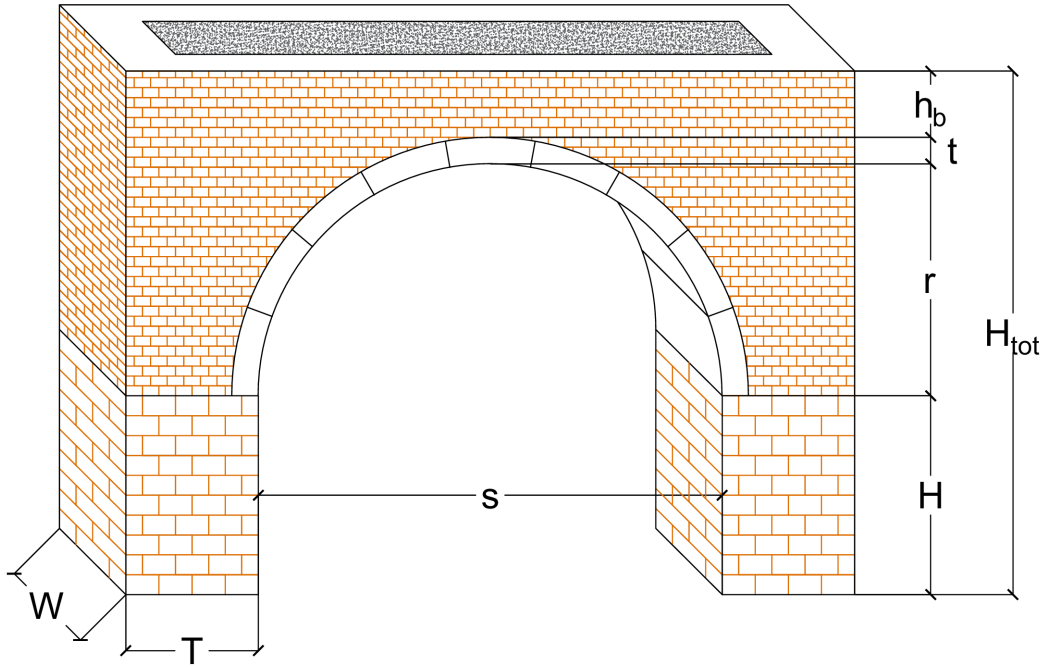
Figure 3.1.   Key geometrical parameters of a masonry arch bridge.

- large span bridge: $s > 15.0m$.

3.2.2   Shape of the arch

The **shape of the arch** is generally described as function of the span s and rise r or, more normally, of the rise to span ratio r/s.

Full circular arches (Roman bridges) had a ratio r/s of $1/2 = 0.5$ [25] [28]. For segmental arches, r/s reached values between $1/6 \approx 0.167$ and $1/9 \approx 0.111$. Sometimes additionally a minimum angle of $60°$ at the springing was required that corresponded to a ratio of $1/7.5 \approx 0.133$ [28]. At the end of the 18th century, the basket arch became more and more popular.

However, in contrast to such rules, bridges with much lower values of the r/s ratio were also constructed, such as the Nemours Bridge by Perronet in 1792 with $r/s = 1/10 = 0.10$ or $r/s = 1/15 \approx 0.067$ [6] [7] [28].

So, considering the rise to span ratio, it's possible to classify the arches [25]:

- shallow arch: $0 < r/s \leq 0.25$;

- semi-shallow arch: $0.25 < r/s \leq 0.40$;

54

- deep arch: $r/s > 0.40$.

Number of circle elements

Additionally to the choice of the r/s value, the number of circle elements in an arch was ruled for basket arches [28]. For example, if the ratio was equal to $1/3 \approx 0.333$ and the span of the arch was higher than $10m$, then three circular elements were suggested. Between $10m$ and $40m$ span, five circular elements were recommended, and for a span greater than $40m$, about seven segments should be chosen. For $r/s = 1/4 = 0.25$, the number of circular segments should then be five, seven, and nine.

For even greater r/s values, it's suggested a circle with a radius R of [7]:

$$R = \frac{s^2 + 4 \cdot r}{8 \cdot r}. \tag{3.1}$$

3.2.3 Thickness of the arch

The **thickness** t of the arch can be constant or variable, generally expressed in function of the span s. For simplicity of the model, a constant thickness will be considered.

To determine the thickness if the arch, there are several empirical formulas, reported in the following Table 3.1 [25] [28] [4], where:

- s: length of the span;

- t: thickness of the arch;

- R: radius of the circle passing through the extrados of the arch;

- ρ: radius of curvature of the arch.

In 1907, the Italian Railways (*Ferrovie dello Stato*) issued the first National Technical Code, in which the crown thickness of arch bridges t was given as a function of the arch span s [4]:

$$t = a + b \cdot s \tag{3.2}$$

where the constants a and b are given in Table 3.2 as a function of the brick compressive strength.

The understanding is that, excluding the resistance of materials, the possibility of adopting thinner thicknesses with more resilient materials is not feasible. Additionally, the collapse analysis would only yield insights into the formation of a more probable collapse mechanism, which implies the kinematic behavior of the entire arch. In practice, increasing the arch thickness, without effectively reducing the relative pressure on the material, would have minimal influence on its value. It would instead elevate the pressure value at the rupture joint where the arches meet.

Table 3.1.   Historical empirical rules for arch thickness [25] [28] [4].

Date	Author	Deep arch	Shallow arch
1452	Alberti	$t = s/10$	
1714	Gautier ($s > 10m$)	$t = 0.32 + s/15$	
1777	Perronet	$t = 0.325 + 0.035s$	$t = 0.325 + 0.0694\rho$
1809	Gauthey ($s < 16m$)	$t = 0.33 + s/48$	
	($16m \leq s < 32m$)	$t = s/24$	
	($s > 32m$)	$t = 0.67 + s/48$	
1809	Sganzin	$t = 0.325 + 0.3472s$	
1845	Déjardin	$t = 0.30 + 0.045s$	$t = 0.30 + 0.025s$
1854	L'Eveillé	$t = 0.333 + 0.033s$	$t = 0.333 + 0.033\sqrt{s}$
1855	Lesguillier	$t = 0.10 + 0.20\sqrt{s}$	$t = 0.10 + 0.20\sqrt{s}$
1862	Rankine	$t = 0.19\sqrt{R}$	
1865	Curioni	$t = 0.24 + 0.05s$	$t = 0.24 + 0.07R$ if
			$t = 0.24 + 0.05R$ if ($\alpha < 60$ř)
1870	Dupuit	$t = 0.20\sqrt{s}$	$t = 0.15\sqrt{s}$
1885	Croizette-Desnoyers	$t = 0.15 + 0.20\sqrt{\rho}$	
1887	Déjardin	$t = 0.15 + 0.10R$	
$19^{th}cent.$	Udine-Pontebba Railway	$t = (1 + 0.10s)/3$	
1914	Séjourné	$t = 0.15 + 0.15\sqrt{s}$	

The imperative to maintain the bridge's dimensions and weight is closely tied to aesthetic and economic factors, underscoring the significance of determining the arch thickness in masonry bridge construction [8].

Stress inside the arch

The axial force N in the arch at the crown is given by:

$$N = H = \frac{q \cdot l^2}{8 \cdot r} \tag{3.3}$$

where q represents the loading.

Table 3.2. Parameters *a* and *b* for equation 3.2 - Italian Railways 1907 [4].

f_b		Deep arch	Shallow arch			
	r/s	1/2	1/4	1/6	1/8	1/10
$10MPa$	a	0.36	0.38	0.39	0.40	0.40
	b	0.046	0.057	0.069	0.081	0.095
$20MPa$	a	0.31	0.31	0.32	0.32	0.32
	b	0.039	0.048	0.057	0.067	0.077
$30MPa$	a	0.25	0.25	0.26	0.26	0.26
	b	0.032	0.039	0.045	0.052	0.059

The axial force can be used to compute the **stress inside the arch**, which can then be compared to the compress strength of the arch. A simplified rule for stress evaluation at an arch crown was given by Dischinger (1949):

$$\sigma = \gamma_i \cdot \frac{s^2}{8 \cdot r} \tag{3.4}$$

where γ_i is the characteristic weight of the bridge. For long span, low pitched arches, γ_i amounts to $30kN/m^3$ and for slender, tall bridges, the value reached $40kN/m^3$.

Deformation of the arch at the crown

Based on these results and Naviers' theory, Ardant [2] was able to compute the **deformation of the arch at the crown** with the following equation :

$$y = \frac{1}{2} \cdot \frac{K \cdot V}{E \cdot I} \cdot l \cdot h^2 \tag{3.5}$$

where:

- y: deformation at crown;

- l: span;

- h: rise;

- V: sum of vertical loads;

- EI: bending stiffness;

- K: factor for the consideration of the load distribution over the arch.

3.2.4 Thickness of the pier

The **thickness** T of the pier is generally expressed in function of span s and thickness t of the arch.

The minimum value of the thickness in correspondence of the springing is generally given by:

$$T_{min} = 2 \cdot t. \tag{3.6}$$

Some of the authors mentioned above also sought to establish historical empirical rules for sizing the thickness of masonry arch bridge piers. Table 3.3 shows the historical relationships for column thickness design depending on the length of the span s and the height of the piers H [21].

Table 3.3.   Historical empirical rules for pier thicknesses [21].

Date	Author	Pier thickness
1452	Alberti	$T = 1/4 \cdot s$
1452	Alberti	$T = 1/4 \cdot H_{pier}$
1570	Palladio	$T = 1/6 \cdot s$
1681	Simon Garcia	$T = 1/4 \cdot s$
1717	Gautier	$T = 1/5 \cdot s$
1768	Perronet	$T = 1/11 \cdot s$
1886	Séjourné	$1/10 \cdot s < T < 1/8 \cdot s$

3.2.5 Height of the bridge

The **total height** H_{tot} of the bridge is given by (Figure 3.1):

$$H_{tot} = H + r + t + h_b \; ;$$

where:

- H: distance from the springing line to the foundation base;

- r: rise of the arch;

- t: thickness of the arch;

- h_b: height of the backing.

3.2.6 Width of the pier

Many different formulas exist for the computation of **width** W of the abutment (Table 3.4).

Table 3.4.   Historical empirical rules for pier width.

Author	Pier width
Semi-circular arches	
Lesguillier	$W = (0.60 + 0.04h)\sqrt{s}$
L'Eveillé	$W = (0.60 + 0.162s)\sqrt{\frac{0.865s(h+0.25s)}{H(0.25s+t)}}$
German-Russian Eng.	$W = 0.305 + \frac{5}{24}s + \frac{h}{6} + \frac{h_1}{12}$
Segmental arches	
Lesguillier	$W = (0.60 + 1.10(\frac{s}{r} - 2) + 0.04h)\sqrt{s}$
L'Eveillé	$W = (0.33 + 0.212s)\sqrt{\frac{sh}{H(r+t)}}$
German Eng.	$W = 0.305 + 0.125s(\frac{3s-r}{s+r} + \frac{2h+h_1}{12})$
Italian Eng.	$W = 0.05h + 0.20s + (\frac{10+0.5s}{100}\frac{s}{r})$
Semi-elliptical arches	
Lesguillier	$W = (0.60 + 0.05(\frac{s}{r} - 2) + 0.04h)\sqrt{s}$
L'Eveillé	$W = (0.43 + 0.154s)\sqrt{\frac{h+0.54r}{H}\frac{0.84s}{0.65r+t}}$
German Eng.	$W = 0.05h + 0.20s + (\frac{10+0.5s}{100} + \frac{s}{r})$
Other formulas	
Manuale dell'Ingegnere	$W = \sqrt{s}(0.42 + \frac{0.17s}{2r+t} + 0.44h)$ for $h_1 < 1.50m$ $W = \sqrt{s}(0.42 + \frac{0.17s}{2r+t} + 0.44h + 0.0185H\sqrt{h_1})$ for $h_1 > 1.50m$
"Hutte's Manual"	$W = \frac{L}{8}(\frac{3s-r}{r+s} + 1.00 + \frac{h}{6})$ $W = \frac{L}{8}(\frac{3s-r}{r+s} + 1.00 + \frac{h}{6})$ semi-circular arches
Croizette-Desnoyers	$W = 0.33 + 0.212s(\frac{sh}{H(r+t)})$
Italian Railway	$W = 0.20 + 0.030(\rho + 2t) + 0.10h$

3.3 Empirical rules obtained from surveys

In recent times, several authors have conducted a survey of the geometric characteristics of masonry arch bridges existing in a certain area, aiming to understand the empirical geometric rules applied in their construction.

Lagomarsino et al. [20] and Gambarotta [10] are among the latest to have made a series of observations on stone masonry arch bridges and subsequent studies, respectively, on the masonry bridges of the Genova-Ovada railway line and the more general study on the masonry bridges of Italy's road and rail systems.

3.3.1 Arch thickness

These two previous authors, after analyzing their data, presented a set of empirical relationships verified between the thickness of the arch t and the length of its span s.

Table 3.5 below presents these relationships, which we will later compare with the considered existing bridges.

Table 3.5. Empirical relationships obtained from surveys for arch thickness [20] [10].

Date	Author	Arch thickness
1999	Lagomarsino et al.	$s/17 < t < s/12$
		$t = 0.33 + 0.033s$
1999	Gambarotta	$t = 0.325 + 0.0347s$
		$t = 0.32 + s/15$
		$t = 0.1 + 0.2\sqrt{s}$
		$t = 0.2\sqrt{s}$
		$t = (1 + 0.1s)/3$
		$t = 0.43 + 0.005s$

3.3.2 Pier thickness

Lagomarsino et al. [20] also related the thickness of the pillars T to their height H and the length of the span s, arriving at the geometric relationships in Table 3.6.

Gambarotta [10], relates the thickness of the pillars with their height, with the length of the arch span and also takes into account the thickness of filling over the arch key and the tympanum, as described in Table 3.6.

The geometric relationships among the thickness in plan of the pillar T, the height of the pillar plus part of the arch arrow h^*, and the thickness of the filling in the crowning area of the arch h_b are illustrated in Figure 3.1. The disparity between dimensions h

Table 3.6.   Empirical relationships obtained from surveys for pier thickness, proposed by Lagomarsino et al. [20] and Gambarotta [10].

Date	Author	Pier thickness
1999	Lagomarsino et al.	$T = 0.125s$
		$T = 0.6 + 0.2H$
1999	Gambarotta	$T = 0.6 + 0.04h^*\sqrt{s}$
		$T = 0.6 + 0.162s\sqrt{s\frac{(h^*+0.25s)0.865s}{H(0.25s+t)}}$
		$T = 0.305 + \frac{5}{24}s + \frac{h^*}{6} + \frac{h_b}{12}$

and h^* arises because the region near the base of the arch is typically filled with a sturdier material, which serves to reinforce this area. This results in a hypothetical pillar height higher than the actual h.

3.4   Existing bridges parameters: cases of study

To derive the parameters used in the model, two case studies were considered. The first case study is Claudia Lemos's thesis [21], which focuses on masonry arch bridges in Spain and Portugal, predominantly in the regions of Minho, Trás-os-Montes, and Galicia. The second case study is João Jorge Carrazedo de Jesus's thesis [18], which examines bridges in the Bragança region.

Claudia Lemos's thesis [21] provides a comprehensive geometric analysis and load-bearing capacity evaluation of masonry arch bridges in Spain and Portugal (Figure 3.2). It includes a detailed study of various bridges, analyzing critical parameters such as the rise/span ratio, thickness/span ratio, and other geometric aspects that influence the structural behavior of these bridges (Table 9.1 in Annex C).

João Jorge Carrazedo de Jesus's thesis [18] involves an in-depth geometric-structural survey of masonry arch bridges in the Bragança region (Figure 3.3). This study includes measuring key parameters such as the number of spans, span lengths, arch heights, arch thicknesses, fill heights over the arch, and pier heights and widths (Table 9.2 in Annex C). The survey aims to characterize these bridges' geometric properties and compare them with historical empirical rules used by ancient builders, contributing to a database for structural analysis and safety assessment.

Both theses provide essential data on the geometric and structural characteristics of masonry arch bridges, which are crucial for validating the FE models and applying the findings to real-world bridges.
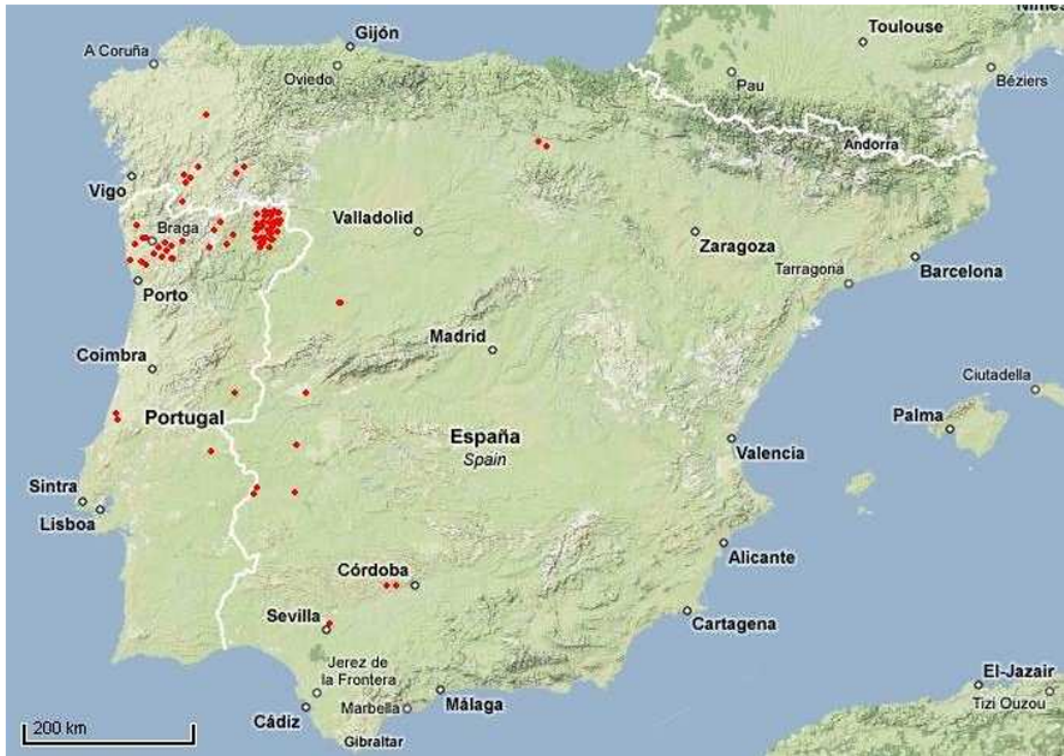
Figure 3.2. Map of the geographical distribution of the sample bridges in Spain and Portugal [21].

3.5 Comparison between empirical rules and existing bridge parameters

3.5.1 Span of the arch

Arched bridges made of natural stone masonry are among the oldest supporting structures still in full function on roads and railways. According to the International Union of Railways (UIC) [17], the number of brick railway bridges in Europe is estimated at around 70000.

Purtak [29] conducted in study in the federal state of Saxony, where several thousand stone masonry arches have been integrated into the transportation network from the 18th to the 20th century. The statistically recorded stone arches had an average span of approximately $10.0m$ with an arch thickness of $60cm$. The percentage ratio of rise to span is approximately 30%.

In addition to very common circular arches, parabolic and segmental arches are the exception. Arches with a constant thickness from the crown to the springing are the norm due to their simple construction using uniform stones. Arches that taper conically towards the springing are more complex to build but are structurally more

Figure 3.3.   Map of the geographical distribution of the sample bridges in Bragança region, Portugal [21].

favorable. The ashlar masonry consists of natural stones across the entire thickness of the arch, usually laid with very thin mortar joints.

3.5.2   Thickness of the arch

Figures 3.4 for deep arches and 3.5 for shallow arches illustrate a comparison between various empirical rules and the actual measurements of existing bridge arches. The analysis yields the following observations:

- there is a significant variation in the rules proposed by different authors.

- the empirical "rules of thumb" suggest a wider dispersion of arch dimensions than what is observed in the actual bridges. This discrepancy is likely because these

empirical rules encompass knowledge from a broad historical period, whereas the Italian bridges were constructed within the last 150 years.

- the methodology recommended by the Italian Railways appears to most accurately reflect the geometries of the existing arches.
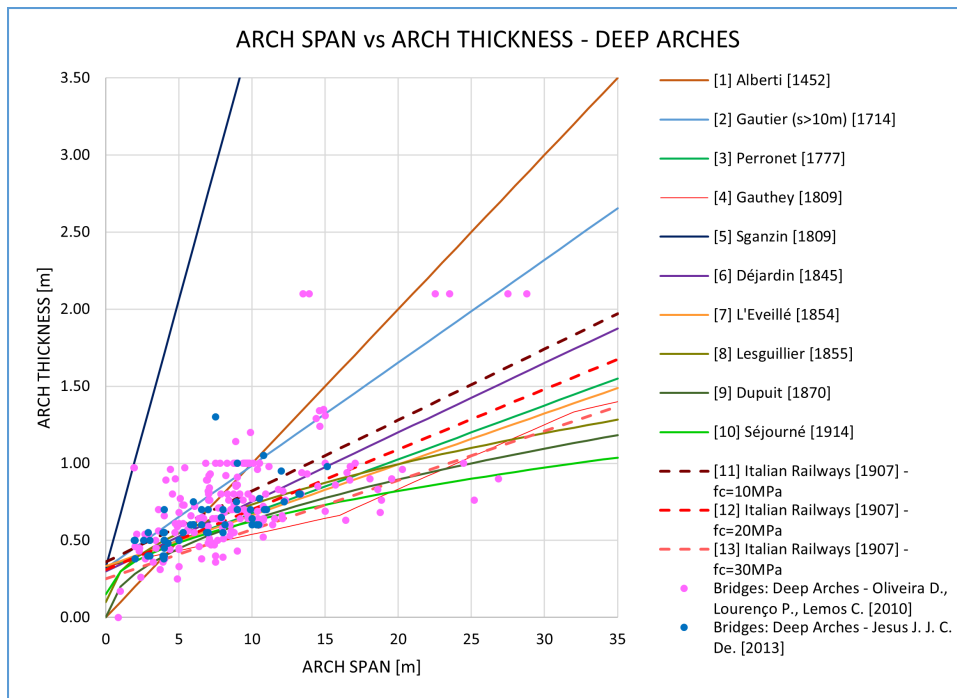
Figure 3.4.   Graph of the arch span versus arch thickness for deep arches.

Figure 3.6 displays the span versus the arch thickness/span ratio for the real bridges considered. Each point on the graph represents actual data from these bridges. Additionally, two trend lines are plotted to represent the general tendency of the data points. The arch thickness/span ratio values range from $t/s = 0.05$ to $t/s = 0.25$.
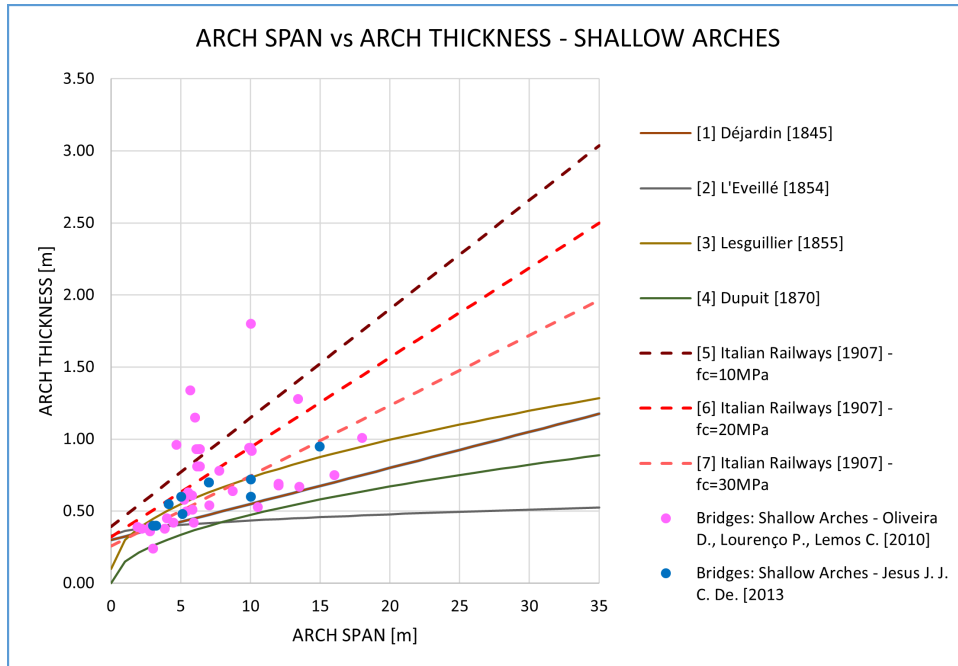
Figure 3.5.   Graph of the arch span versus arch thickness for shallow arches.
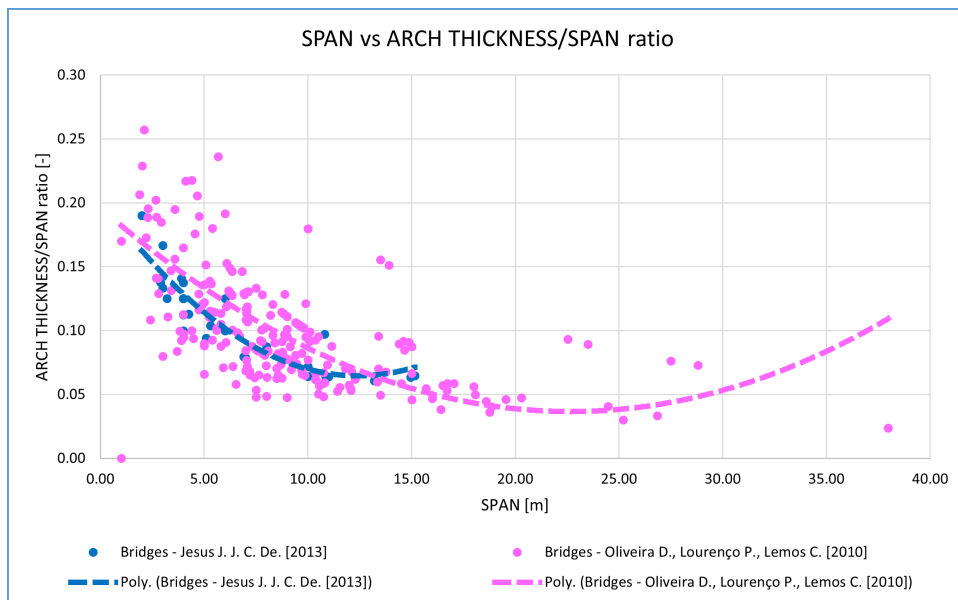
Figure 3.6.   Graph of the arch span versus the arch thickness/arch span ratio.

3.5.3 Shape of the arch

Figure 3.7 depicts the span versus the rise for the collection of real-world bridges. The data points predominantly cluster within a rise/span ratio range of $r/s = 0.25$ to $r/s = 0.50$, indicating a common proportional relationship between span and rise in the existing bridges.
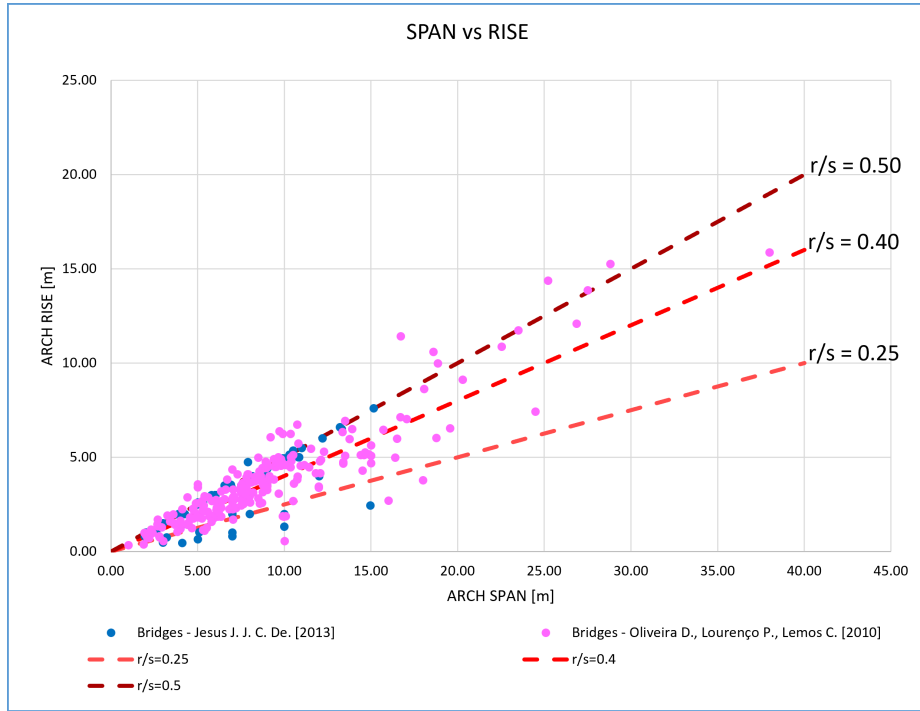
Figure 3.7. Graph of the arch span versus the arch rise.

Figure 3.8 illustrates the span versus the rise/span ratio for the selection of real-world bridges. Each point represents actual data from these bridges. A trend line is observed, highlighting a general pattern where the rise/span ratio tends to fall between $r/s = 0.10$ and $r/s = 0.70$, indicating a common proportional relationship in the dataset of existing bridges.

Figure 3.9 shows the rise/span ratio versus the arch thickness/span ratio for considered real bridges. Each point corresponds to actual bridge data. A trend line indicates that the arch thickness/span ratio generally ranges from $t/s = 0.05$ to $t/s = 0.25$, demonstrating a consistent relationship between these two ratios in the examined bridge data.

Figure 3.10 depicts the rise/span ratio versus the arch thickness/rise ratio for real-world bridges. There is an observable trend where the arch thickness/rise ratio decreases as the rise/span ratio increases. The data points span a range from $t/r = 0.10$

66
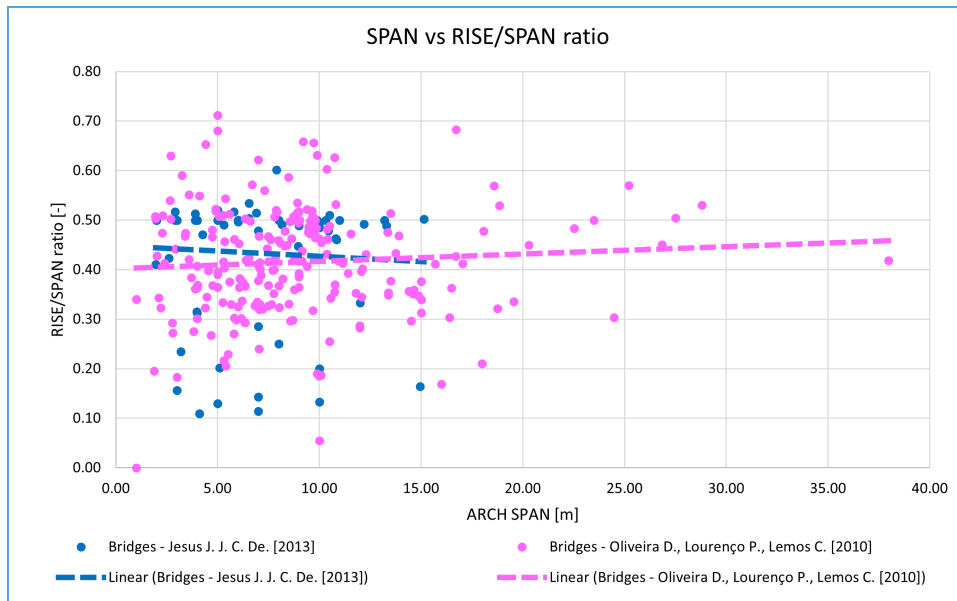
Figure 3.8.   Graph of the arch span versus the arch rise/arch span ratio.
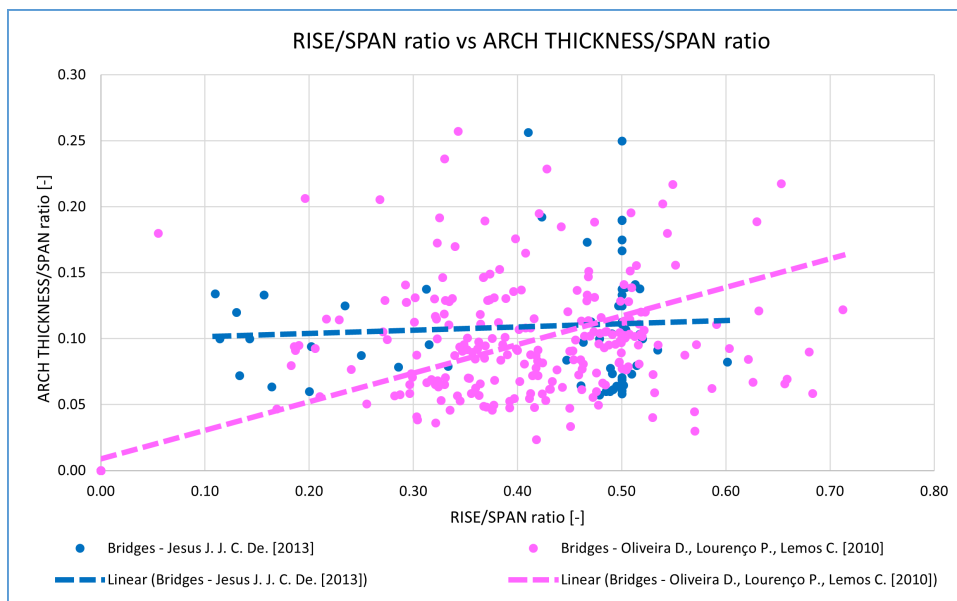
Figure 3.9.   Graph of the arch rise/arch span ratio versus the arch thickness/arch span ratio.

to $t/r = 1.00$, illustrating a consistent inverse relationship between these two ratios in the examined bridges.
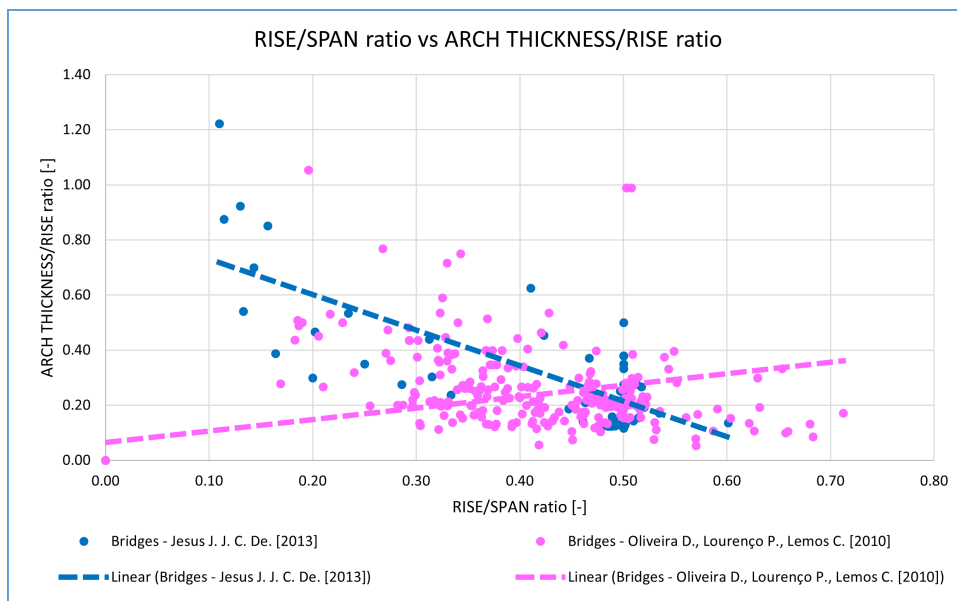
Figure 3.10.   Graph of the arch rise/arch span ratio versus the arch thickness/arch rise ratio.

3.5.4   Thickness of the piers

Figure 3.11 displays the span versus the pier thickness for the collection of real-world bridges. Notably, the majority of the data points lie above the recommended values suggested by authors in previous literature. This indicates that the piers of existing bridges tend to be thicker than what is commonly advised in the literature.
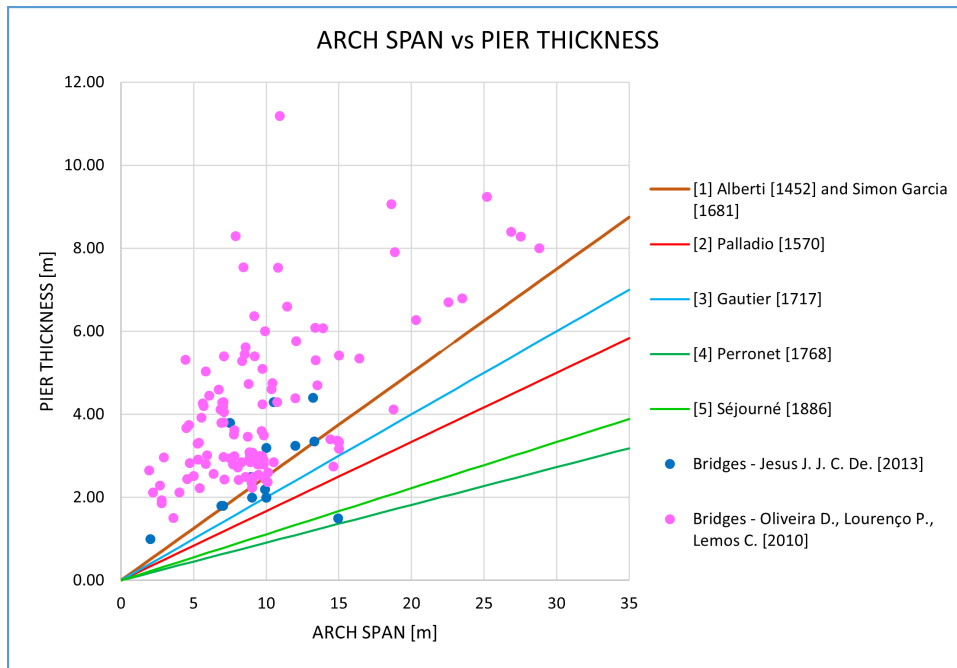
Figure 3.11.   Graph of the arch span versus the pier thickness.

Figure 3.12 depicts the span versus the pier thickness/arch span ratio. As the span increases, the pier thickness/arch span ratio decreases, a trend that is clearly illustrated by the trend lines. The values for the pier thickness/arch span ratio range from $T/s = 0.20$ to $T/s = 1.20$, highlighting a consistent inverse relationship between these two variables.
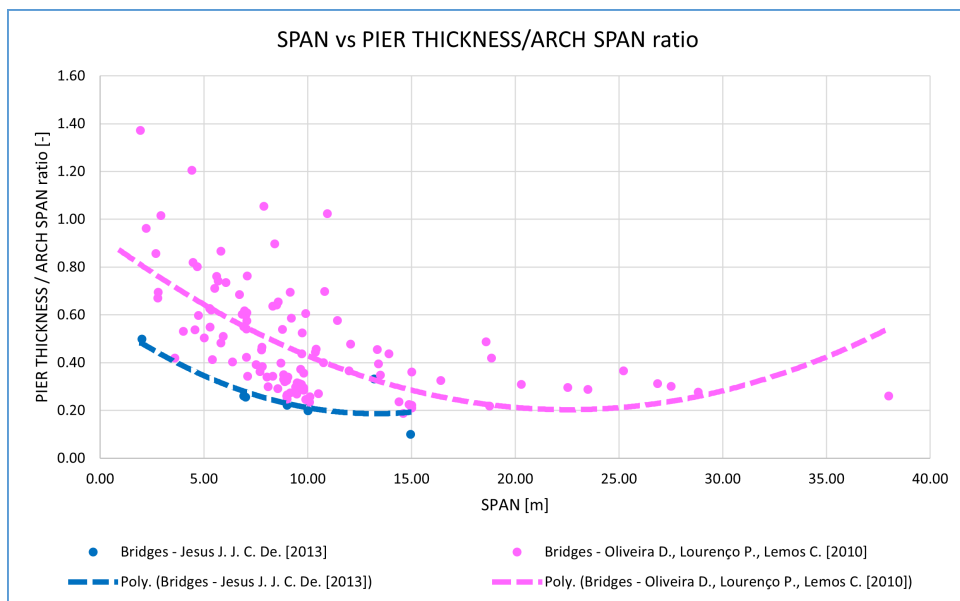
Figure 3.12.   Graph of the arch span versus the pier thickness/arch span ratio.

3.5.5 Width of the bridge

Figure 3.13 illustrates the maximum arch span versus the bridge width for the considered real-world bridges. The values of bridge width over span range from $W/s = 0.2$ to $W/s = 1.6$, showing a varied relationship between the maximum arch span and bridge width across the dataset.
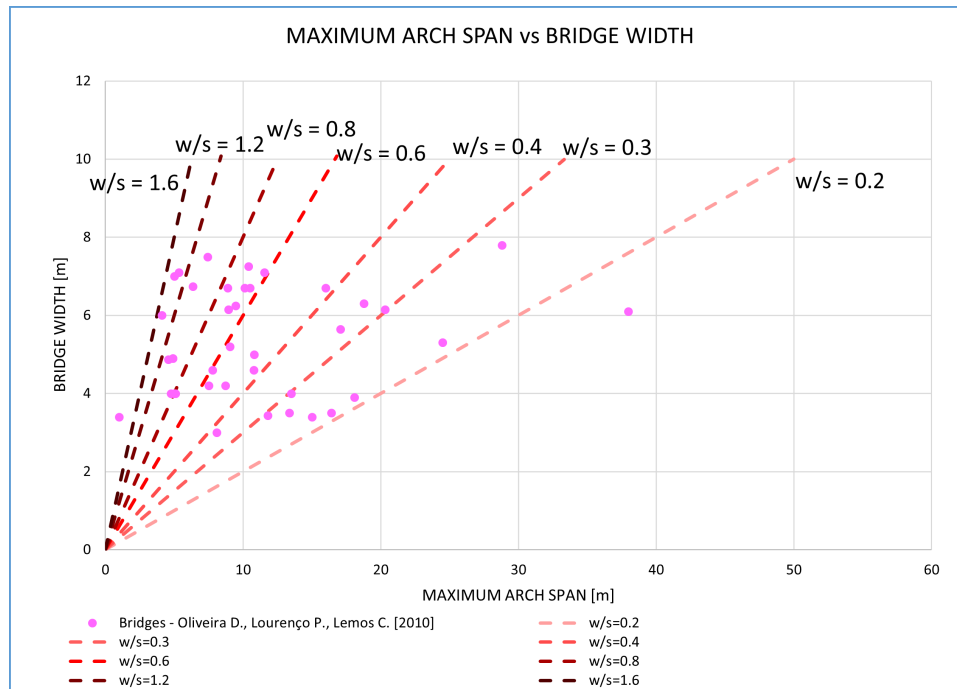
Figure 3.13.   Graph of the arch span versus the bridge width.

3.5.6 Height of the backing

Regarding the **height of the backing**, there is no universally agreed criterion. However, to provide a practical guideline, it is commonly suggested that the key of the vault be covered by a layer of embankment of at least $0.50m$. This recommendation is based on the belief that such coverage enhances the distribution of mobile loads [30]. In the absence of a fixed standard, it is proposed that an alternative approach be adopted: considering an height equal to $1/4$ of the arch rise, with a minimum of $0.50m$, to serve as a suitable starting point for determining the height of the backing.

3.5.7 Thickness of the spandrel walls

Traditionally, the **thickness of spandrel walls** is determined based on specific criteria. However, due to the absence of a fixed criterion, we consider an alternative method. Generally the thickness is calculated as $1/3$ of the height of the embankment,

augmented by $0.50m$ for road bridges and $1.00m$ for railway bridges. This entails maintaining a consistent thickness throughout the tympanum, starting from the maximum thickness at the starts and extending to the minimum thickness at the key, which should ideally not be less than $0.50m$ [30].

In the case of the designed model, a simplified rectangular shape will be adopted, with a constant thickness of 1/5 of the bridge width, ensuring both structural stability and construction efficiency.

3.5.8   Final considerations

In this concluding paragraph, the aim is to summarize the results obtained from the geometric study of the existing bridges of Claudia Lemos's thesis [21] and João Jorge Carrazedo de Jesus's thesis [18]. For each parameter examined, also also for ratios, the extreme values of the possible range and the most common value identified in the analysis are provided in Tables 3.7 and 3.8.

Table 3.7.   Common values of the considered parameters.

Parameter	[m]	Min	Max	Common
Arch Span	s	2.00	20.00	7.00
Arch Thickness	t	0.25	1.30	0.60
Arch Rise	r	0.45	7.60	2.80
Pier Thickness	T	1.00	5.00	2.00
Pier Height	H	1.50	15.00	5.00
Pier Width	W	3.00	7.80	5.35

Table 3.8.   Common values of the considered ratios.

Ratio	[-]	Min	Max	Common
Arch Rise / Arch Span	r/s	0.10	0.70	0.40
Arch Thickness / Arch Span	t/s	0.05	0.25	0.10
Arch Thickness / Arch Rise	t/r	0.10	1.00	0.30
Pier Thickness / Arch Span	T/s	0.20	1.00	0.40
Pier Thickness / Pier Heigth	T/H	0.10	2.00	1.00
Pier Width / Arch Span	W/s	0.15	0.70	0.20

Chapter 4

Design of the Model

4.1 Software: STKO

©**STKO (Scientific ToolKit for OpenSees)** (Figure 4.1) is an advanced software platform of **Asdea Software** (Figure 4.2) [1] that significantly enhances the functionality of **OpenSees** through its graphical user interface (GUI).

Figure 4.1. STKO Software logo.

Figure 4.2. Asdea Software logo.

Its potential in the realm of civil engineering and specifically in the modeling of

masonry arch bridges can be understood through several of its key features [1]:

- **All-encompassing Integration:** STKO is not a mere GUI layer but an integrated environment that fully harnesses the capabilities of OpenSees, including support for all its materials, elements, conditions, and interactions. This comprehensive approach ensures that every facet of OpenSees can be leveraged to its fullest, which is vital for modeling the complex behaviors of masonry arch bridges.

- **Efficient Data Handling:** The introduction of the MPCO recorder allows for efficient management of large data sets within the HDF5 database structure. This capability is critical when dealing with the extensive amount of data generated in the simulation of masonry arch bridges, where each element's performance under various loads and conditions needs to be meticulously recorded and analyzed.

- **Sophisticated Modeling:** STKO enables the creation of sophisticated and complex models, which is essential for representing the intricate geometries and composite materials found in masonry arch bridges. The level of detail attainable in these models allows for a more accurate simulation of real-world behavior under static and dynamic loads.

- **Python Scripting Interface:** The Python API allows for extensive customization and automation of tasks, which can include the development of bespoke modeling tools, parametric analyses, and the incorporation of AI algorithms. This flexibility is crucial when tailoring models to specific bridge geometries and conditions or when incorporating innovative design methodologies.

- **Interoperability and Collaboration:** STKO's compatibility with various major 3D modeling programs and its collaborative features, like the open-source external solver library available on GitHub, enable seamless integration into broader engineering workflows. This interoperability is particularly beneficial for masonry arch bridge modeling, where the integration of different software tools may be required to address the multidisciplinary aspects of bridge engineering.

- **State-of-the-Art Development:** Continuous updates and developments in STKO, in tandem with advancements in OpenSees, ensure that users have access to the latest materials, theories, and modeling techniques. This aspect is particularly pertinent for masonry arch bridges, which may require the latest analytical methods to assess their structural integrity and historical value accurately.

Incorporating these features, STKO positions itself as an essential tool for civil engineers focused on the assessment, design, and retrofitting of masonry arch bridges. By facilitating the detailed analysis of these structures, STKO aids in preserving their historical significance while ensuring their safety and functionality within modern infrastructure.

4.2 Model Characteristics

4.2.1 Geometric Parameters

The **geometric model** of the bridge, consisting of vertices and lines, has been developed parametrically using Python within STKO (Annex A). Initially, a 2D model of nodes and lines is generated with Python (Figure 4.3), which is then extruded in STKO to obtain a 3D model (Figure 4.4).

This approach allows for a dynamic and flexible creation process: by inputting initial key dimensions, this method enables the generation of a virtually infinite variety of masonry arch bridge designs. Each parameter acts as a seed value that, when altered, can systematically transform the entire geometry of the bridge, thereby facilitating the exploration of a wide range of bridge configurations .

The input **variable parameters** are here reported:

- Number and Length of the Spans;

- Height, Thickness and Width of the Piers;

- Thickness and Rise of the Arches;

- Number of bricks in the Vault;

- Height of the backing over the crown;

- Thickness of infill and spandrel walls.

This parametric modeling is particularly advantageous for performing sensitivity analyses, optimizing structural performance, and understanding the influence of various design parameters on the behavior of masonry arch bridges under different load conditions.

4.2.2 Physical Properties

The **physical properties** of the masonry arch bridge model within STKO (Figure 4.5) are defined as isotropic elastic materials, because only a linear analysis has to be performed. These properties are crucial in influencing the structural behavior and durability of the bridge (Table 4.1).

For the pillars and the upper portion of the bridge, which are typically subject to different stresses and environmental conditions, distinct brick materials are used. The pillars, bearing the majority of the structural load, are composed of a denser, more robust type of brick. This brick is characterized by high compressive strength and lower porosity to resist compressive forces and minimize water ingress, which can lead to weathering and degradation. The upper portion of the bridge, while still constructed of brick, may use a less dense variant, which could have a higher degree of porosity.
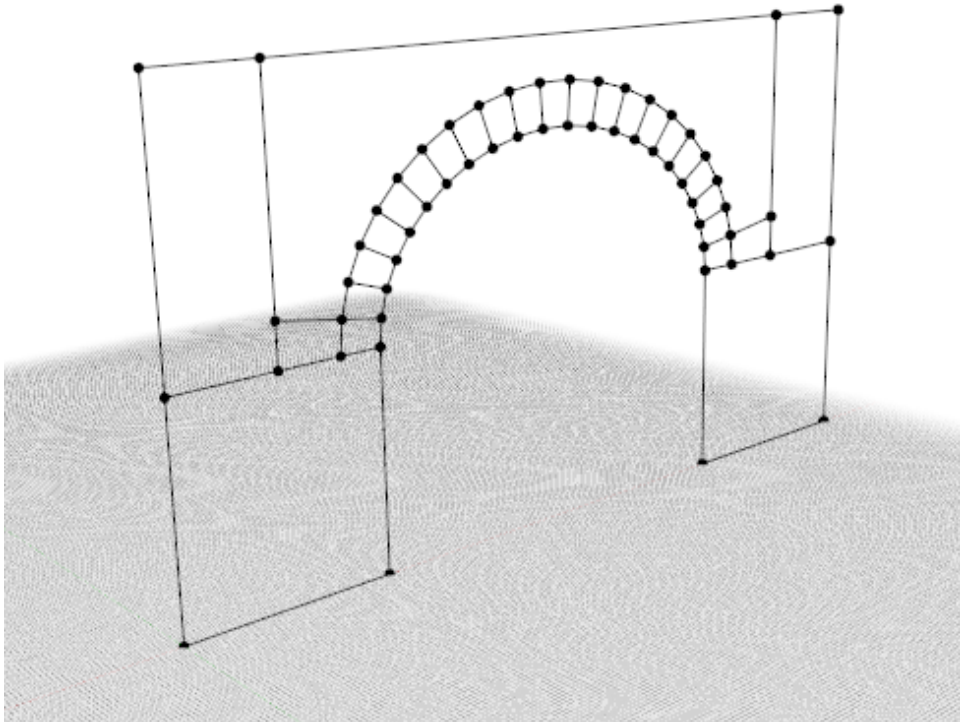
Figure 4.3.   Example of a STKO Model: 2D geometry generated by the Python script.

This choice is often made to reduce the overall weight of the structure and to account for the different load-bearing requirements compared to the pillars.

The fill material, situated between the arches and often used to support the roadway, is a composite material that can include a mixture of rubble, mortar, and smaller brick pieces. This fill serves to distribute weight and absorb tension within the structure, and its composition is selected for its ability to compact under load while providing a degree of flexibility.

In the STKO model, each material's Young's modulus, Poisson's ratio, density, and compressive and tensile strengths are input parameters that can be adjusted to simulate the behavior of these materials under load. For a truly representative model, these material properties can be sourced from empirical data or laboratory tests on samples of the actual bridge materials. The differentiation of materials in the model is essential for analyzing the bridge's response to dynamic loads, thermal expansion, and long-term deterioration processes.
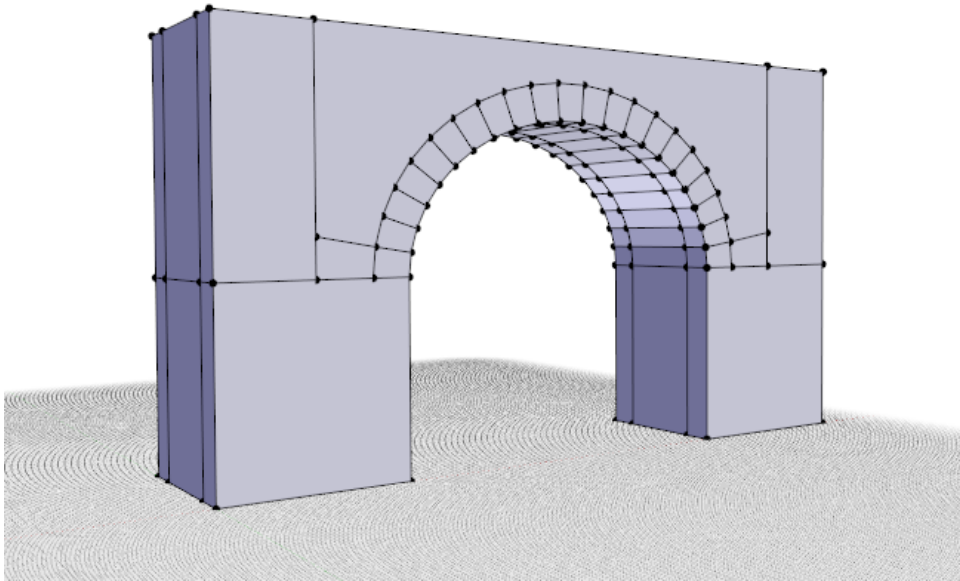
Figure 4.4.   Example of a STKO Model: 3D geometry generated by extrusion in the orthogonal direction.

4.2.3   Boundary Conditions

Boundary conditions in the STKO model (Figure 4.6) play a pivotal role in defining how the masonry arch bridge interacts with its environment and supports the loads it carries. For a comprehensive simulation, the following conditions are meticulously specified:

- **Fixed Base:** The base of the bridge's pillars is typically fixed, representing the connection to the foundation. This condition assumes that there is no movement at the base, simulating a rigid connection to the earth. In practice, this translates to zero degrees of freedom in terms of translation or rotation at the base nodes within the model.

- **Self-Weight of the Fill, Pier, and Masonry:** Each component of the bridge—be it the fill material, the masonry of the arches, or the piers—is subject to gravity. The self-weight is intrinsically considered in the model to account for the primary constant load acting on the structure. This condition is essential for stress analysis and for evaluating the overall stability of the bridge.

- **Adjacent Constraint to Soil:** Bridges are not isolated structures; the adjacent soil can exert significant lateral pressure and support. In the model, this is represented through constraints that mimic the soil-structure interaction, affecting both the global stability and the local stress distribution of the bridge.
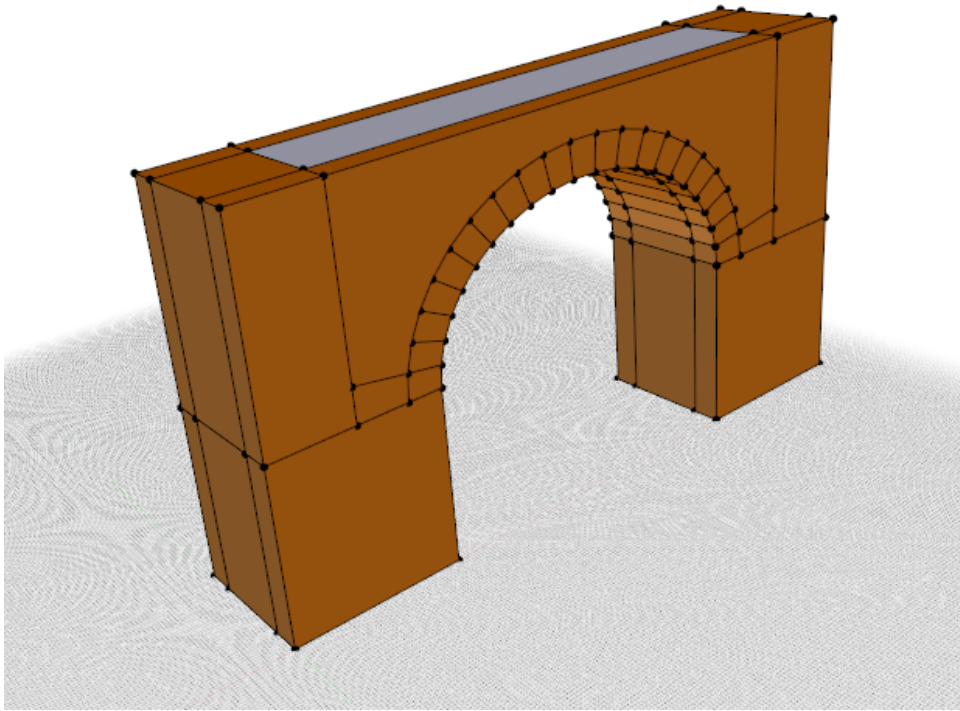
Figure 4.5.   Example of a STKO Model: physical properties assessment.

- **Mass of Masonry, Pier, and Fill:** The mass properties of the bridge components are critical for dynamic analysis, such as seismic simulation. The mass affects the bridge's inertia, influencing how it will respond to dynamic loads like earthquakes or passing vehicles.

- **Applied Loads:** In addition to the self-weight, bridges are designed to carry additional loads. These can include the weight of vehicles, pedestrians, or even snow. In STKO, these loads are applied to the model to simulate various loading conditions the bridge might encounter throughout its service life. This could be in the form of concentrated loads, distributed loads, or dynamic loads, depending on the type of traffic and environmental conditions anticipated.

By defining these boundary conditions and loads, the STKO model can provide a realistic simulation of how the bridge would behave under actual service conditions. It allows for the analysis of the structural response, identification of potential failure modes, and aids in the design of reinforcement or retrofitting strategies to ensure the bridge's longevity and safety.

Table 4.1. **Table C8.5.I from Circolare 21 gennaio 2019, n. 7 C.S.LL.PP.** [24] - Reference values of the mechanical parameters of masonry, to be used in the specified resistance criteria (short-term behavior), and average specific weight for different types of masonry. The values refer to: f = average compressive strength, τ_0 = average shear strength in the absence of normal stresses (with reference to the formula given, concerning capacity models, in §C8.7.1.3), f_v0 = average shear strength in the absence of normal stresses (with reference to the formula given, concerning capacity models, in §C8.7.1.3), E = average value of the normal modulus of elasticity, G = average value of the tangential modulus of elasticity, w = average specific weight.

Masonry typology	f $[N/mm^2]$	E $[N/mm^2]$	G $[N/mm^2]$	w $[kN/m^3]$
Random rubble masonry (pebbles, erratic stones, and irregular stones)	1.0 - 2.0	690 - 1050	230 - 350	19
Rough ashlar masonry, with uneven thickness of faces	2.0	1020 - 1440	340 - 480	20
Masonry in split stones with a good texture	2.6 - 3.8	1500 - 1980	500 - 660	21
Irregular masonry of soft stone (tuff, limestone, etc.)	1.4 - 2.2	900 - 1260	300 - 420	13 - 16
Masonry with regular ashlar of soft stone (tuff, limestone, etc.)	2.0 - 3.2	1200 - 1620	400 - 500	13 - 16
Squared stone block masonry	5.8 - 8.2	2400 - 3300	800 - 1100	22
Solid brick masonry with lime mortar	2.6 - 4.3	1200 - 1800	400 - 600	18
Semi-solid brick masonry with cement mortar (e.g., double UNI perforation 40%)	5.0 - 8.0	3500 - 5600	875 - 1400	15

4.2.4 Mesh generation

After generating the 3D geometry and assigning properties and boundary conditions, **creating the mesh is crucial** (Figure 4.7). In this study, we used a mesh with the following characteristics:

- **Uniform by Size**: ensures that the entire geometry is divided into elements
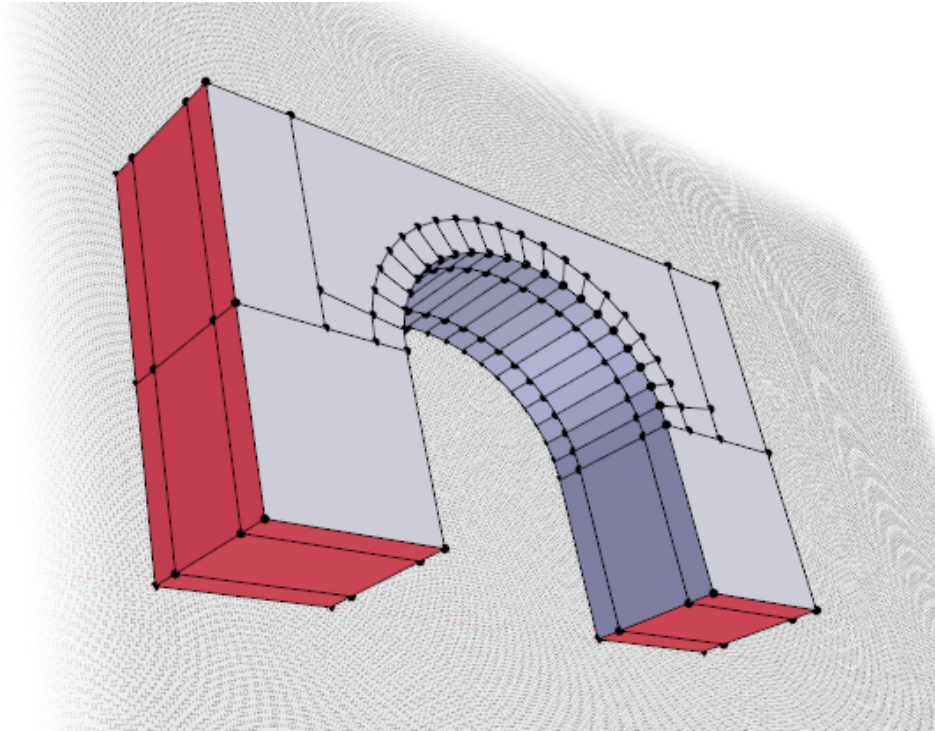
Figure 4.6.   Example of a STKO Model: boundary conditions.

of consistent size, balancing accuracy and computational efficiency. The characteristic element size is chosen to accurately capture the geometry and stress distribution.

- **Solids of Tetrahedral Elements**: ideal for complex 3D structures. They fit irregular shapes well and can be generated automatically, making them suitable for the intricate geometry of masonry bridges.

- **Linear Elements**: used for their computational efficiency. Although less accurate than higher-order elements, a sufficiently refined linear mesh provides reliable results for dynamic analysis.

4.3   Analysis Steps

The **Analysis Steps** in the STKO model of a masonry arch bridge follow a systematic approach to simulate the bridge's behavior under various conditions:

- **Creation of Time Series:** This initial step involves defining the time series for the dynamic analysis. Time series data can represent different types of loads that may vary over time, such as seismic events, vehicle loads, or thermal loads due to
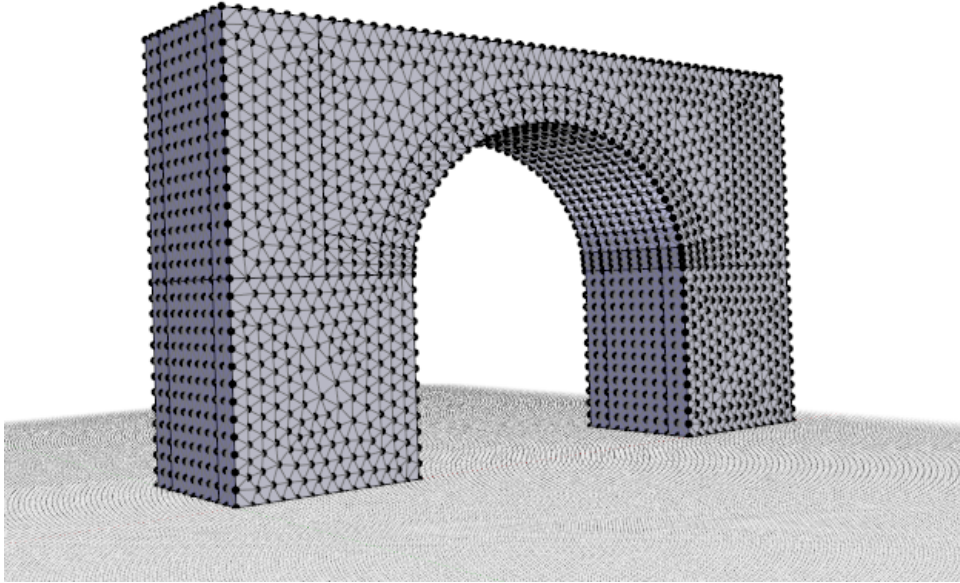
Figure 4.7.   Example of a STKO Model: mesh.

seasonal temperature changes. In STKO, time series are essential for capturing the variation of loads and boundary conditions in a time-dependent analysis.

- **Recording of Values:** To monitor the bridge's response to the applied loads, a record of key values is maintained. These values may include displacements, stresses, strains, and reactions at supports, which are crucial for evaluating the performance of the bridge. The recording is set up so that data output is organized and readily available for post-processing and detailed analysis.

- **Application of Boundary Conditions and Loads:** Before commencing the actual analysis, the defined boundary conditions and loads are applied to the model. This step is critical as it establishes the foundational constraints and forces acting on the structure. The boundary conditions fix or restrict movements at certain points, while the loads simulate the external forces that the bridge is expected to carry.

- **Final Analysis:** With all parameters set, the final analysis can begin. This comprehensive analysis might encompass several types, including static, modal, transient, or nonlinear time-history analysis. The type of analysis is chosen based on the goals of the study, whether it's understanding the basic load-carrying capacity of the bridge or its complex response to dynamic and seismic activity.

During the final analysis, the previously created time series and recorded values serve as a basis for the software to compute the bridge's response over time, yielding

insights into how it might behave under real-world conditions. The outcomes of this analysis provide invaluable data, which are then used to evaluate the bridge's structural integrity, guide the maintenance and rehabilitation processes, and inform future bridge design efforts.

4.4   Analysis Results and Visualization

In the dynamic analysis of masonry arch bridges, the results can be effectively visualized through various deformation plots. These plots provide critical insights into the structural behavior under different loading conditions. The primary plots of interest in this analysis include displacement, reaction force, and mode shapes, which are essential for understanding the dynamic response of the bridge.

Displacement Plot

The displacement plot (Figure 4.8) illustrates how the structure deforms under applied loads. This plot is crucial for identifying the maximum deflections and understanding how the bridge responds to dynamic forces. It helps in assessing the structural integrity and the potential for damage or failure.

- **Maximum Displacement**: Indicates areas of greatest movement, which are critical for evaluating serviceability and safety.

- **Deformation Patterns**: Show how the structure deforms globally and locally, providing insights into stress distribution.

Reaction Force Plot

The reaction force plot (Figure 4.9) shows the forces at the supports and constraints. These forces are essential for ensuring that the support conditions are accurately modeled and that the structure can sustain the applied loads.

- **Support Reactions**: Reveal the load distribution to the supports, which is vital for designing the foundations.

- **Force Magnitudes**: Help in verifying that the reactions are within acceptable limits and that the supports are adequately designed.
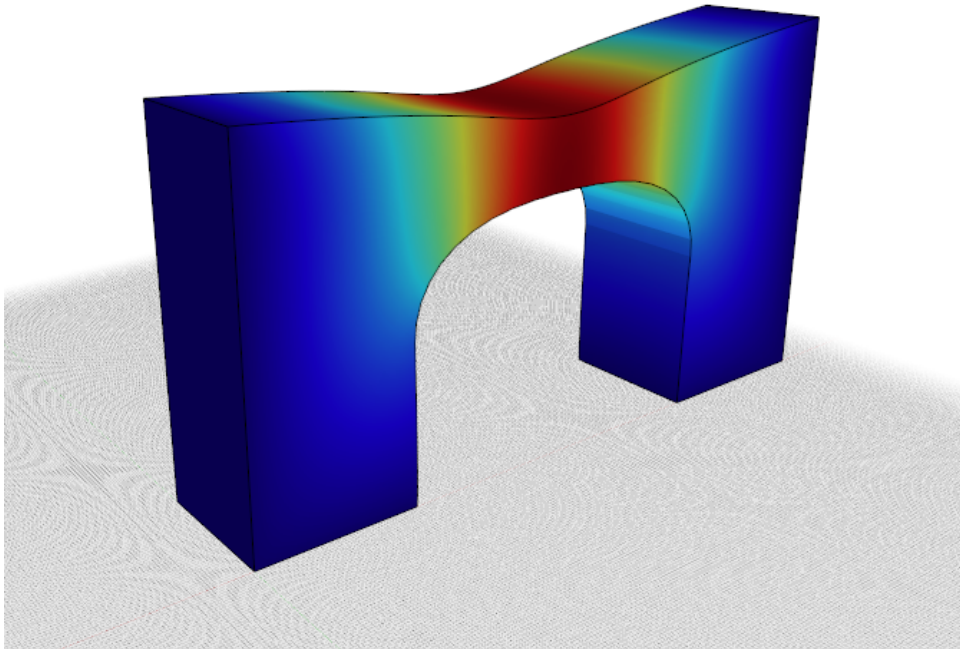
Figure 4.8.   Example of a STKO Model: displacements plot.
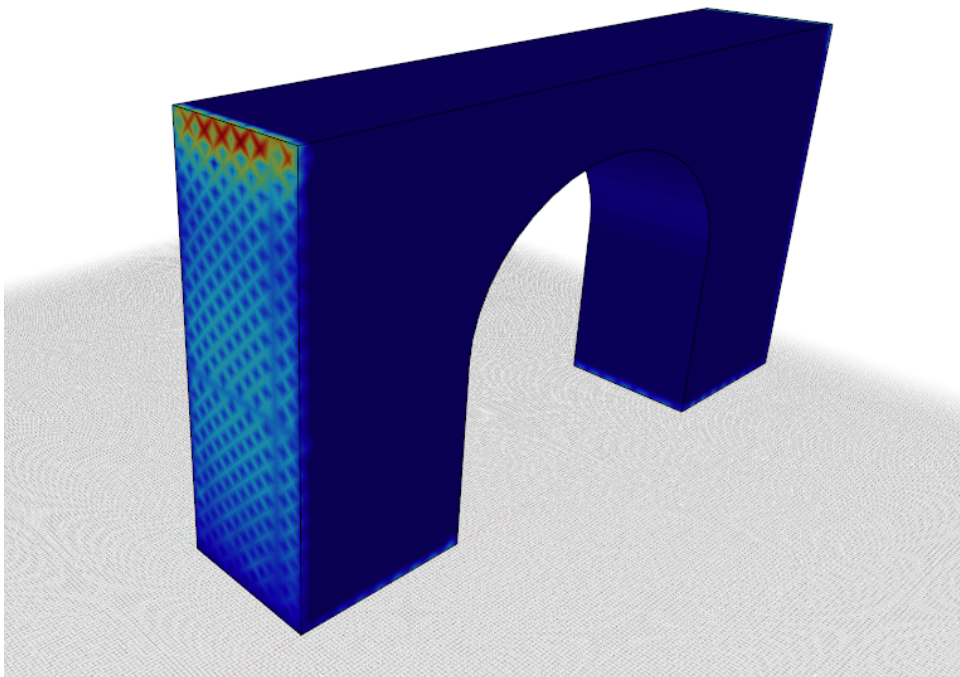
Figure 4.9.   Example of a STKO Model: reaction forces plot.

Mode Shape Plots

Mode shape plots depict the deformation patterns of the structure at different natural frequencies. These are critical for understanding the dynamic behavior of the bridge.

- **Transversal Mode Shape**: Shows the deformation pattern perpendicular to the length of the bridge (Figure 4.10). This mode is important for understanding lateral stability and potential sway under dynamic loads.

- **Vertical Mode Shape**: Depicts the vertical vibration patterns (Figure 4.11), which are crucial for assessing the vertical stiffness and the impact of dynamic vertical loads.

- **First Longitudinal Mode Shape**: Illustrates the primary mode of vibration along the length of the bridge (Figure 4.12). This mode is typically associated with the global bending behavior of the structure.
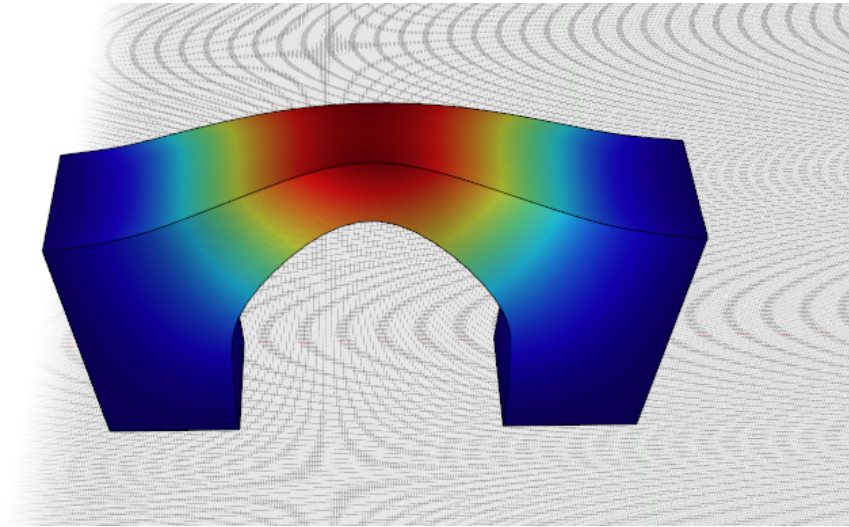
Figure 4.10.   Example of a STKO Model: first transversal mode-shape plot.
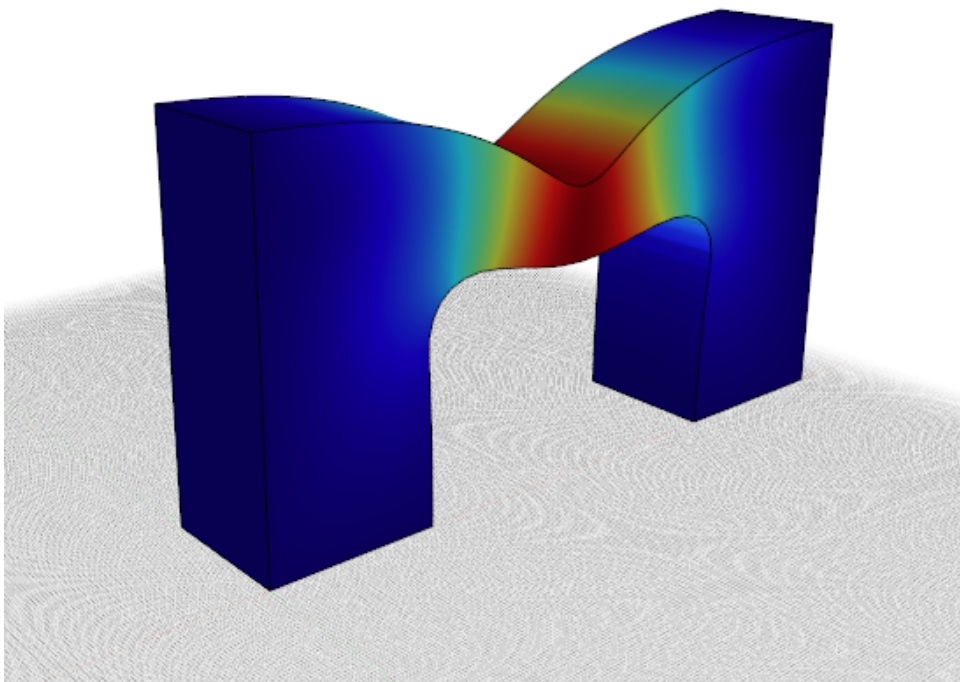
Figure 4.11.   Example of a STKO Model: first vertical mode-shape plot.
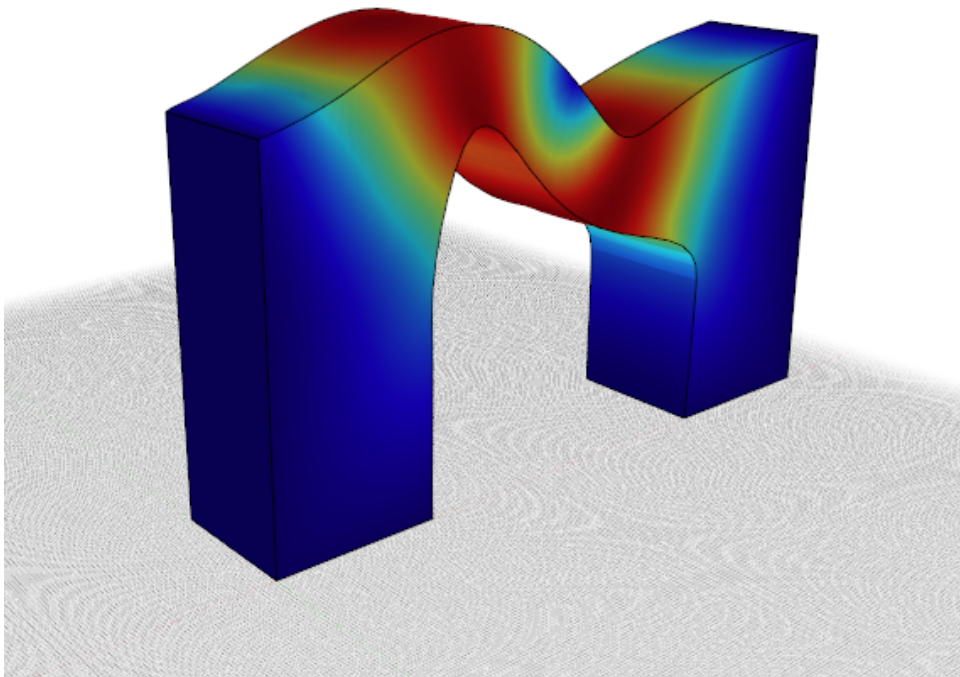
Figure 4.12.   Example of a STKO Model: first longitudinal mode-shape plot.

4.5   Summary of STKO items used in the Analysis

The following Table 4.2 lists the items used in STKO to generate the 3D FEM model and initiate the analysis. These functions are crucial for translating the parametric 2D geometry developed in Python into a comprehensive 3D model. Additionally, it is necessary to assign material and element properties, define boundary conditions, apply loads, and generate the mesh. Functions must also be selected to record and output the mode shapes and dynamic properties of the bridge, enabling detailed structural analysis and evaluation.

Table 4.2: Items used in the STKO model.

Items used in the STKO model	
Geometries	
Constant Time Series	A constant time series for load application, typically used for static loads that do not vary with time.
Physical Properties	
Brick iso	Isotropic elastic material. Used for elements representing brick materials in upper structure.
Fill iso	Isotropic elastic material. Used for fill material within the structure.
Stone iso	Isotropic elastic material. Used for elements representing stone materials in piers.
Element Properties	
Solid	Tetrahedron elements. These are likely used for the 3D meshing of the geometric structure.
Boundary Conditions	
Fixed base	Fixes degrees of freedom at the base, ensuring no movement.
Fixed lateral surfaces	Fixes degrees of freedom at the lateral surfaces, ensuring no movement.
Loads	
Mass Fill	Volume mass assignment for fill material.

Table 4.2 – continued from previous page

Items used in the STKO model	
Self-Weight Fill	Volume Force. Description: Self-weight of the fill material with a density of $19kN/m^3$.
Mass Stone	Volume mass assignment for stone material.
Self-Weight Stone	Volume Force. Description: Self-weight of the stone material with a density of $22kN/m^3$.
Mass Masonry	Volume mass assignment for masonry with specific properties.
Self-Weight Masonry	Volume Force. Description: Self-weight of the masonry material with a density of $18kN/m^3$.
Analysis Steps	
Record	Setup for recording analysis results.
Boundary Conditions	Application of boundary conditions.
Patterns Loads	Application of load patterns.
Gravitational analysis	Static analysis to consider gravitational forces.
Eigen analysis	Likely a modal analysis to determine natural frequencies.
Modal Properties	Extraction of modal properties.
Recorder Modal Properties	Setup for recording modal analysis results.

Chapter 5

Eigenvalue Parametric Analysis of single span bridges

5.1 Parametric Analysis Workflow: from geometric definition to dynamic characterization

To perform a parametric analysis of masonry arch bridges, a systematic approach is essential to comprehensively investigate the dynamic behavior and structural responses across various design scenarios. Here's a structured outline of the process:

1. **Define Bridge Dimensions in CSV Format**: Begin by specifying the key geometric parameters of the bridge in a CSV file. This serves as the foundation for generating multiple bridge configurations for analysis.

2. **Import CSV Data into Python Script**: Utilize a Python script to read the CSV data, enabling efficient handling and manipulation of the bridge geometries and associated parameters.

3. **Integration with Structural Analysis Software (e.g., STKO)**: Integrate the Python script into specialized structural analysis software like STKO. This facilitates seamless data transfer and preparation for subsequent modeling and analysis steps.

4. **Create 3D Structural Models**: Extrude the bridge geometries based on the CSV data within STKO to create accurate 3D representations of each bridge configuration. This step ensures that the physical dimensions and proportions are accurately simulated.

5. **Assign Material Properties and Boundary Conditions**: Define the mechanical properties of the materials used in the bridge construction, such as

89

masonry, within STKO and specify appropriate boundary conditions, ensuring realistic structural behavior.

6. **Define Load Cases and Analysis Steps**: Set up the load cases and define the sequence of analysis steps to simulate load applications and structural responses.

7. **Generate Finite Element Mesh**: Generate a finite element mesh over the 3D bridge models to discretize the structure into smaller elements. This mesh refinement ensures accurate representation of the structural behavior and facilitates efficient numerical computations.

8. **Perform Structural Analysis**: Execute the structural analysis within STKO to compute the dynamic responses of the bridge models under the specified loading conditions. This analysis provides insights into critical factors such as stresses, displacements, and frequencies.

9. **Investigate Mode Shapes and Frequencies**: Post-analysis, investigate the mode shapes of interest, particularly the first transverse, vertical, and longitudinal modes. Analyze and interpret the corresponding frequencies associated with these mode shapes to understand the dynamic characteristics of each bridge configuration.

This structured approach ensures a thorough parametric analysis of masonry arch bridges, enabling engineers to optimize designs, assess structural integrity, and make informed decisions based on detailed simulations and analytical results.

5.2 Sensitivity Analysis #1: varying Pier Height

Sensitivity Analysis #1 meticulously evaluate the potential impact of **varying piers heights** on the structural behavior of the bridge. Three distinct scenarios were meticulously examined (Table 5.1):

- Case A: $H = 2.00m$;

- Case B: $H = 5.00m$;

- Case C: $H = 8.00m$.

In each scenario, the pillars were rigorously constrained laterally, employing boundary conditions that strictly prohibited any rotational or displacement effects. It is imperative to note that the bridge, in this analysis, was subjected solely to its self-weight, without any additional external loads.

Remarkably, despite the significant alterations in pillar height across the different cases, the structural response of the bridge remained remarkably consistent. Notably, the **deformability, mode shapes, period and frequency of the bridge exhibited negligible deviations, regardless of the varying pillar heights** (Table 5.2 and Figures 5.1 and 5.2).

This resilience can be attributed to the robust lateral fixation of the pillars, which effectively mitigates any potential influences stemming from height discrepancies. Moreover, the absence of external loads ensures that the structural integrity of the bridge is primarily governed by its intrinsic properties, rather than external factors.

Therefore, based on the outcomes of this meticulous sensitivity analysis, it can be confidently concluded that variations in pillar height do not exert a discernible influence on the structural behavior of the bridge under the specified conditions.

Table 5.1. Values adopted for Sensitivity Analysis #1: varying Pier Height.

Varying Parameter				
Pier Height	Case A	$H = 2.00m$		
	Case B	$H = 5.00m$		
	Case C	$H = 8.00m$		
Fixed Parameters				
Stone material	$E = 2400MPa$	$w = 22kN/m^3$		
Filling material	$E = 800MPa$	$w = 19kN/m^3$		
Arch Span	$s = 10.00m$	Arch Thickness	$t = 1.00m$	
Arch Rise	$r = 4.00m$	Backing Height	$h_b = 1.00m$	
Bridge Width	$W = 5.00m$	Pier Thickness	$T = 5.00m$	
Spandrels Thickness	$t_s = 1.00m$	Infill Thickness	$t_i = 3.00m$	

Table 5.2. Eigenvalue Sensitivity Analysis #1: varying Pier Height.

Eigenvalue Sensitivity Analysis #1		
Mode-Shape	**Frequency [Hz]**	
	A: $H = 2.00m$ **B:** $H = 5.00m$ **C:** $H = 8.00m$	

Mode-Shape	A: $H = 2.00m$	B: $H = 5.00m$	C: $H = 8.00m$
Transversal	0.3808	0.4130	0.3674
Vertical	0.5554	0.5297	0.5334
Longitudinal	0.7769	0.7346	0.7436

91
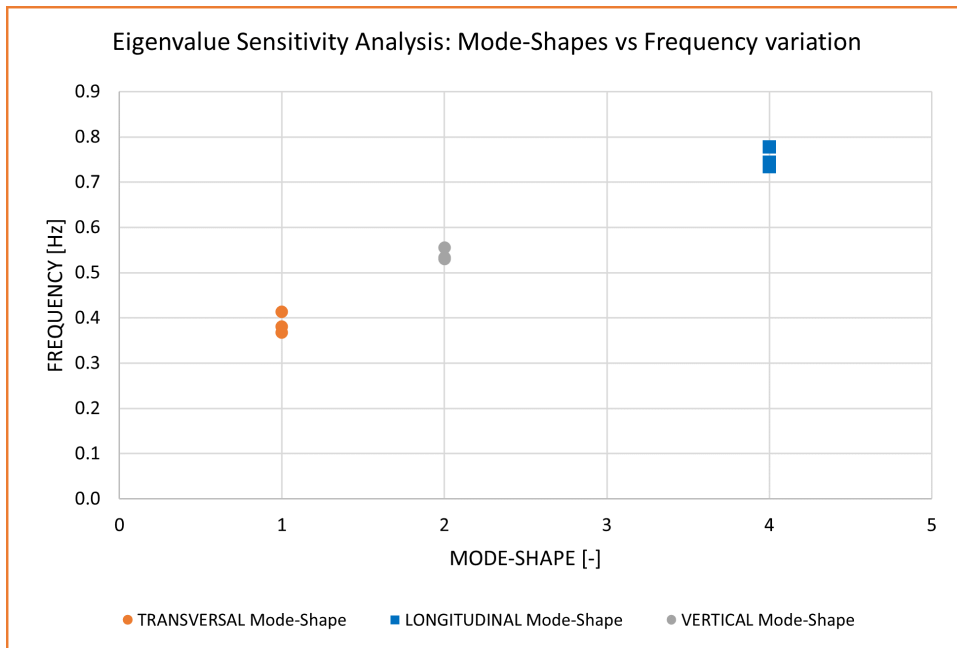
Figure 5.1.   Sensitivity Analysis #1: varying Pier Height - Mode Shape vs Frequency variation.
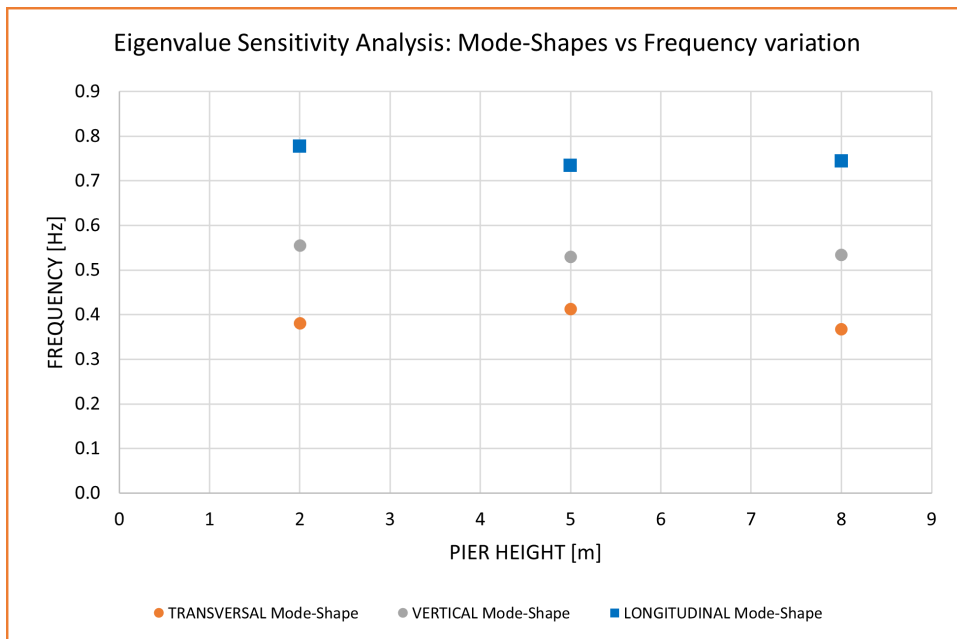
Figure 5.2.   Sensitivity Analysis #1: varying Pier Height - Pier Height vs Frequency variation.

5.3   Sensitivity Analysis #2: varying Pier Thickness

Sensitivity Analysis #2 meticulously assessed the potential effects of **varying the thickness of the bridge piers** on its structural behavior. Three distinct scenarios were meticulously examined (Table 5.3):

- Case A: $T = 4.00m$;

- Case B: $T = 5.00m$;

- Case C: $T = 6.00m$.

In each scenario, the piers were rigorously constrained laterally, employing boundary conditions that strictly prohibited any rotational or displacement effects. Importantly, the bridge was subjected solely to its self-weight, without any additional external loads.

Remarkably, despite the significant alterations in pier thickness across the different cases, the structural response of the bridge remained remarkably consistent. Notably, the **deformability, mode shapes, period, and frequency of the bridge exhibited negligible deviations, regardless of the varying pier thicknesses** (Table 5.4 and Figures 5.3 and 5.4).

This resilience can be attributed to the robust lateral fixation of the piers, which effectively mitigates any potential influences stemming from thickness discrepancies. Moreover, the absence of external loads ensures that the structural integrity of the bridge is primarily governed by its intrinsic properties, rather than external factors.

Therefore, based on the outcomes of this meticulous sensitivity analysis, it can be confidently concluded that variations in pier thickness do not exert a discernible influence on the structural behavior of the bridge under the specified conditions.

Table 5.3.   Values adopted for Sensitivity Analysis #2: varying Pier Thickness.

Varying Parameter			
Pier Thickness	Case A	$T = 4.00m$	
	Case B	$T = 5.00m$	
	Case C	$T = 6.00m$	
Fixed Parameters			
Stone material	$E = 2400MPa$	$w = 22kN/m^3$	
Filling material	$E = 800MPa$	$w = 19kN/m^3$	
Arch Span	$s = 10.00m$	Arch Thickness	$t = 0.50m$
Arch Rise	$r = 4.00m$	Backing Height	$h_b = 1.00m$
Bridge Width	$W = 5.00m$	Pier Height	$H = 5.00m$
Spandrels Thickness	$t_s = 1.00m$	Infill Thickness	$t_i = 3.00m$

Table 5.4.   Eigenvalue Sensitivity Analysis #2: varying Pier Thickness.

Eigenvalue Sensitivity Analysis #2			
Mode-Shape	**Frequency [Hz]**		
	A: $T = 4.00m$	**B:** $T = 5.00m$	**C:** $T = 6.00m$
Transversal	0.4273	0.3812	0.3443
Vertical	0.5471	0.5319	0.5220
Longitudinal	0.7820	0.7280	0.6871
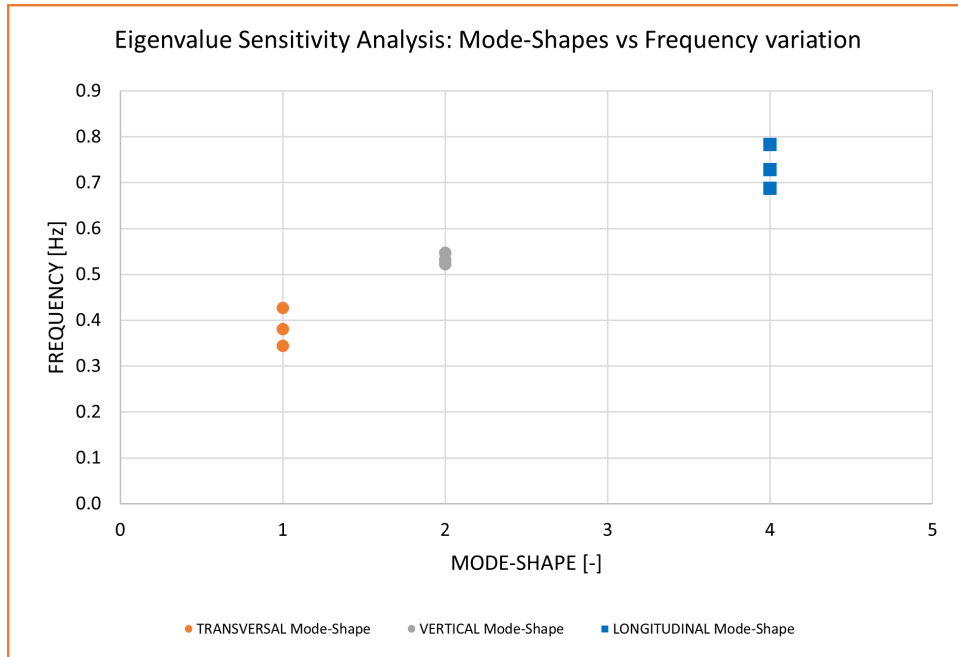
Figure 5.3. Sensitivity Analysis #2: varying Pier Thickness - Mode Shape vs Frequency variation.
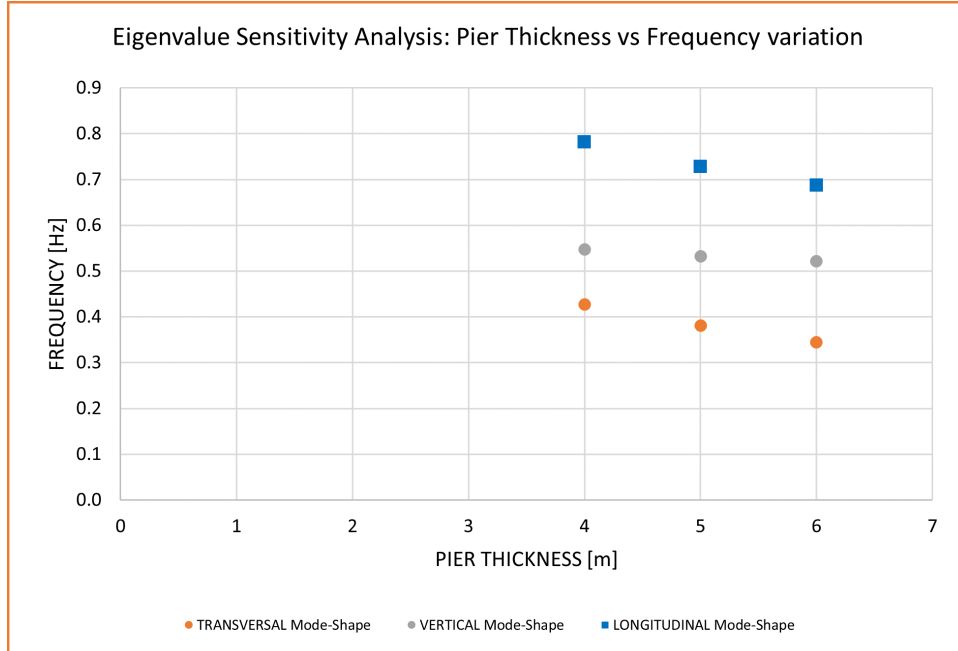
Figure 5.4. Sensitivity Analysis #2: varying Pier Thickness - Pier Thickness vs Frequency variation.

5.4 Sensitivity Analysis #3: varying Material's Young modulus

Sensitivity Analysis #3 examined the impact of **changing the material properties of the masonry, specifically the Young's modulus**. Three distinct scenarios were meticulously examined (Table 5.5):

- Case A: $E = 1600 MPa$;

- Case B: $E = 2000 MPa$;

- Case C: $E = 2400 MPa$.

In each scenario, the masonry properties were rigorously tested to assess their influence on the overall structural behavior. The bridge's response to these variations in Young's modulus was systematically analyzed, ensuring that all other conditions remained constant.

The findings indicated that **variations in the Young's modulus of the masonry had a significant effect on the stiffness and overall deformation characteristics of the bridge**. However, the mode shapes, period, and frequency showed only minor deviations across the different scenarios (Table 5.6 and Figures 5.5 and 5.6).

It is important to note that **the mode shapes do not change order; only the frequencies change, and these changes have to be considered and evaluated in a correct way**. In this sensitivity analysis, the study is limited, so it has to be taken into account in future works.

Based on the results of this comprehensive sensitivity analysis, it can be concluded that changes in the Young's modulus of the masonry significantly affect the stiffness and deformation of the bridge, while the dynamic characteristics remain relatively stable under the specified conditions.

Table 5.5.   Values adopted for Sensitivity Analysis #3: varying Material's Young modulus.

Varying Parameter		
Material's Young modulus	Case A	$E = 1600MPa$
	Case B	$E = 2000MPa$
	Case C	$E = 2400MPa$
Fixed Parameters		
Stone material		$w = 22kN/m^3$
Filling material	$E = 800MPa$	$w = 19kN/m^3$
Arch Span	$s = 10.00m$	Arch Thickness $t = 1.00m$
Arch Rise	$r = 4.00m$	Backing Height $h_b = 2.00m$
Bridge Width	$W = 5.00m$	Pier Height $H = 5.00m$
Pier Thickness	$H = 5.00m$	
Spandrels Thickness $t_s = 1.00m$		Infill Thickness $t_i = 3.00m$

Table 5.6.   Eigenvalue Sensitivity Analysis #3: varying Material's Young modulus.

Eigenvalue Sensitivity Analysis #3			
Mode-Shape	Frequency [Hz]		
	A: $E = 1600MPa$	**B:** $E = 2000MPa$	**C:** $E = 2400MPa$
Transversal	0.2987	0.3238	0.3454
Vertical	0.4417	0.4839	0.5221
Longitudinal	0.6551	0.7153	0.7687
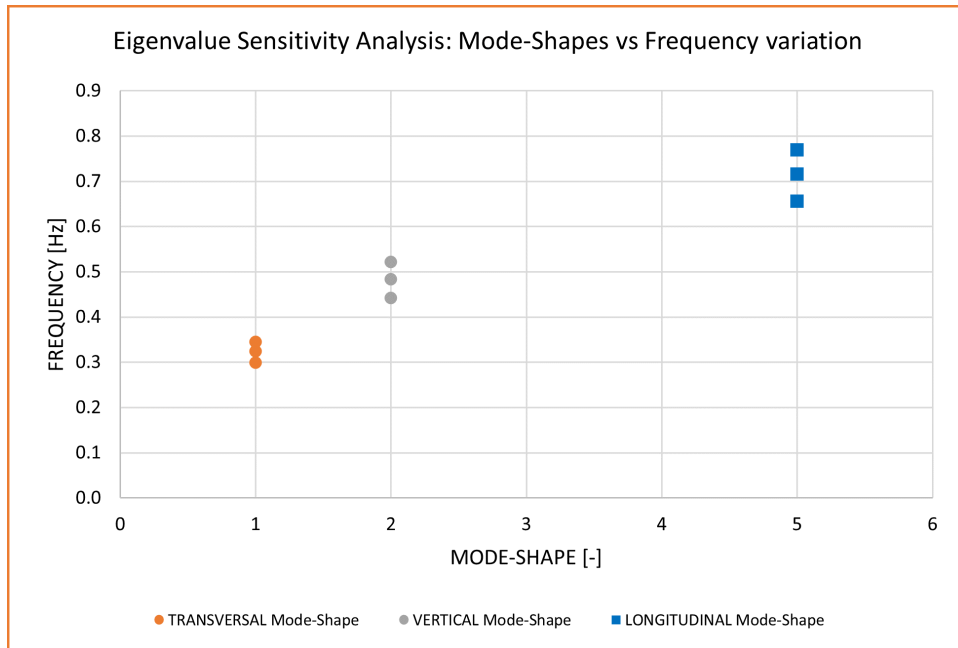
Figure 5.5.   Sensitivity Analysis #3: varying Material's Young modulus - Mode Shape vs Frequency variation.
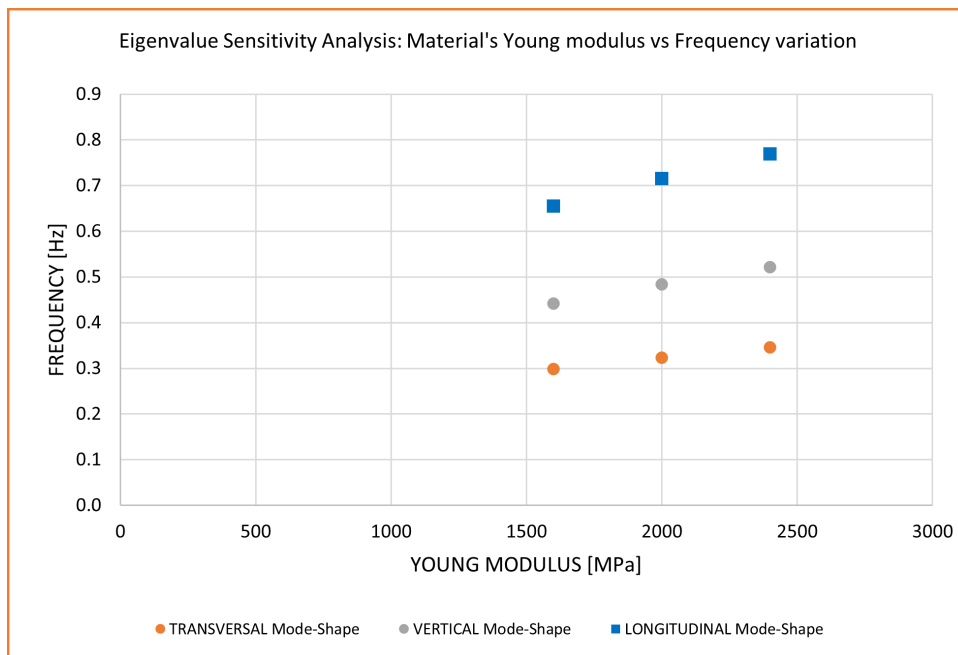
Figure 5.6.   Sensitivity Analysis #3: varying Material's Young modulus - Material's Young modulus vs Frequency variation.

5.5   Sensitivity Analysis #4: varying Material's specific weight

Sensitivity Analysis # examined the impact of **changing the specific weight of the masonry**. Three distinct scenarios were meticulously examined (Table 5.7):

- Case A: $w = 18kN/m^3$;

- Case B: $w = 22kN/m^3$;

- Case C: $w = 26kN/m^3$.

In each scenario, the masonry properties were rigorously tested to assess their influence on the overall structural behavior. The bridge's response to these variations in specific weight was systematically analyzed, ensuring that all other conditions remained constant.

The findings indicated that **variations in the specific weight of the masonry had a significant effect on the stiffness and overall deformation characteristics of the bridge**. However, the mode shapes, period, and frequency showed only minor deviations across the different scenarios (Table 5.8 and Figures 5.7 and 5.8).

It is important to note that **the mode shapes do not change order; only the frequencies change, and these changes have to be considered and evaluated in a correct way**. In this sensitivity analysis, the study is limited, so it has to be taken into account in future works.

Based on the results of this comprehensive sensitivity analysis, it can be concluded that changes in the specific weight of the masonry significantly affect the stiffness and deformation of the bridge, while the dynamic characteristics remain relatively stable under the specified conditions.

Table 5.7. Values adopted for Sensitivity Analysis #4: varying Material's specific weight.

Varying Parameter		
Material's specific weight	Case A	$w = 18kN/m^3$
	Case B	$w = 22kN/m^3$
	Case C	$w = 26kN/m^3$
Fixed Parameters		
Stone material	$E = 2000MPa$	
Filling material	$E = 800MPa$	$w = 19kN/m^3$
Arch Span	$s = 10.00m$	Arch Thickness $t = 1.00m$
Arch Rise	$r = 4.00m$	Backing Height $h_b = 2.00m$
Bridge Width	$W = 5.00m$	Pier Height $H = 5.00m$
Pier Height	$H = 5.00m$	
Spandrels Thickness	$t_s = 1.00m$	Infill Thickness $t_i = 3.00m$

Table 5.8. Eigenvalue Sensitivity Analysis #4: varying Materuial's specific weight.

Eigenvalue Sensitivity Analysis #4		
Mode-Shape	**Frequency [Hz]**	
	A: $w = 18kN/m^3$ **B:** $w = 22kN/m^3$ **C:** $w = 26kN/m^3$	
Transversal	0.3423	0.3238	0.3080
Vertical	0.5128	0.4839	0.4593
Longitudinal	0.7577	0.7153	0.6794
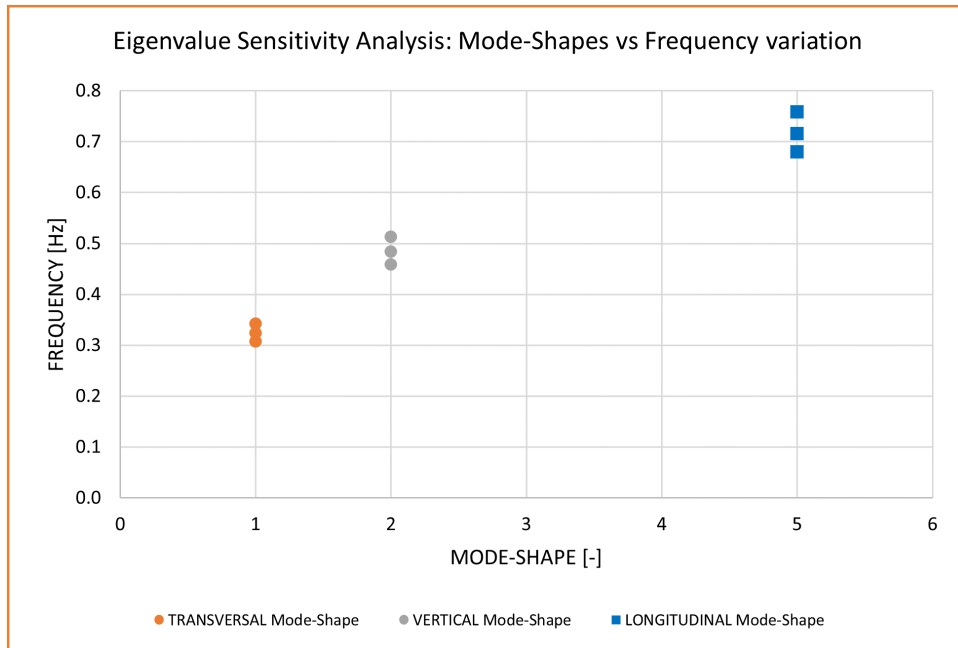
Figure 5.7.   Sensitivity Analysis #4: varying Material's specific weight - Mode Shape vs Frequency variation.
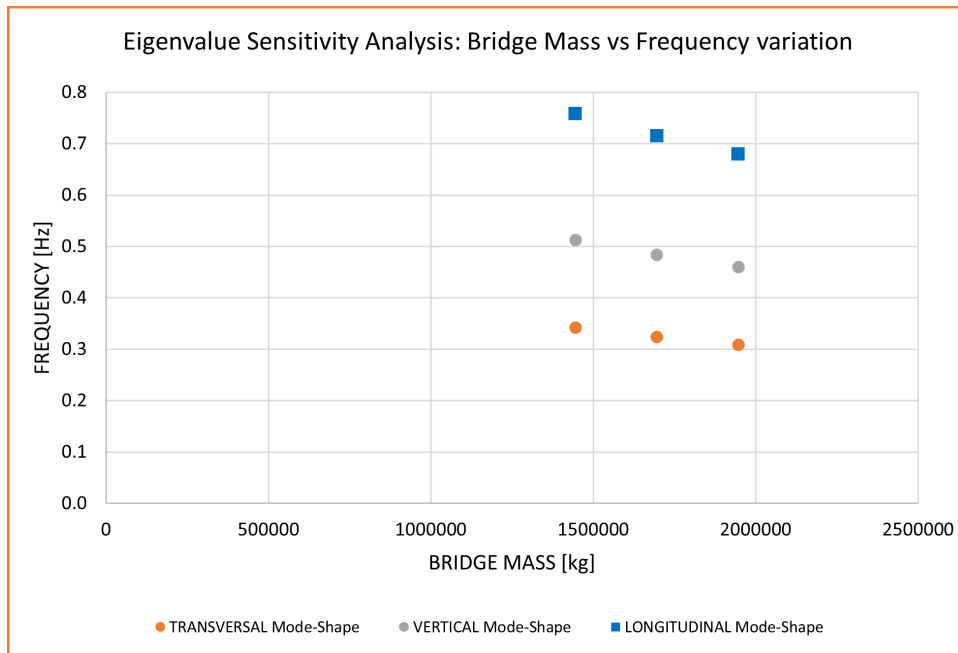
Figure 5.8.   Sensitivity Analysis #4: varying Material's specific weight - Material's specific weight vs Frequency variation.

5.6   Parametric analysis

A parametric analysis of **75 single span masonry arch bridges** has been performed, focusing on identifying the oscillation frequencies of the first three vibration modes in longitudinal, transverse, and vertical directions. The analysis examines how variations in several parameters affect these frequencies; the **variables** are here reported:

- Arch Span s;

- Arch Thickness/Arch Span t/s;

- Arch Rise/Arch Span r/s;

- Bridge Width W;

- Backfill Height over the crown h_b.

Certain parameters were kept constant throughout the analysis for consistency and control. These **constants** included:

- Pier Height $H = 5.00m$;

- Pier Thickness $T =$ Arch Span $/2$;

- Spandrel Wall Thickness $=$ Bridge Width $/5$;

- Infill Thickness $=$ Bridge Width $\times 3/5$.

Fixing these parameters allowed for a more controlled examination of how variations in the primary parameters impact the structural response, ensuring that changes in oscillation frequencies could be attributed primarily to the variables of interest.

The ranges for the chosen variables were determined through a **Monte Carlo simulation**, consisting of a statistical technique used to understand the impact of risk and uncertainty in prediction and forecasting models. It involves generating random values for each parameter within specified ranges (Table 9.3 in Annex C), repeatedly solving the model, and analyzing the resulting output distributions (Table 9.4 in Annex C). The use of this technique allows for a comprehensive exploration of possible scenarios and their effects on the bridge's dynamic behavior. The extreme values used in this analysis were sampled from a **uniform distribution**, as derived from a literature review discussed in Paragraph 3.5.8 of this Master Thesis, ensuring that the chosen ranges were realistic and based on empirical data (Table 5.9).

Graphical representations were created for each parameter, followed by the computation of Pearson's correlation coefficient and Spearman's rank correlation coefficient to quantify the relationships between the parameters and the oscillation frequencies.

Pearson's correlation coefficient r measures the linear relationship between two continuous variables. It ranges from -1 to +1, where +1 indicates a perfect positive

Table 5.9. Ranges of the considered parameters for the parametric analysis.

Parameter		Min	Max
Arch Span	s [m]	5.00	25.00
Arch Thickness / Arch Span	t/s [-]	0.03	0.25
Arch Rise / Arch Span	r/s [-]	0.10	0.50
Bridge Width	W [m]	4.00	8.00
Backfill height above the arch crown	h_b [m]	0.30	2.50

linear relationship, -1 indicates a perfect negative linear relationship, and 0 indicates no linear relationship. This coefficient is sensitive to outliers and assumes that the relationship between the variables is linear. By calculating Pearson's correlation, we aimed to identify direct linear relationships between the structural parameters and the oscillation frequencies.

Spearman's rank correlation coefficient ρ assesses the strength and direction of the monotonic relationship between two ranked variables. It also ranges from -1 to +1, where +1 signifies a perfect positive monotonic relationship, -1 signifies a perfect negative monotonic relationship, and 0 indicates no monotonic relationship. Unlike Pearson's correlation, Spearman's rank correlation does not assume a linear relationship and is less sensitive to outliers, making it suitable for non-linear and ordinal data. This coefficient was used to uncover more complex, non-linear relationships that might exist between the parameters and the dynamic behavior of the bridges.

Through this dual approach, the study aims to provide a comprehensive understanding of how structural parameters influence the dynamic behavior of masonry arch bridges. By combining graphical analysis with robust statistical methods, we were able to identify key trends and correlations, providing valuable insights for the design and assessment of these structures. The findings from this study underscore the importance of accurately characterizing and controlling key parameters to predict and optimize the dynamic performance of masonry arch bridges effectively.

5.6.1 Parametric analysis results and plots

Frequency vs Mode Shape variation

The graphical analysis of frequencies against mode shapes (Figure 5.9) in masonry arch bridges reveals distinct patterns.

- The **first mode shape** consistently corresponds to **transverse vibration**, characterized by lower frequencies. This mode reflects the lateral oscillations primarily influenced by the bridge's geometry and structural configuration.

- Moving to the **second and third mode shape**, which often represents **vertical vibration**, frequencies tend to increase to moderate levels. Vertical modes indicate movements along the vertical axis of the bridge, influenced by load distributions, support conditions, and material properties.

- The **fourth and fifth mode shape**, observed occasionally, typically corresponds to **longitudinal vibration**. These modes exhibit higher frequencies, indicating movements along the length of the bridge. Longitudinal vibrations are influenced by dynamic loads such as traffic, wind, and seismic events, which can induce longitudinal waves through the structure.

Understanding these mode shapes and their associated frequencies allows for the precise prediction of dynamic behavior and resonance phenomena, ensuring that the bridge remains within safe operational limits.
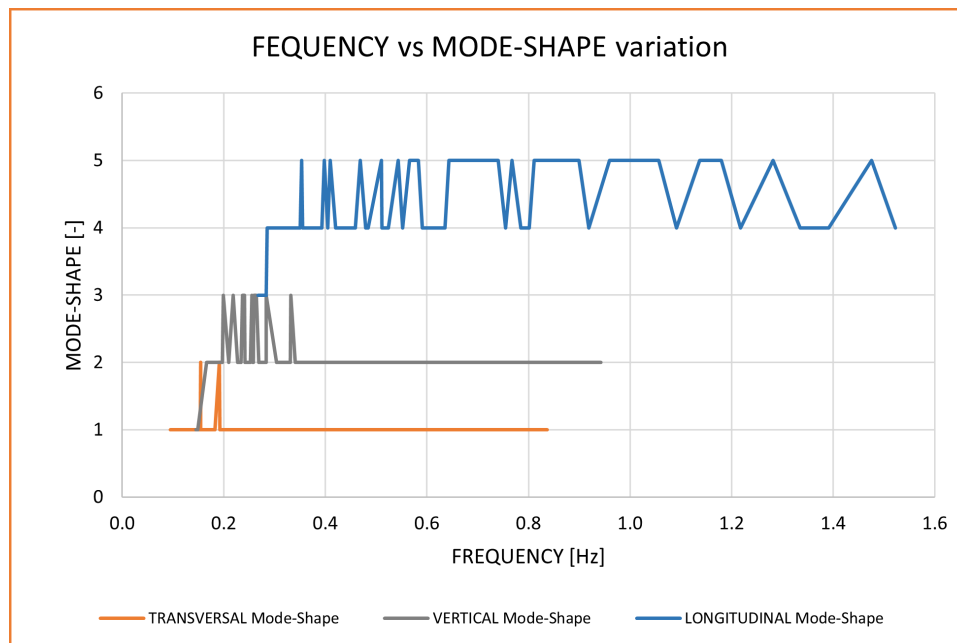
Figure 5.9.   Parametric Analysis - Frequency vs Mode Shape variation.

Parameter: Arch Span

The analysis reveals a **strong monotonic decreasing relationship** between the bridge span length and its corresponding natural frequencies (Figures 5.10 and 5.11). This trend is supported by low Pearson's correlation coefficient and Spearman's rank correlation values (Table 5.10), indicating a significant but inverse association between these variables.

Furthermore, the investigation identified distinct trend lines for the three investigated mode shapes (Figure 5.12): transversal, vertical, and longitudinal. These trend lines provide mathematical models that describe the relationship between span length and natural frequency for each mode shape. The equations derived from these trend lines offer predictive capabilities for estimating frequency variations as the span length is altered.

The findings underscore the significance of considering span length in the design and assessment of masonry arch bridges, highlighting its critical role in determining dynamic performance and resonance characteristics.
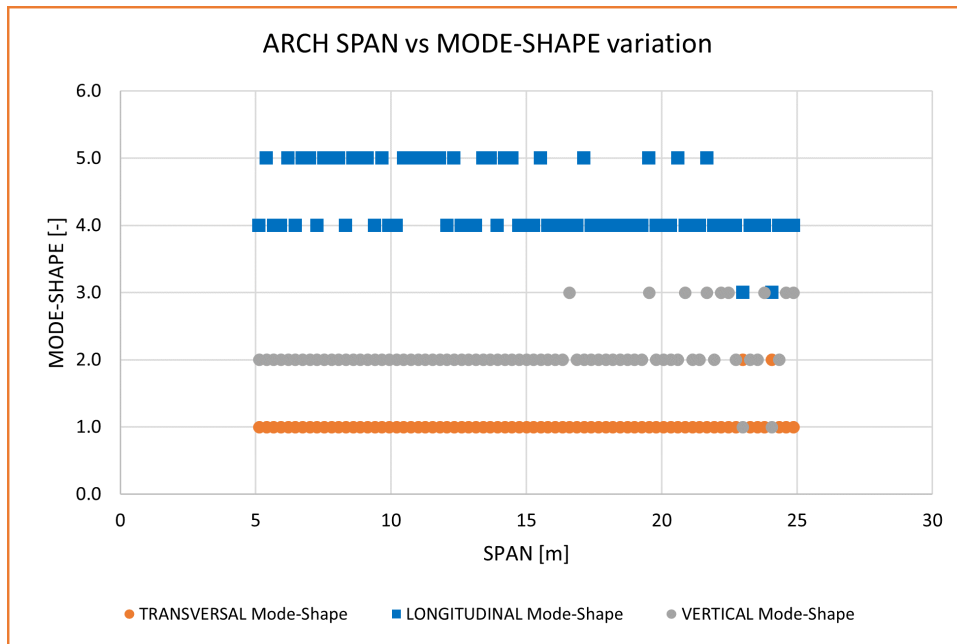
Figure 5.10.   Parametric Analysis - Arch Span vs Mode-Shape variation.
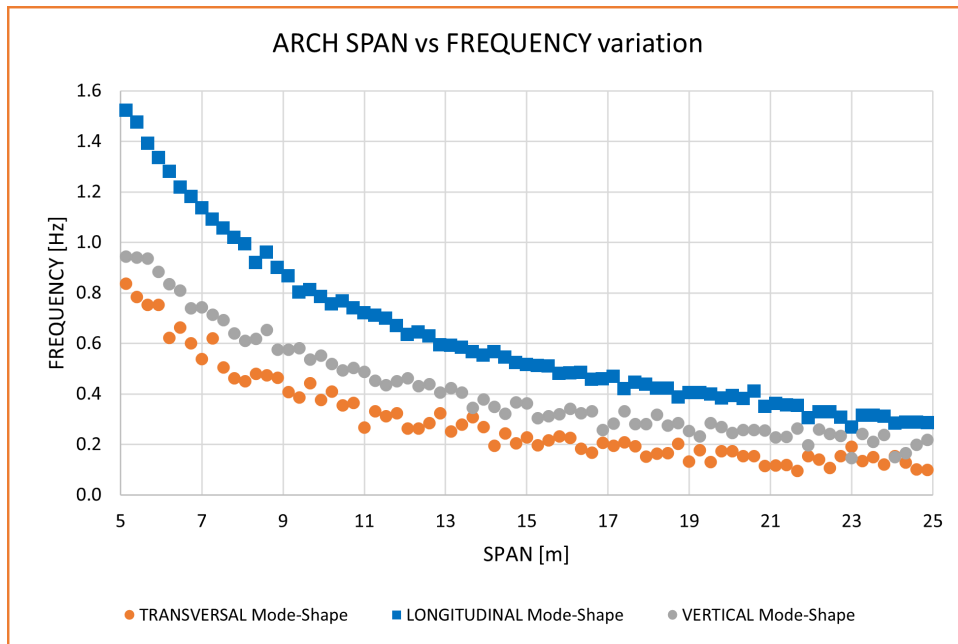
Figure 5.11. Parametric Analysis - Arch Span vs Frequency variation.
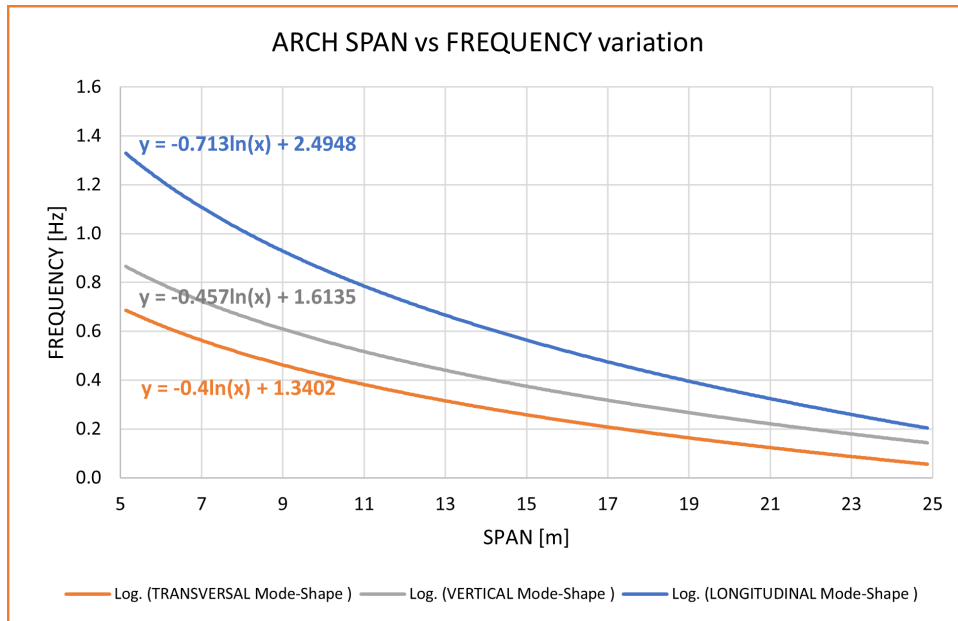
Figure 5.12. Parametric Analysis - Arch Span vs Frequency variation - Trend Lines with equations.

Table 5.10. Pearson's correlation coefficient and Spearman's rank correlation for Mode-Shapes Parametric Analysis - Span vs Frequencies.

Parametric Analysis - Span vs Frequencies			
Mode-Shape Coefficient	Transversal	Vertical	Longitudinal
Pearson's correlation coefficient	-0.8938	-0.9261	-0.9265
Spearman's rank correlation	-0.9628	-0.9815	-0.9961

Parameter: Arch Rise

The analysis indicates that natural frequencies in masonry arch bridges exhibit a **monotonic decreasing relationship** with arch rise, although less pronounced compared to arch span (Figures 5.13 and 5.13). This trend is supported by low values of both Pearson's correlation coefficient and Spearman's rank correlation (Table 5.11), which are smaller in magnitude compared to those observed for span.

The influence of arch rise on frequencies reflects its impact on the bridge's dynamic characteristics. While span length primarily governs the overall stiffness and geometrical configuration affecting natural frequencies, arch rise contributes to modifications in structural dynamics, particularly in altering the distribution of stresses and strains within the arch.

The lower correlation coefficients suggest a weaker but still significant association between arch rise and frequency variations. This relationship underscores the need for comprehensive parametric studies that consider both span length and arch rise to accurately predict and optimize bridge performance under dynamic loading conditions.
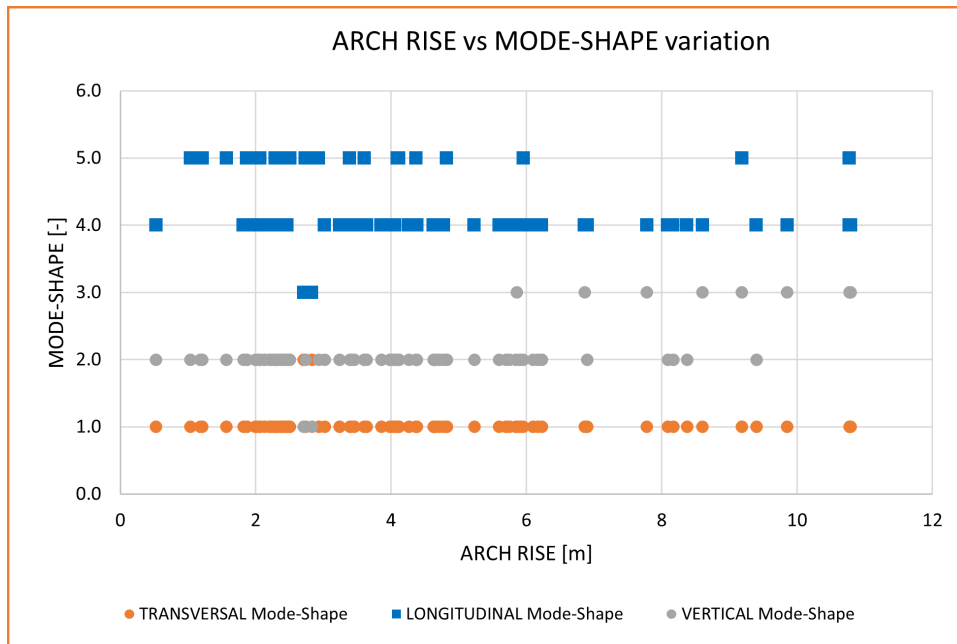
Figure 5.13.   Parametric Analysis - Arch Rise vs Mode-Shape variation.
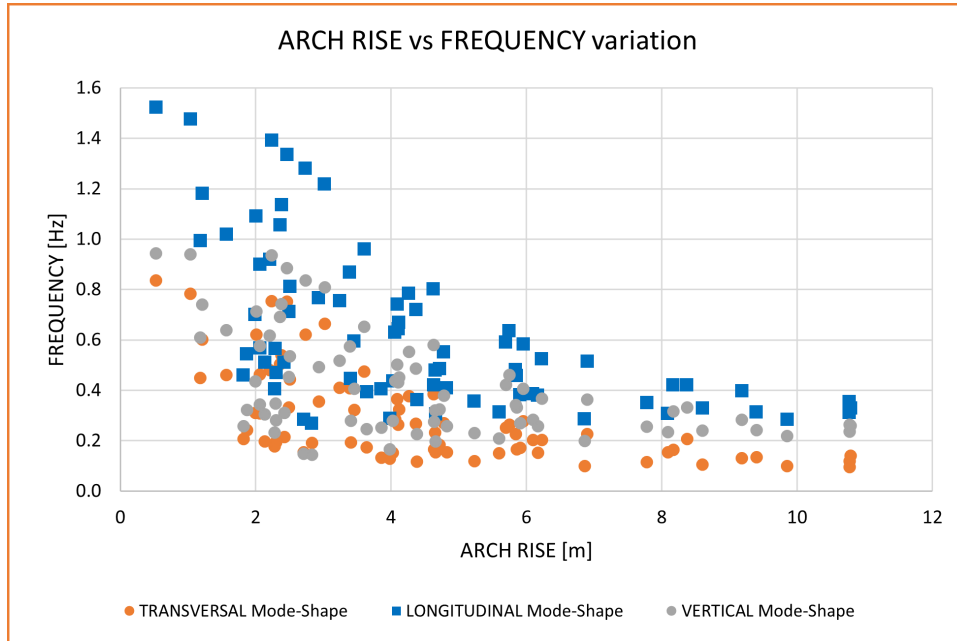
Figure 5.14.   Parametric Analysis - Arch Rise vs Frequency variation.

Table 5.11.   Pearson's correlation coefficient and Spearman's rank correlation for Mode-Shapes Parametric Analysis - Arch Rise vs Frequencies.

Parametric Analysis - Rise vs Frequencies			
Mode-Shape Coefficient	**Transversal**	**Vertical**	**Longitudinal**
Pearson's correlation coefficient	-0.6133	-0.5282	-0.6097
Spearman's rank correlation	-0.6739	-0.5198	-0.6427

The analysis of natural frequencies in masonry arch bridges reveals that they do not exhibit a clear trend with arch rise/span ratio, as depicted in Figures 5.15 and 5.16. The distribution of data points is scattered, indicating a **lack of a pronounced monotonic relationship** similar to that observed with arch span.

This observation is supported by low values of both Pearson's correlation coefficient and Spearman's rank correlation (Table 5.12), suggesting weak associations compared to those observed for span. The influence of arch rise/span ratio on frequencies reflects its role in modifying the bridge's dynamic characteristics, albeit less prominently than span length, which primarily governs stiffness and geometric configuration affecting natural frequencies.
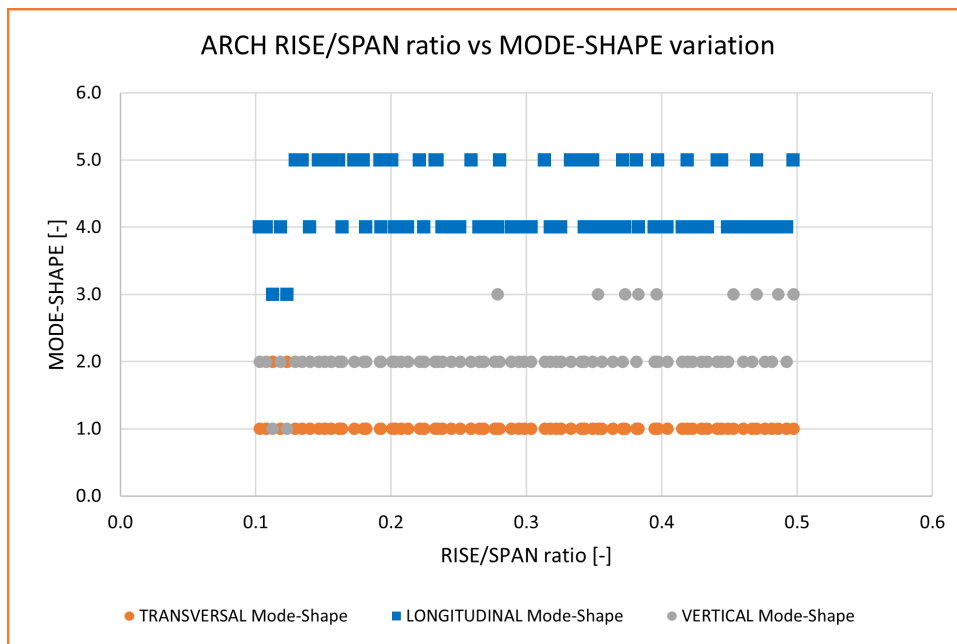
Figure 5.15.   Parametric Analysis - Arch Rise/Span ratio vs Mode-Shape variation.
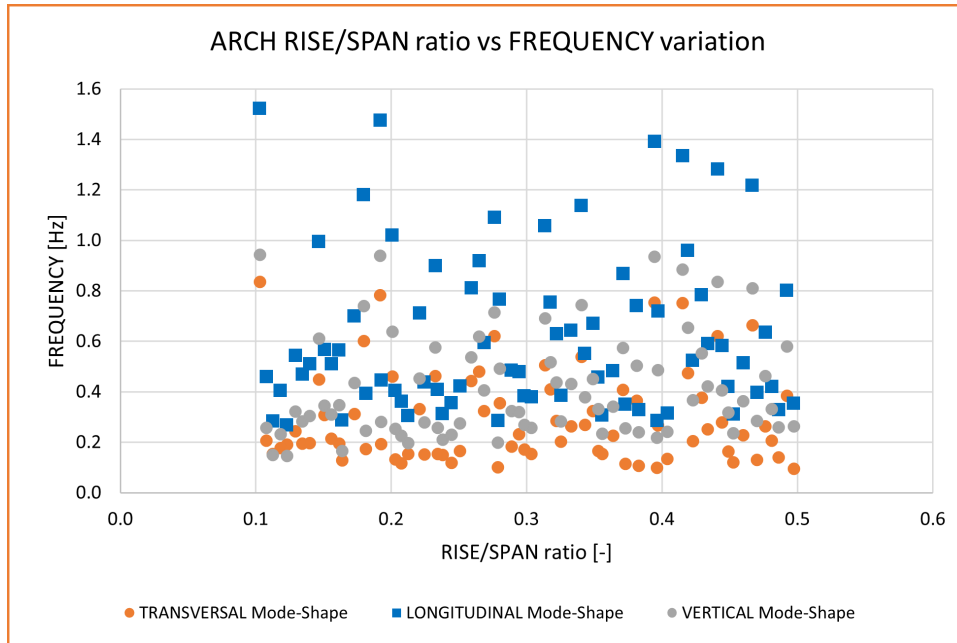
Figure 5.16.   Parametric Analysis - Arch Rise/Span ratio vs Frequency variation.

Table 5.12.   Pearson's correlation coefficient and Spearman's rank correlation for Mode-Shapes Parametric Analysis - Arch Rise/Span ratio vs Frequencies.

Parametric Analysis - Rise/Span ratio vs Frequencies			
Mode-Shape Coefficient	**Transversal**	**Vertical**	**Longitudinal**
Pearson's correlation coefficient	+0.0086	+0.1478	+0.0339
Spearman's rank correlationn	-0.0078	+0.1958	+0.0503

Parameter: Arch Thickness

The analysis reveals that natural frequencies in masonry arch bridges exhibit a nuanced relationship with arch thickness. Unlike span and arch rise, arch thickness shows a **dual trend** where frequencies tend to accumulate around two distinct lines. The first trend line shows a slight increase, while the second trend line exhibits a pronounced decrease (Figure 5.18).

This observation is supported by the analysis of Pearson's correlation coefficient and Spearman's rank correlation, which indicate moderate to low values (Table 5.13). The correlations for arch thickness are typically smaller in magnitude compared to span but demonstrate a significant influence on frequency distribution across different mode shapes.

Arch thickness plays a critical role in modifying the structural dynamics of arch bridges. The slight increase observed in the first trend line suggests that within a certain range, thicker arches may slightly increase frequencies, possibly due to increased stiffness or mass distribution effects. Conversely, the pronounced decrease along the second trend line indicates that excessively thick arches can significantly reduce frequencies, potentially leading to undesirable resonance conditions.
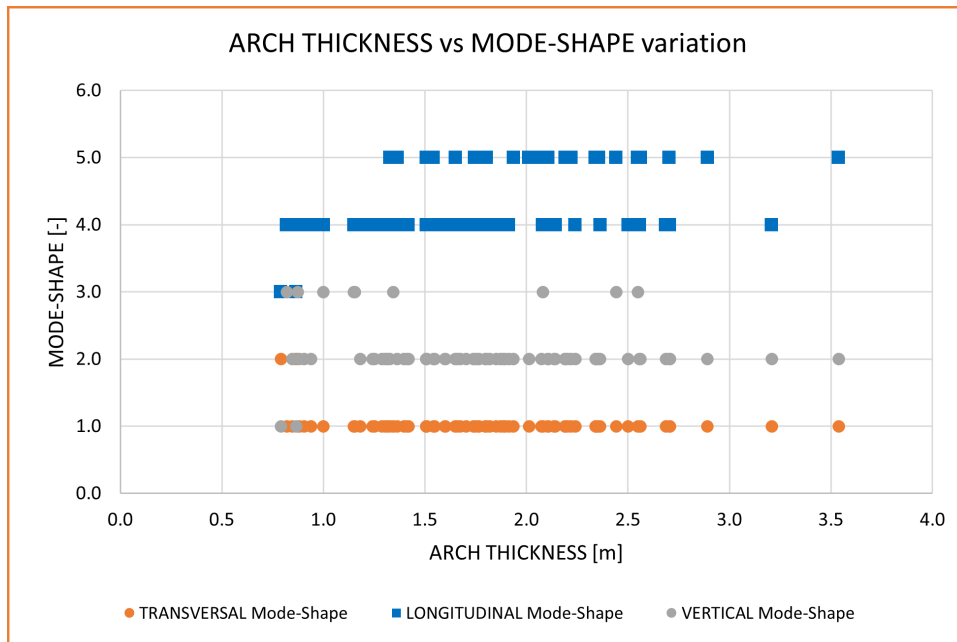
Figure 5.17.   Parametric Analysis - Arch Thickness vs Mode-Shape variation.
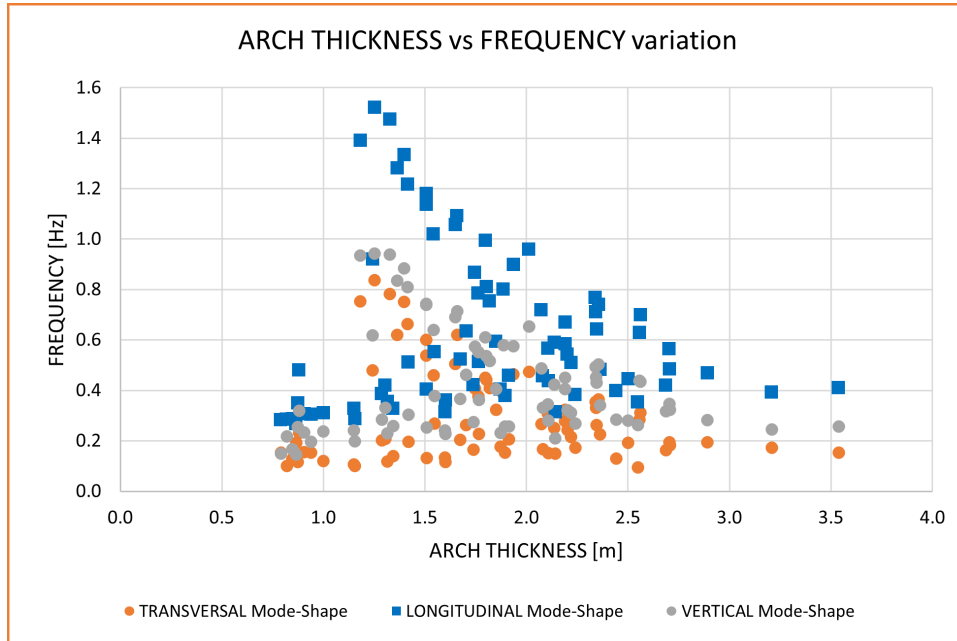
Figure 5.18.   Parametric Analysis - Arch Thickness vs Frequency variation.

Table 5.13.   Pearson's correlation coefficient and Spearman's rank correlation for Mode-Shapes Parametric Analysis - Arch Thickness vs Frequencies.

Parametric Analysis - Arch Thickness vs Frequencies			
Mode-Shape Coefficient	Transversal	Vertical	Longitudinal
Pearson's correlation coefficientt	-0.1401	-0.0834	-0.0753
Spearman's rank correlation	+0.0405	+0.1146	+0.1476

The analysis of natural frequencies in masonry arch bridges with respect to arch thickness/span ratio reveals a **scattered distribution** of data points (Figures 5.19 and 5.20).

The arch thickness/span ratio exhibits a not pronounced influence, as indicated by slightly positive values of both Pearson's correlation coefficient and Spearman's rank correlation (Table 5.14).
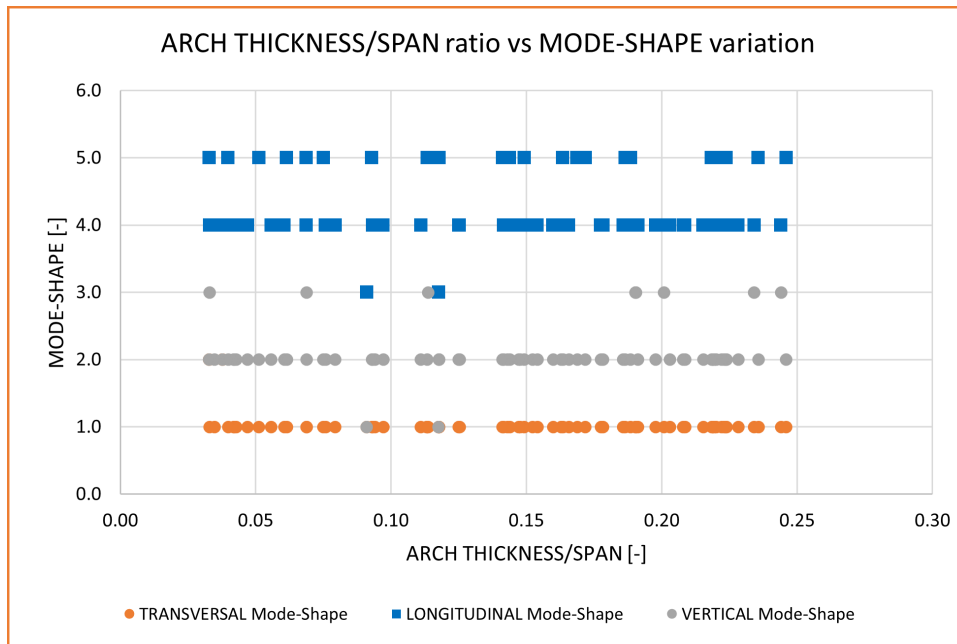
Figure 5.19.   Parametric Analysis - Arch Thickness/Span ratio vs Mode-Shape variation.

Table 5.14.   Pearson's correlation coefficient and Spearman's rank correlation for Mode-Shapes Parametric Analysis - Arch Thickness/Span ratio vs Frequencies.

Parametric Analysis - Arch Thickness/Span ratio vs Frequencies			
Mode-Shape Coefficient	**Transversal**	**Vertical**	**Longitudinal**
Pearson's correlation coefficient	+0.7828	+0.8232	+0.8321
Spearman's rank correlation	+0.8477	+0.8904	+0.9150
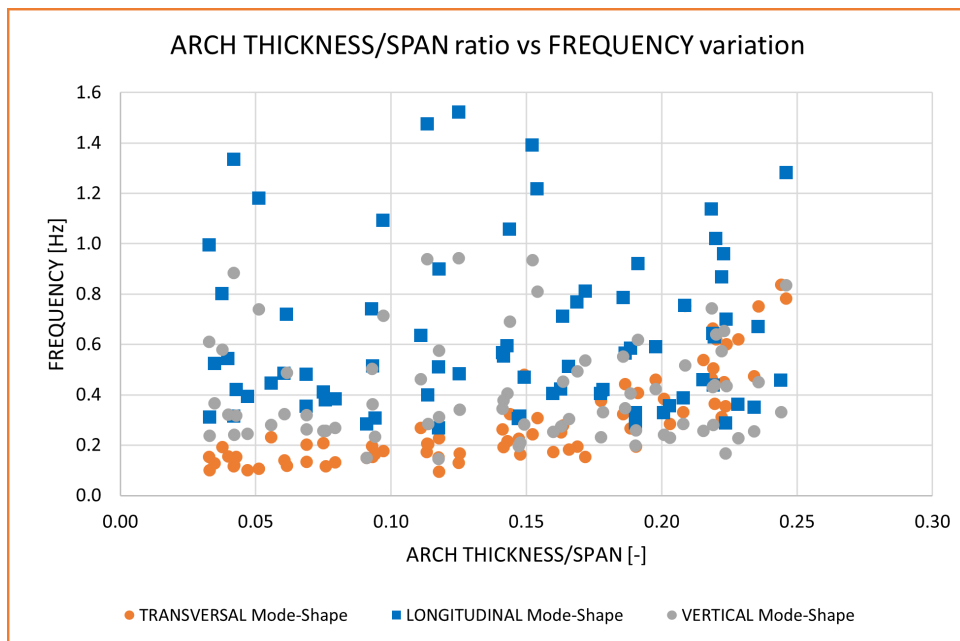
Figure 5.20.   Parametric Analysis - Arch Thickness/Span ratio vs Frequency variation.

Parameter: Bridge Width

The investigation into the relationship between bridge width and natural frequencies in masonry arch bridges reveals that **there is no discernible correlation** between these two parameters. The graphical representation shows scattered points distributed uniformly across the plot, indicating no clear trend or pattern (Figures 5.21 and 5.22).

This observation is further supported by the analysis of Pearson's correlation coefficient and Spearman's rank correlation, which both yield coefficients close to zero (Table 5.15). These values suggest that there is negligible linear relationship between bridge width and frequencies of vibration modes.

The absence of a significant trend implies that varying the width of the bridge does not notably influence its dynamic characteristics in terms of natural frequencies. Unlike parameters such as span, arch rise, and arch thickness, which exhibit distinct trends impacting frequency distribution, changes in bridge width do not result in predictable shifts in vibration modes.
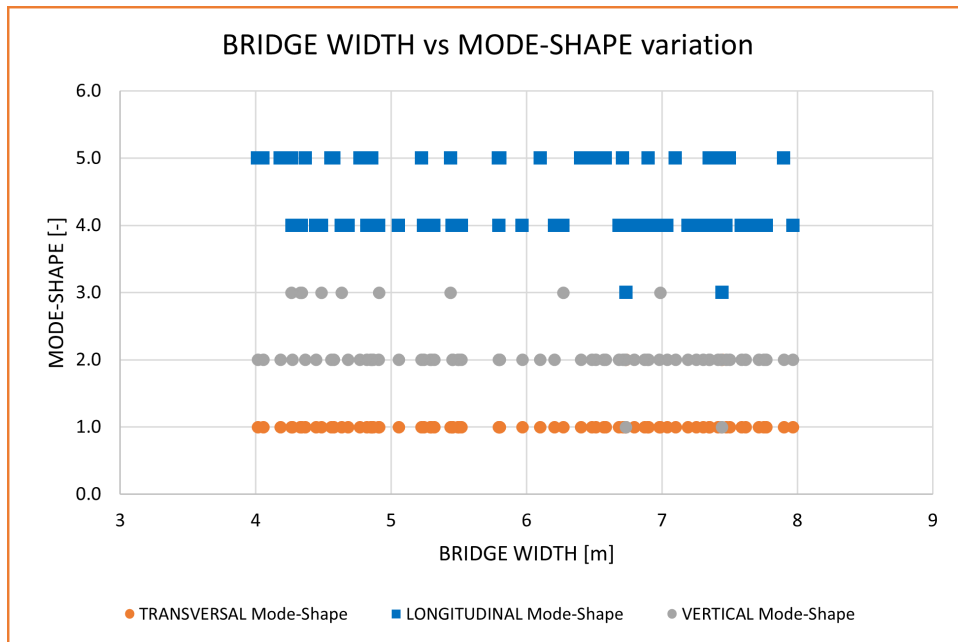
Figure 5.21. Parametric Analysis - Bridge Width vs Mode-Shape variation.
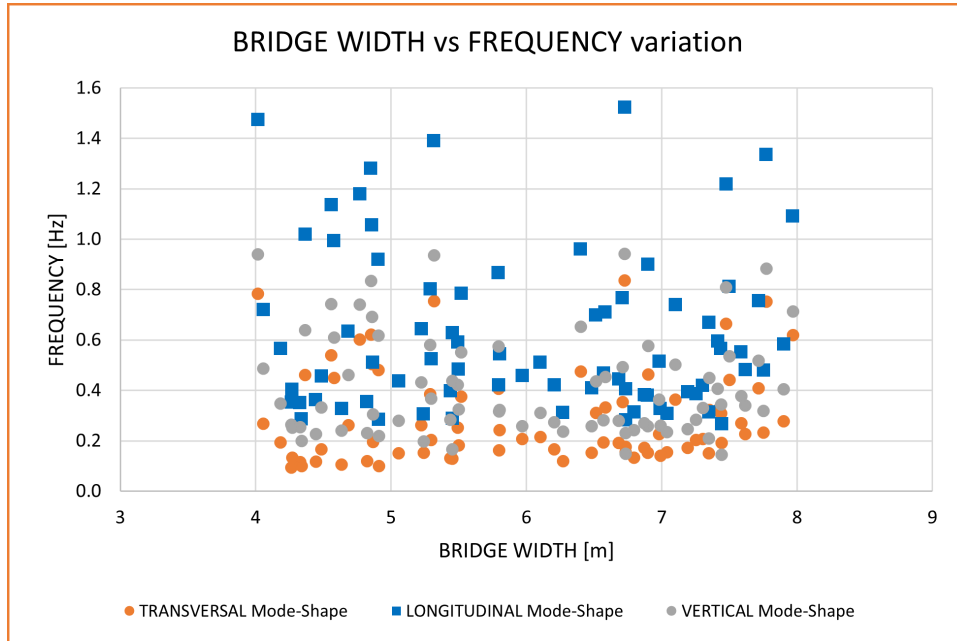
Figure 5.22.   Parametric Analysis - Bridge Width vs Frequency variation.

Table 5.15.   Pearson's correlation coefficient and Spearman's rank correlation for Mode-Shapes Parametric Analysis - Bridge Width vs Frequencies.

Parametric Analysis - Bridge Width vs Frequencies			
Mode-Shape Coefficient	**Transversal**	**Vertical**	**Longitudinal**
Pearson's correlation coefficient	+0.0657	-0.0616	-0.0684
Spearman's rank correlation	+0.1861	+0.0044	-0.0076

117

Parameter: Backfill Height

The investigation into the relationship between backfill height over the arch crown and natural frequencies in masonry arch bridges reveals that **there is no discernible correlation** between these two parameters. The graphical representation shows scattered points distributed uniformly across the plot, indicating no clear trend or pattern (Figures 5.23 and 5.24).

This observation is further supported by the analysis of Pearson's correlation coefficient and Spearman's rank correlation, which both yield coefficients close to zero (Table 5.16). These values suggest that there is negligible linear relationship between backfill height and frequencies of vibration modes.

The absence of a significant trend implies that varying the backfill height over the arch crown does not notably influence its dynamic characteristics in terms of natural frequencies. Unlike parameters such as span, arch rise, and arch thickness, which exhibit distinct trends impacting frequency distribution, changes in backfill height do not result in predictable shifts in vibration modes.
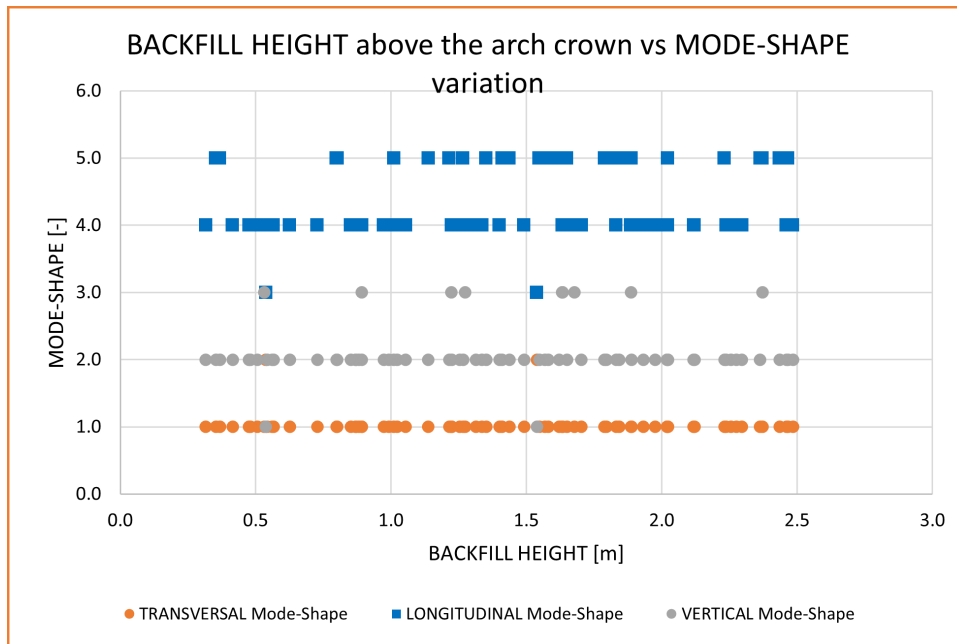
Figure 5.23. Parametric Analysis - Backfill Height vs Mode-Shape variation.
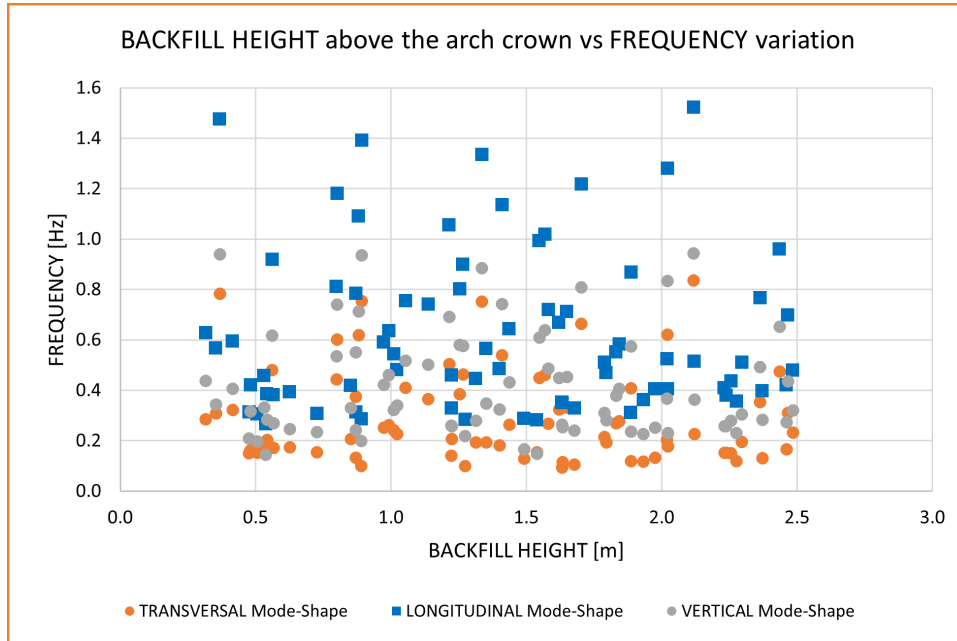
Figure 5.24.   Parametric Analysis - Backfill Height vs Frequency variation.

Table 5.16.   Pearson's correlation coefficient and Spearman's rank correlation for Mode-Shapes Parametric Analysis - Backfill Height vs Frequencies.

Parametric Analysis - Backfill Height vs Frequencies			
Mode-Shape Coefficient	Transversal	Vertical	Longitudinal
Pearson's correlation coefficient	-0.0968	-0.0462	-0.0194
Spearman's rank correlation	-0.1138	-0.0335	+0.0183

119

Parameter: Bridge Mass

The investigation into the relationship between bridge mass and natural frequencies in masonry arch bridges reveals a **notable monotonic decreasing trend**. This trend suggests that as the mass of the bridge increases, the natural frequencies of its vibration modes decrease (Figures 5.25 and 5.26).

The graphical representation of bridge mass versus frequencies shows a clear pattern where frequencies decrease consistently as bridge mass increases. This observation aligns with the understanding that heavier bridges tend to exhibit lower natural frequencies due to increased inertia and damping effects.

This relationship is **likely influenced by the span of the bridge** as well. Larger spans typically result in greater structural mass, as materials and dimensions scale proportionally to support longer spans. Therefore, the correlation between bridge mass and natural frequencies indirectly reflects the impact of span length on structural dynamics—larger spans not only increase bridge mass but also tend to lower natural frequencies.

Analyzing Pearson's correlation coefficient and Spearman's rank correlation further supports this finding, indicating a moderate to strong negative correlation between bridge mass and natural frequencies (Table 5.17). These coefficients suggest that changes in bridge mass are inversely related to variations in vibration frequencies, underscoring the influence of mass on dynamic response.
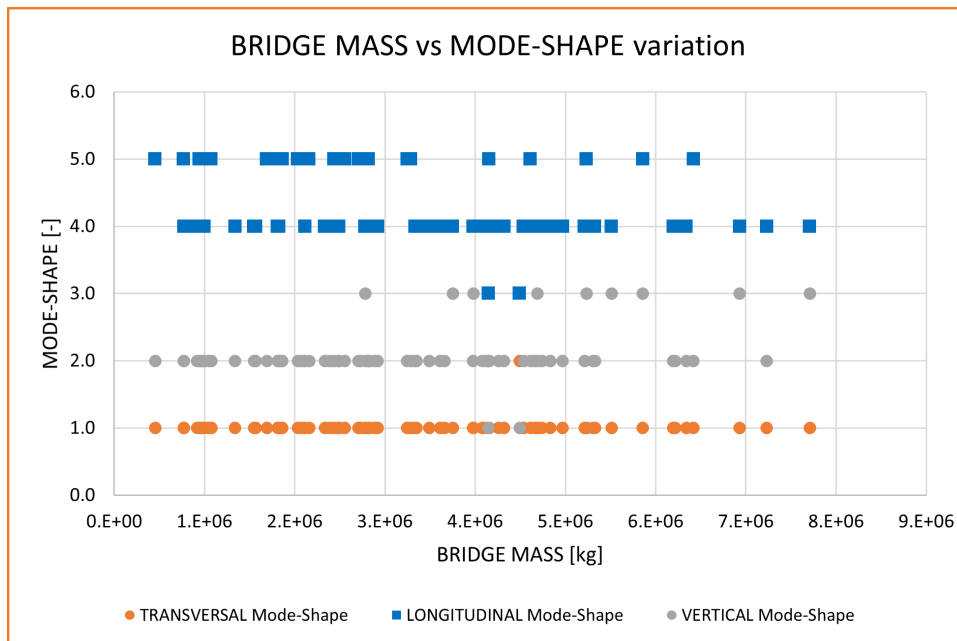
Figure 5.25.   Parametric Analysis - Bridge Mass vs Mode-Shape variation.
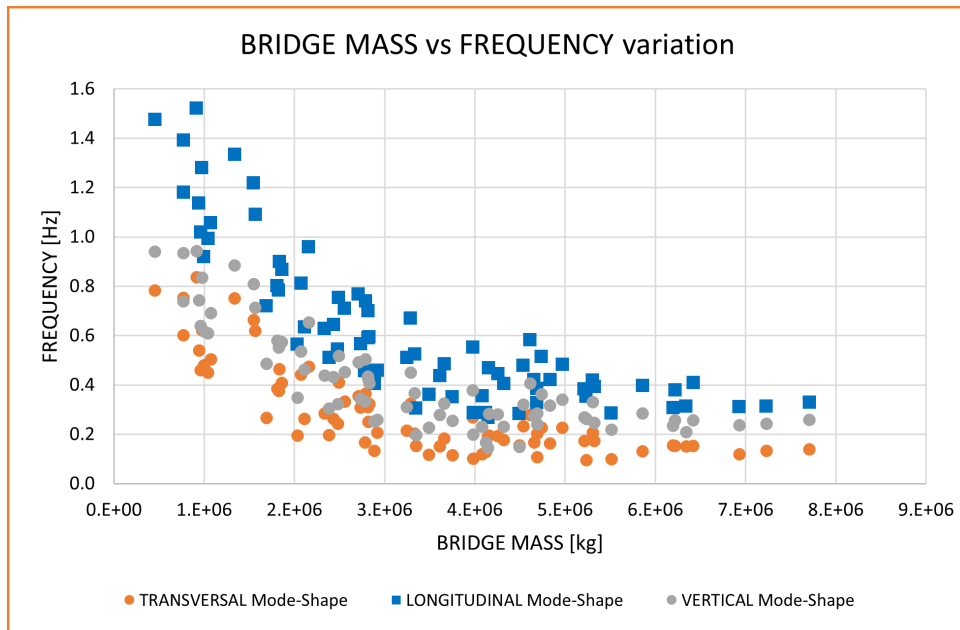
Figure 5.26.   Parametric Analysis - Bridge Mass vs Frequency variation.

Table 5.17.   Pearson's correlation coefficient and Spearman's rank correlation for Mode-Shapes Parametric Analysis - Bridge Mass vs Frequencies.

Parametric Analysis - Bridge Mass vs Frequencies			
Mode-Shape Coefficient	Transversal	Vertical	Longitudinal
Pearson's correlation coefficient	-0.7676	-0.7842	-0.8113
Spearman's rank correlation	-0.7808	-0.7722	-0.8084

Parameter: Bridge and Arch Slenderness

In this study, it was decided to also represent two parameters: **Bridge Slenderness** and **Arch Slenderness**, both versus frequencies. These parameters provide additional insights into the structural behavior of the masonry arch bridges.

Bridge Slenderness is defined as the ratio of the bridge length to the product of the bridge width and the sum of the arch thickness and the backfill height:

$$\text{Bridge Slenderness} = \frac{\text{Arch Span} + 2 \times \text{Pier Width}/2}{\text{Bridge Width} \times (\text{Arch Thickness} + \text{Backfill Height})}$$

Arch Slenderness is defined as the ratio of the span plus twice the arch thickness to the product of the bridge width and the sum of the arch thickness and the backfill height:

$$\text{Arch Slenderness} = \frac{\text{Span} + 2 \times \text{Arch Thickness}}{\text{Bridge Width} \times (\text{Arch Thickness} + \text{Backfill Height})}$$

These slenderness ratios help in understanding how the geometric proportions of the bridge influence its dynamic characteristics, such as oscillation frequencies.

Bridge slenderness exhibits a **monotonic decreasing trend** when plotted against natural frequencies (Figures 5.27 and 5.28). As bridge slenderness increases—indicating longer and narrower spans relative to width—the natural frequencies of the bridges decrease. This trend suggests that longer and narrower bridges tend to have lower natural frequencies compared to shorter and wider ones.

This behavior is supported by correlation coefficients, such as Pearson's and Spearman's, which indicate a moderate negative correlation between bridge slenderness and natural frequencies (Table 5.18). These coefficients suggest that changes in bridge slenderness have a measurable impact on the dynamic characteristics of masonry arch bridges.

Similarly, **arch slenderness** also exhibits a **monotonic decreasing trend** in relation to natural frequencies (Figures 5.29 and 5.30). When arch slenderness increases, indicating taller arches relative to their span, the natural frequencies of the bridges decrease. This observation implies that taller and narrower arches tend to have lower natural frequencies compared to shorter and wider ones.

This trend is evident in both the Pearson's and Spearman's correlation coefficients, which indicate a strong negative correlation between arch slenderness and natural frequencies (Table 5.19). These coefficients underscore the significant influence of arch slenderness on the dynamic behavior of masonry arch bridges.

122
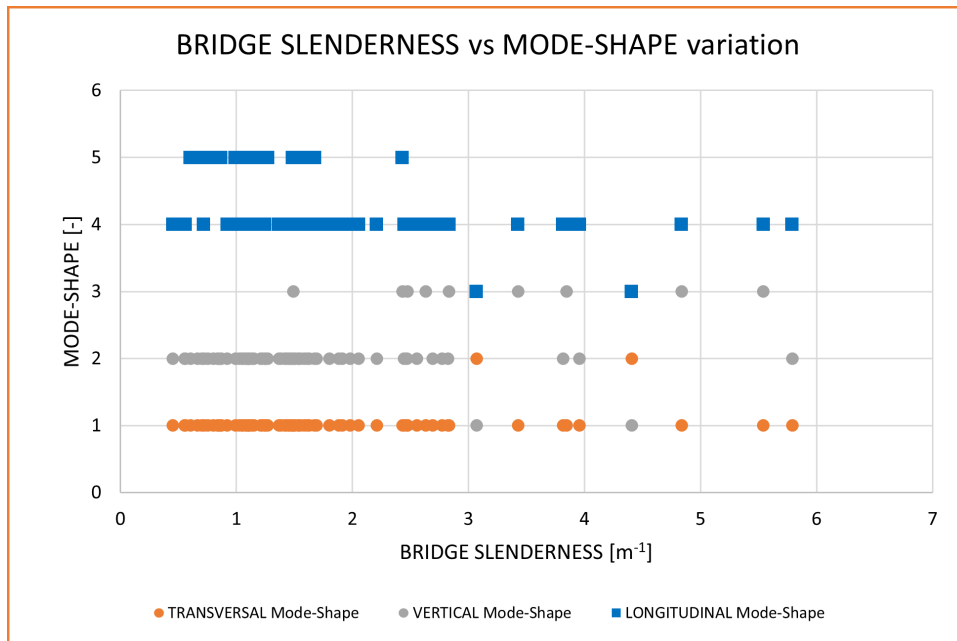
Figure 5.27.   Parametric Analysis - Bridge Slenderness vs Mode-Shape variation.
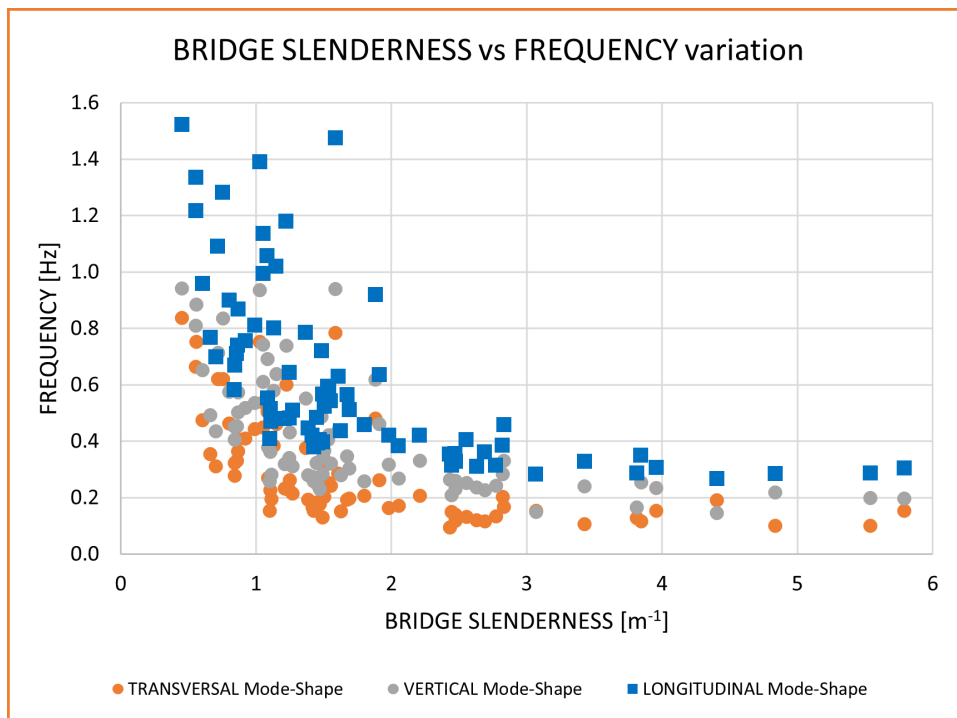
Figure 5.28.   Parametric Analysis - Bridge Slenderness vs Frequency variation.

Table 5.18.   Pearson's correlation coefficient and Spearman's rank correlation for Mode-Shapes Parametric Analysis - Bridge Slenderness vs Frequencies.

Parametric Analysis - Bridge Slenderness vs Frequencies			
Mode-Shape Coefficient	Transversal	Vertical	Longitudinal
Pearson's correlation coefficient	-0.5708	-0.6056	-0.6129
Spearman's rank correlation	-0.8183	-0.8210	-0.8673
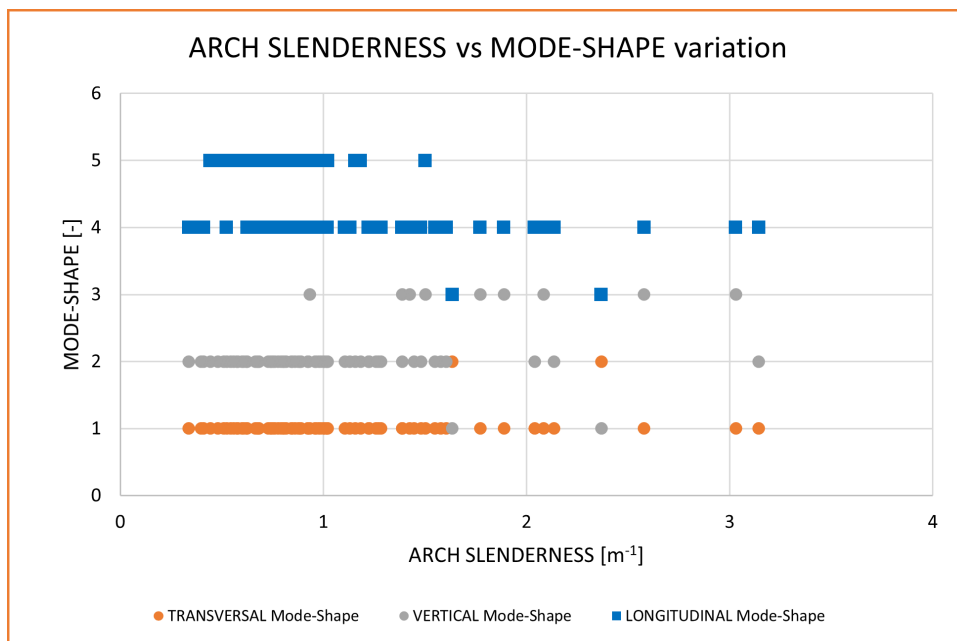
Figure 5.29.   Parametric Analysis - Arch Slenderness vs Mode-Shape variation.
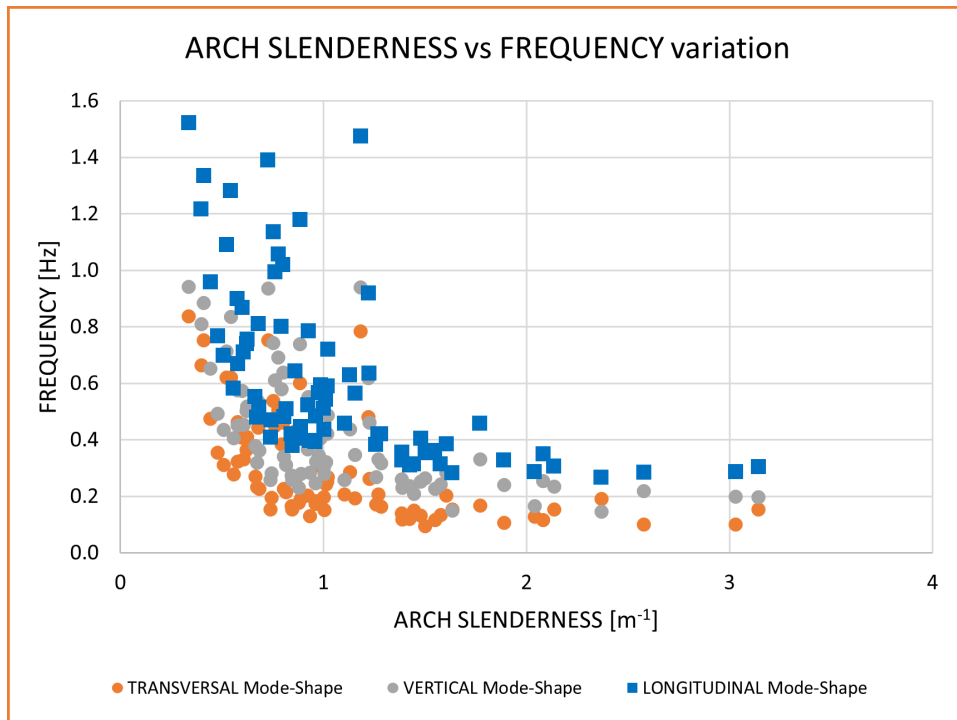
Figure 5.30.   Parametric Analysis - Arch Slenderness vs Frequency variation.

Table 5.19.   Pearson's correlation coefficient and Spearman's rank correlation for Mode-Shapes Parametric Analysis - Arch Slenderness vs Frequencies.

Parametric Analysis - Arch Slenderness vs Frequencies			
Mode-Shape Coefficient	Transversal	Vertical	Longitudinal
Pearson's correlation coefficient	-0.5555	-0.5817	-0.5900
Spearman's rank correlation	-0.7412	-0.7234	-0.7628

5.6.2 3D plots

This study employs **3D graphical analysis** to deepen the exploration of the relationship between geometric parameters and the dynamic behavior of masonry arch bridges. These graphs illustrate how modal frequencies, represented on the vertical axis (Z-axis), vary in response to changes in two key parameters: arch span along the X-axis and another variable parameter along the Y-axis.

The variable parameters analyzed include bridge width, arch thickness, bridge width, arch rise, and other critical dimensions identified in the study. Each graph provides a clear visual depiction of how these geometric factors influence modal frequencies, offering insights into their relative impacts on the bridge's dynamic characteristics (Figures 5.31; 5.32; 5.33; 5.34; 5.35; 5.36; 5.37; 5.38; 5.39).

By using 3D visualization, this approach allows for a comprehensive examination of the multidimensional effects of geometric variations on bridge dynamics. The graphs serve not only to illustrate trends but also to facilitate a deeper understanding of the complex interplay between geometry and structural behavior in masonry arch bridges.

These graphical representations are integral to interpreting the empirical findings of this study, providing a visual framework that complements quantitative analyses.

Frequencies vs Span and Rise
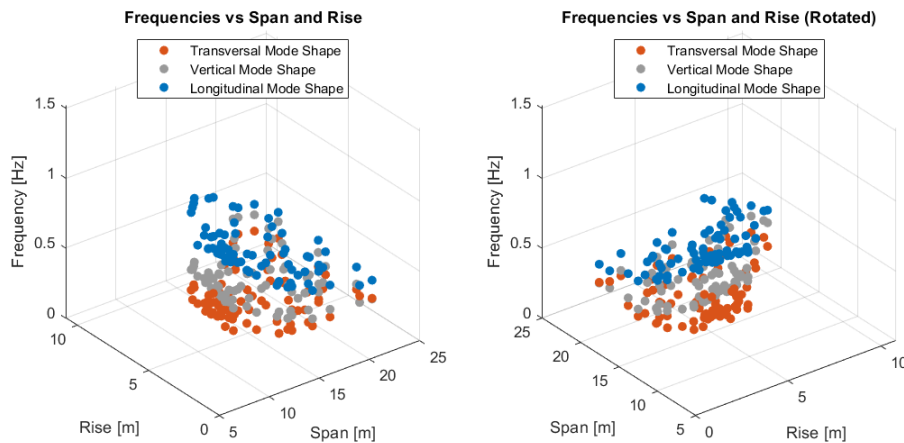
Figure 5.31.   Parametric Analysis - Frequencies vs Span and Rise.

126
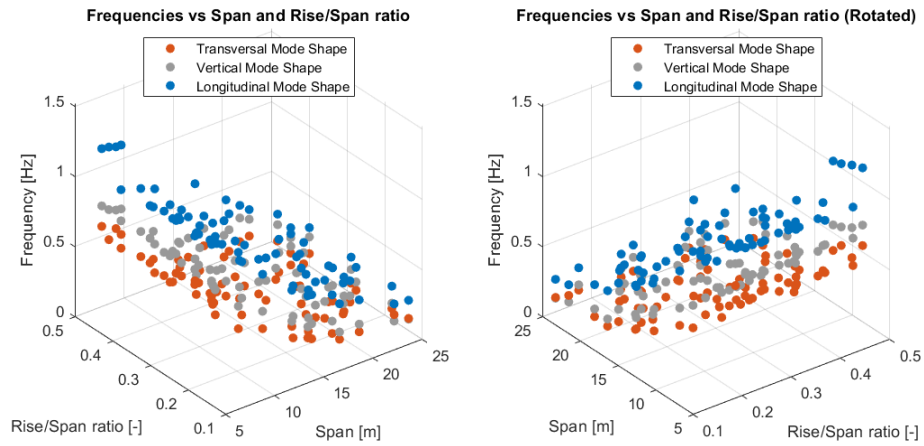
Figure 5.32.   Parametric Analysis - Frequencies vs Span and Rise/Span ratio.

Frequencies vs Span and Arch Thickness
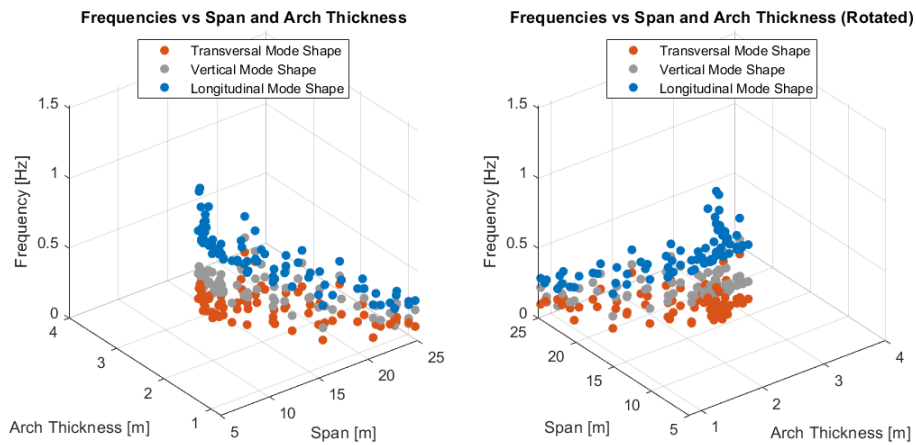
Figure 5.33.   Parametric Analysis - Frequencies vs Span and Arch Thickness.

127
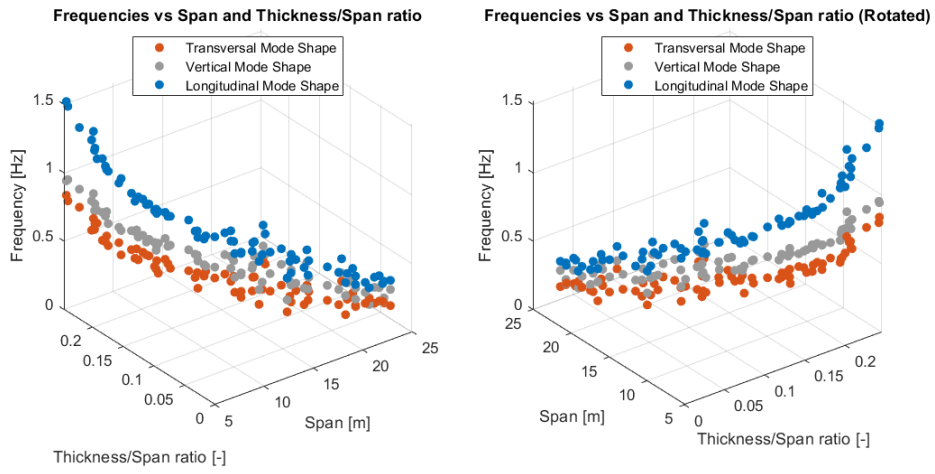
Figure 5.34.   Parametric Analysis - Frequencies vs Span and Thickness/Span ratio.

Frequencies vs Span and Width
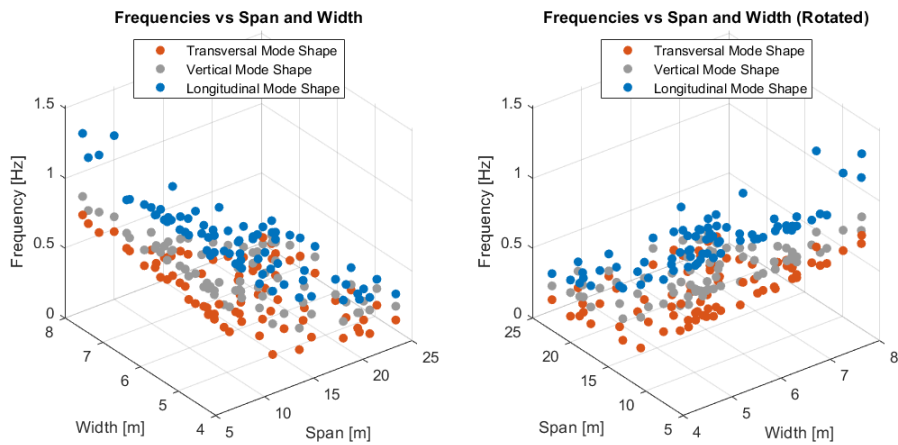
Figure 5.35.   Parametric Analysis - Frequencies vs Span and Width.

Frequencies vs Span and Backfill Height
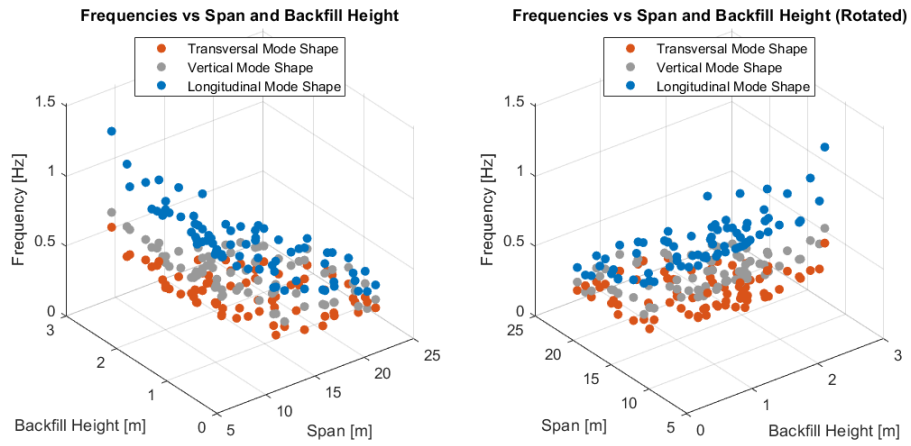
Figure 5.36.   Parametric Analysis - Frequencies vs Span and Backfill Height.

Frequencies vs Span and Mass
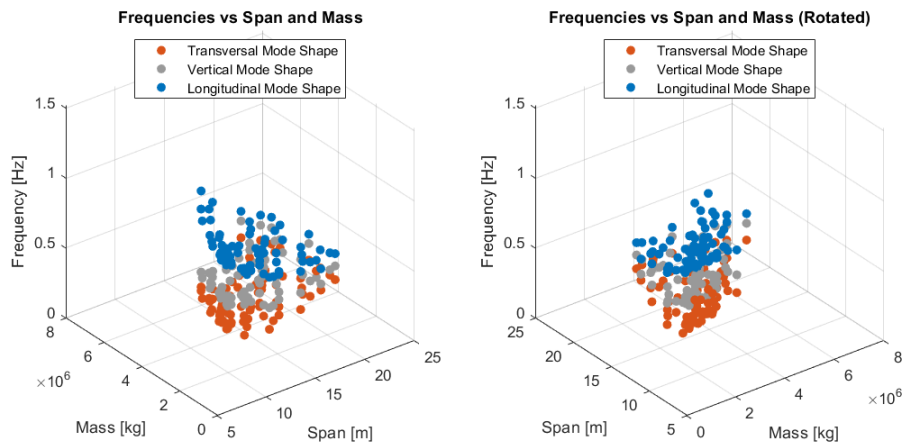
Figure 5.37.   Parametric Analysis - Frequencies vs Span and Mass.

129

Frequencies vs Span and Bridge Slenderness
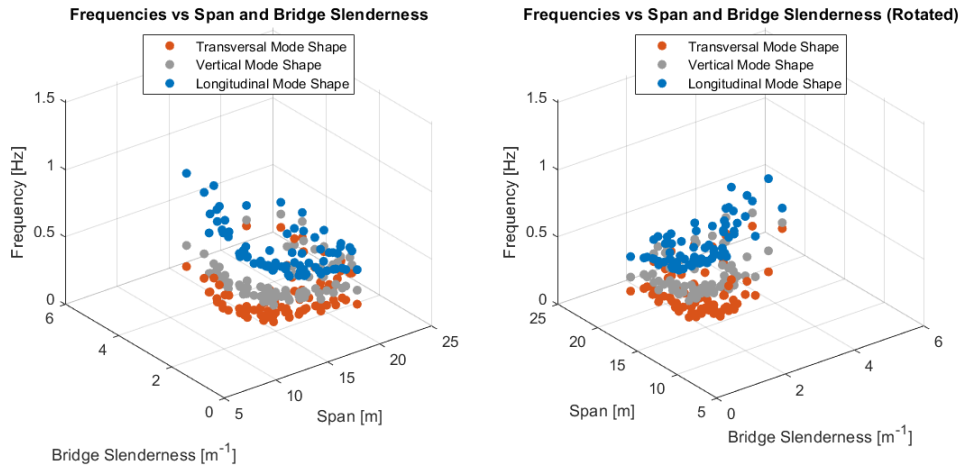
Figure 5.38.   Parametric Analysis - Frequencies vs Span and Bridge Slenderness.

Frequencies vs Span and Arch Slenderness
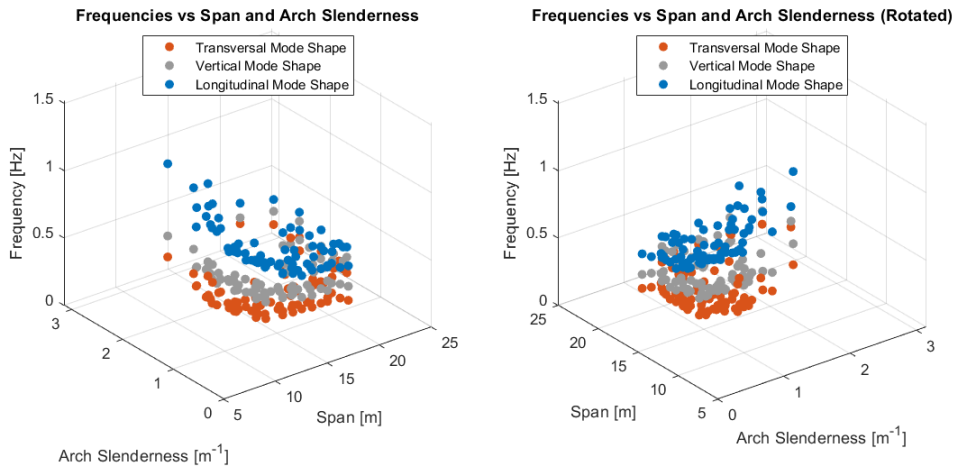
Figure 5.39.   Parametric Analysis - Frequencies vs Span and Arch Slenderness.

Chapter 6

Conclusions

6.1 Summary

This thesis aimed to **explore the correlation between the geometrical characteristics of masonry arch bridges and their dynamic behavior**, focusing specifically on modal frequencies and mode shapes. A comprehensive methodology was implemented, involving historical analysis, geometric parameterization, advanced finite element modeling, and empirical validation. The findings provided valuable insights into the dynamic properties of masonry arch bridges, contributing to their assessment, maintenance, and design.

The structure of this thesis was organized as follows:

- **Chapter 1: Introduction** - This chapter provided an overview of the background, motivation, objectives, and methodology of the study. It highlighted the importance of masonry arch bridges in global infrastructure and identified the research gap in understanding their dynamic behavior.

- **Chapter 2: State of the Art** - This chapter reviewed the current literature and previous research on the dynamic behavior of masonry arch bridges, focusing on methodologies and findings related to modal analysis. It discussed various approaches and identified the limitations and gaps in existing studies.

- **Chapter 3: Empirical Rules and Geometrical Parameters** - This chapter examined historical empirical rules and identified critical geometrical parameters that influence the dynamic behavior of masonry arch bridges. It provided a detailed analysis of traditional design principles and their relevance to modern engineering practices.

- **Chapter 4: Design of the Model** - This chapter detailed the process of parameterizing the geometrical characteristics of masonry arch bridges and creating 3D finite element (FE) models. It described the development of a custom Python code for generating parametric geometric models and the use of STKO for finite element analysis.

- **Chapter 5: Eigenvalue Sensitivity Analysis of Single Span Bridges** - This chapter discussed the influence of different geometrical parameters on the dynamic properties of the bridges. It presented the results of modal analyses, highlighting the correlation between modal frequencies and parameters such as arch span, thickness, rise, bridge width, and pier dimensions.

- **Chapter 6: Conclusions** - This chapter summarized the findings, discussed their implications, and provided recommendations for future research and practical applications. It highlighted the main contributions of the study, such as the development of empirical equations for predicting natural frequencies. Suggestions for future work included expanding the database, exploring material properties, investigating boundary conditions, developing advanced FE models, conducting field tests, and utilizing advanced computational techniques.

Overall, this thesis offered a systematic and comprehensive approach to understanding the dynamic behavior of masonry arch bridges, providing valuable insights and practical tools for engineers and researchers in the field.

6.2   Main Contributions

This study has made several significant and original contributions to advancing the understanding of the dynamic behavior of masonry arch bridges. The findings highlight key correlations between geometric parameters and dynamic properties, offering insights crucial for both theoretical developments and practical applications in structural engineering.

From the analysis, it was observed that modal frequencies exhibit strong correlations with specific geometrical parameters of masonry arch bridges:

- **Significant Influence of Arch Span**: The study found a significant, monotonically decreasing relationship between arch span and modal frequencies. This trend was robustly supported by Pearson's correlation coefficient and Spearman's rank correlation, indicating a strong negative correlation. Larger spans corresponded to lower modal frequencies, emphasizing the critical role of arch span in bridge dynamics.

- **Impact of Arch Rise**: Similarly, arch rise demonstrated a decreasing trend with respect to modal frequencies, though the correlation was slightly weaker compared to arch span. Nonetheless, the correlation coefficients for arch rise still highlighted its notable influence on the dynamic behavior of the bridges.

- **Complex Pattern of Arch Thickness**: Arch thickness exhibited a unique pattern with two distinct trend lines in relation to modal frequencies. One trend showed a slight increase in frequencies with increased thickness, while the other showed a strong decrease. This complexity suggests that arch thickness affects modal frequencies in a nuanced manner compared to other parameters.

- **Less Influential Parameters**: Parameters such as bridge width and backfill height over the crown did not show significant relationships with modal frequencies. The dispersion of data points and near-zero correlation coefficients indicated that these parameters have minimal impact on the dynamic behavior of masonry arch bridges under the study conditions.

- **Influence of Bridge Mass**: The study identified a monotonically decreasing relationship between bridge mass and modal frequencies. This relationship is likely influenced by the bridge span, where larger spans generally result in greater mass and consequently lower modal frequencies.

- **Slenderness Effects**: Both bridge slenderness and arch slenderness exhibited monotonically decreasing trends with frequencies. Bridge slenderness values were generally higher than those of arch slenderness, reflecting their differing contributions to the dynamic behavior of the bridge structure.

These findings significantly enhance the understanding of how specific geometric characteristics influence the dynamic behavior of masonry arch bridges. They provide a foundation for optimizing bridge design, assessing structural integrity, and guiding maintenance strategies in the field of civil engineering.

6.3   Suggestions for the future works

Based on the findings of this study, several avenues for future research could further advance the understanding and application of dynamic analysis in masonry arch bridges. However, it's important to note the **limitations of this study**, which include the following assumptions:

- constant pier height;

- pier thickness always equal to half of the span;

- constant number of arch bricks;

- constant material properties (Young's modulus and Poisson ratio);

- spandrel wall thickness equal to 1/5 of the bridge width;

- infill thickness equal to 3/5 of the span width.

Moving forward, the following areas are recommended for exploration and development:

- **Enhancement of Database and Empirical Equations**: Expand the existing database to encompass a broader spectrum of bridge types, materials, and environmental conditions. This expansion would improve the accuracy and reliability of empirical equations for predicting modal frequencies and mode shapes.

133

- **Integration of Material Properties**: Investigate the combined effects of material properties, such as different types and qualities of masonry, on the dynamic behavior of bridges. Understanding these interactions alongside geometric parameters could provide deeper insights into structural performance and durability.

- **Boundary Condition Analysis**: Explore the influence of varying boundary conditions on modal frequencies and mode shapes. Analyzing how different support conditions and environmental factors affect bridge dynamics would enhance the predictive capabilities of numerical models.

- **Development of Advanced Finite Element Models**: Develop more sophisticated finite element models capable of capturing non-linear behaviors, including the effects of damage and aging. Incorporating these aspects into simulations would improve the accuracy of dynamic predictions and support more realistic assessments of bridge conditions over time.

- **Field Validation Studies**: Conduct comprehensive field tests on existing masonry arch bridges to validate the numerical models and empirical equations developed in this study. Field validation would confirm the applicability of theoretical findings in real-world scenarios and enhance confidence in engineering decisions.

- **Exploration of Machine Learning Techniques**: Explore the application of advanced computational techniques, such as machine learning algorithms, to predict the dynamic behavior of masonry arch bridges. Machine learning models could leverage large datasets to uncover complex relationships between input parameters and bridge performance, offering new insights and predictive capabilities.

- **Extension to Multi-Span Bridges**: While this study focuses on single-span bridges, future research should be extended to include multi-span masonry arch bridges. Investigating the dynamic behavior of multi-span bridges will provide a more comprehensive understanding and broaden the applicability of the findings.

Addressing these research directions would contribute to refining the understanding of masonry arch bridge dynamics, improving design practices, and supporting more effective maintenance and rehabilitation strategies in civil engineering.

Bibliography

[1] **ASDEA Software Technology.** Scientific ToolKit for OpenSees, STKO. Pescara (Italy); 2023. https://asdea.eu/software/ (accessed on 18 June 2024)

[2] **Ardant P-J** Theoretisch-praktische Abhandlung über Anordnung und Construction der Sprengwerke von grosser Spannweite mit besonderer Beziehung auf Dach- und Brücken-Constructionen aus geraden Theilen, aus Bögen, oder aus der Verbindung beider; für praktische Baumeister, so wie für Vorträge über Ingenieur-Mechanik; mit einem Atlas von 28 Tafeln und in den Text gedruckten Holzschnitten. Auf Befehl des Französischen Kriegsministeriums gedruckte Abhandlung. Deutsch hrsg. von Aug[ust] von Kaven. Hannover (Hahn); 1847.

[3] **Bien J., Elfgren L., Olofsson J.** Sustainable Bridges. Assessment for Future Traffic Demands and Longer Lives. 2007. Available online ad D9.2 from: www.sustainablebridges.net (accessed on 13 February 2024)

[4] **Brencich A., Morbiducci R.** Masonry Arches: Historical Rules and Modern Mechanics *International Journal of Architectural Heritage* **165-189** 1:2; Genova, Italy; 2007.

[5] **Busch P., Zumpe G.** Load capacity, load safety and load reserves Arch bridges. *5th Dresden Bridge Building Symposium* **153-169** Faculty of Civil Engineering, Technical University of Dresden, Germany; 1995.

[6] **Corradi M.** Empirical methods for the construction of masonry arch bridges in the 19th century. Arch Bridges: history, analysis, assessment, maintenance and repair. *Proceedings of the second international arch bridge conference* **25-36** Venice, Italy; 6–9 October 1998.

[7] **Corradi M., Filemio V.** A brief comparison between mechanical aspects and construction of arch bridges during the XVIIIth and XIXth centuries. Arch Bridges IV *Advances in Assessment, Structural Design and Construction* **79-86** CIMNE, Barcelona, Spain; 2004.

[8] **Dupuit J.** Treatise on the balance of vaults and the construction of masonry bridges (in French). *Dunod.* Paris, France; 1870.

[9] **Fuentes MD** An endeavour to identify Roman bridges built in former Hispania. *First international Congress on Construction History.* **775–86**; Madrid, Spain; 2003.

[10] **Gambarotta L.** Sperimentazione e Modellazione di Ponti ad Arco in Muratura. *Pubblicazione Serie I, n.º 11. Atti Giornata di Studio sulla Sperimentazione dei ponti, CIAS.* **250-277** Milan and Trento, Italy; 1999.

135

[11] **Gilbert M.** The behaviour of masonry arch bridges containing defects. *PhD Thesis.* University of Manchester, UK; 1993.

[12] **Gilbert M., Cole G., Smith C., Melbourne C.** Guidance on the assessment of masonry arch bridges. *CIRIA* London, UK; 2022. Available online ad D9.2 from: www-ciria.org (accessed on 13 February 2024)

[13] **Heinrich B.** Bridges - from beams to arches. *Rowohlt paperback* Verlag GmbH, Hamburg, Germany; 1983.

[14] **Hodgson J.A.** The behaviour of skewed masonry arch bridges. *PhD Thesis.* University of Salford, UK; 1996.

[15] **Hughes T.G., Blackler M.J.** A review of the UK masonry arch assessment methods. Proceedings of the ICE-Structures and Buildings. **3** 122, 305-315; 1997.

[16] **Indian Railways Institute of Civil Engineering** Inspection, Assessment, repairs and retrofitting of masonry arch bridges. *Indian Railways Institute of Civil Engineering, Pune - 411 001* Available online: https://indianrailways.gov.in/railwayboard/uploads/directorate/Heritage (accessed on 30 January 2024)

[17] **International Union of Railways (UIC)** Improving Assessment, Optimization of Maintenance and Development of Database for Masonry Arch Bridges. 2005.

[18] **João Jorge Carrazedo de Jesus** Caraterização Geométrico-Estrutural de Pontes em Arco de Alvenaria na Região de Bragança. Master Thesis. Instituto Politécnico de Bragança, Portugal; 2013.

[19] **Kurrer K-E, Kahlow A.** Arch and vault from 1800 to 1864. *Second international conference on arch bridges.* **37-42**, 1998.

[20] **Lagomarsino S., Resemini S., Rossi B.** Analisi teorico-sprimentale per la sicurezza dei ponti della linea ferroviaria Genova-Ovada. *Atti del corso CIAS: Progetto, costruzione e controllo dei ponti: il ruolo della sperimentazione.* Milan and Genova, Italy; 1999.

[21] **Lemos C.** Geometric analysis and load capacity of masonry arch bridges. Master Thesis. University of Minho, Portugal; 2009.

[22] **Melbourne C., Wang J., Tomor A., Holm G., Smith M., Bengtsson P.E., Bien J., Kaminski T., Rawa P., Casas J.R., Roca P., Molins C.** Masonry Arch Bridges: Sustainable Bridges. Background document 4.7 2007. Retrieved from https://urn.kb.se/resolve?urn=urn:nbn:se:ltu:diva-75318

[23] **Ministero delle Infrastrutture e dei Trasporti** Aggiornamento delle «Norme techniche per le costruzioni». *Supplemento ordinario alla "Gazzetta Ufficiale„ n. 42 del 20 febbraio 2018 - Serie generale* DECRETO 17 Genuary 2018. Rome, Italy; 20 february 2018.

[24] **Ministero delle Infrastrutture e dei Trasporti** Istruzioni per l'applicazione dell'«Aggiornamento delle "Norme techiche per le costruzioni"» di cui al decreto ministeriale 17 gennaio 2018. *Supplemento ordinario alla "Gazzetta Ufficiale„ n. 35 del 11 febbraio 2019 - Serie generale* CIRCOLARE 21 gennaio 2019, n. 7 C.S.LL.PP. Rome, Italy; 11 february 2019.

[25] **Oliveira D., Lourenço P., Lemos C.** Geometric issues and ultimate load capacity of masonry arch bridges from the northwest Iberian Peninsula. *Engineering*

Structures. 3955-3965 32. 2010.

[26] **Page J.** TRL State of the Art Review: Masonry Arch Bridges. Her Majesty's Stationery Office, London, UK; 1993.

[27] **Pont3.** Universitat Politècnica de València, Universitat Politècnica de Catalunya, Universidade de Vigo. Spain; 2022. https://pont3.es/ (accessed on 21 June 2024)

[28] **Proske D., van Gelder P.** Safety of historical stone arch bridges. *Springer.* 2009.

[29] **Purtak F.** For the nonlinear calculation of arch bridges made of natural stone masonry (in German). *CAD-FEM Users Meeting 2004 – International Congress on FEM Technology with ANSYS CFX & ICEM CFD Conference,* **22** Dresden, Germany; 2004.

[30] **Ribera, J.E.** Puentes de Fábrica y Hormigon Armado, Tomo III. Spain; 1936.

[31] **Stone Arch Bridges.** Architecture standing the test of time. 2023. https://stonearchbridges.com/2023/01/27/the-structural-significance-of-solid-backing-part-1/ (accessed on 22 June 2024)

[32] **Wang, J.** The three-dimensional behaviour of masonry arches. *PhD Thesis.* University of Salford, UK; 2004.

137

Chapter 7

Annex A - Python Code

The following Listing is the Python Code used to generate the geometry of the bridge.

```python
# Master Degree Thesis: INVESTIGATION OF THE DYNAMIC PROPERTIES
    OF MASONRY ARCH BRIDGES VIA 3D FINITE ELEMENT MODELLING

# Universitat Politecnica de Catalunya - ETSECCPB: Escola
    Tecnica Superior d'Enginyeria de Camins, Canals i Ports de
    Barcelona (Barcelona, Spain)
# Polytechnic University of Turin - DISEG: Dipartimento di
    Ingegneria Strutturale, Edile e Geotecnica (Turin, Italy)

# Student: Francesco Pino
# Supervisors: Luca Pela, Semih Gonen, Pietro Cornetti,
    Gianfranco Piana



# ----- IMPORT PACKAGES ----- #

import csv
import os
import sys
import math
import numpy as np
from PyMpc import *
from PySide2.QtCore import Qt
from PySide2.QtWidgets import (
    QApplication,
    QDialog,
    QVBoxLayout,
    QProgressBar,
    QLabel,
    QListWidget,
    QListWidgetItem,
```

```python
28          QDialogButtonBox ,
29          QMessageBox ,
30          QInputDialog ,
31          QFileDialog ,
32     )
33
34     import Configuration_data          # Import the configuration
              script
35
36     print ("All␣modules␣imported␣successfully.")
37
38
39
40     # ----- INITIATING ----- #
41
42     App.clearTerminal()                # Clear the terminal
43     doc = App.caeDocument()      # Initialize the CAE document
44
45     print ("Application␣commands␣executed␣successfully.")
46
47
48
49     # ----- DEFINING VARIABLES ----- #
50
51     NumberSpans = 1
52
53     # Read data from CSV file
54     with open('data.csv', newline='') as csvfile:
55          reader = csv.DictReader(csvfile)
56          for index, row in enumerate(reader, start=1):
57                     # Select the desired n. analysis
58              if index == 1:
59                  n = int(row['n'])
60                  Span = float(row['Span'])
61                  Rise_Span_Ratio = float(row['Rise/Span␣Ratio'])
62                  Arch_thickness_Span_Ratio = float(row['Thickness/
                       Span␣Ratio'])
63                  Backfill_height = float(row['Backfill␣height'])
64
65                  # Process the data for the selected row
66                  ArchSpan = Span
67                  ArchRise = ArchSpan * Rise_Span_Ratio
68                  ArchThickness = ArchSpan *
                       Arch_thickness_Span_Ratio
69                  PierHeight = 5000.0
70                  PierThickness = ArchSpan/2
71                  BricksNumber = 21.0
72                  TotalOffset = 0
```

```python
# Print the values to debug
print("n:", n)
print("ArchSpan (mm):", ArchSpan)
print("ArchRise (mm):", ArchRise)
print("ArchThickness (mm):", ArchThickness)
print("Backfill height (mm):", Backfill_height)



# ----- CREATING GEOMETRIES ----- #

for i in range(NumberSpans):
    if i > 0:
        TotalOffset += ArchSpan + PierThickness

    pier_vertices = [
        FxOccBuilder.makeVertex(TotalOffset, 0.0, 0.0),
        FxOccBuilder.makeVertex(TotalOffset, 0.0, PierHeight),
        FxOccBuilder.makeVertex(TotalOffset + PierThickness,
            0.0, 0.0),
        FxOccBuilder.makeVertex(TotalOffset + PierThickness,
            0.0, PierHeight),
    ]

    for vertex in pier_vertices:
        next_id = doc.geometries.getlastkey(0) + 1
        geom = MpcGeometry(next_id, '', vertex)
        doc.addGeometry(geom)

    pier_edges = [
        FxOccBuilder.makeEdge(pier_vertices[0], pier_vertices
            [1]),
        FxOccBuilder.makeEdge(pier_vertices[0], pier_vertices
            [2]),
        FxOccBuilder.makeEdge(pier_vertices[1], pier_vertices
            [3]),
        FxOccBuilder.makeEdge(pier_vertices[2], pier_vertices
            [3]),
    ]

    for edge in pier_edges:
        next_id = doc.geometries.getlastkey(0) + 1
        geom = MpcGeometry(next_id, '', edge)
        doc.addGeometry(geom)

    # Calculate the center X position for the arch based on the
        current span's position
```

```python
114        center_x = TotalOffset + PierThickness + ArchSpan / 2.0
115
116        # Create vertices for two arches (arch1 and arch2 with a
              thickness offset)
117        arch1_vertices = []
118        arch2_vertices = []
119        a = ArchSpan / 2.0   # Half of the major axis
120        b = ArchRise         # Minor axis
121
122        for j in range(int(BricksNumber) + 1):
123            # Calculate the angle for the division of the arch
124                    angle = np.pi * j / BricksNumber
125            # Calculate and add the vertices for the first arch
126                x1 = center_x + a * np.cos(angle)
127            z1 = PierHeight + b * np.sin(angle)
128            vertex1 = FxOccBuilder.makeVertex(x1, 0.0, z1)
129            arch1_vertices.append(vertex1)
130
131                    # Calculate and add the vertices for the second
                          arch with the thickness offset
132            x2 = center_x + a * np.cos(angle) + ArchThickness * np.
                  cos(angle)
133            z2 = PierHeight + b * np.sin(angle) + ArchThickness *
                  np.sin(angle)
134            vertex2 = FxOccBuilder.makeVertex(x2, 0.0, z2)
135            arch2_vertices.append(vertex2)
136
137            # Add the vertices to the document
138            next_id1 = doc.geometries.getlastkey(0) + 1
139            geom1 = MpcGeometry(next_id1, '', vertex1)
140            doc.addGeometry(geom1)
141
142            next_id2 = doc.geometries.getlastkey(0) + 1
143            geom2 = MpcGeometry(next_id2, '', vertex2)
144            doc.addGeometry(geom2)
145
146        # Connect the vertices to form the edges of each arch
147        for k in range(len(arch1_vertices) - 1):
148            edge1 = FxOccBuilder.makeEdge(arch1_vertices[k],
                  arch1_vertices[k + 1])
149            next_id1 = doc.geometries.getlastkey(0) + 1
150            geom1 = MpcGeometry(next_id1, '', edge1)
151            doc.addGeometry(geom1)
152
153            edge2 = FxOccBuilder.makeEdge(arch2_vertices[k],
                  arch2_vertices[k + 1])
154            next_id2 = doc.geometries.getlastkey(0) + 1
155            geom2 = MpcGeometry(next_id2, '', edge2)
```

```
156        doc.addGeometry(geom2)

157

158    # Create the edges connecting the corresponding vertices of
           arch1 and arch2 to simulate the thickness
159    min_len = min(len(arch1_vertices), len(arch2_vertices))
160    for k in range(min_len):
161        connecting_edge = FxOccBuilder.makeEdge(arch1_vertices[
               k], arch2_vertices[k])
162        next_id_connecting = doc.geometries.getlastkey(0) + 1
163        geom_connecting = MpcGeometry(next_id_connecting, '',
               connecting_edge)
164        doc.addGeometry(geom_connecting)

165

166    # Add nodes at height = PierHeight + ArchRise/4
167    height_node_z = PierHeight + ArchRise/4
168    left_node_vertex = FxOccBuilder.makeVertex(TotalOffset +
           PierThickness/2, 0.0, height_node_z)
169    right_node_vertex = FxOccBuilder.makeVertex(TotalOffset +
           PierThickness + PierThickness/2 + ArchSpan, 0.0,
           height_node_z)

170

171    next_id_left_node = doc.geometries.getlastkey(0) + 1
172    geom_left_node = MpcGeometry(next_id_left_node, '',
           left_node_vertex)
173    doc.addGeometry(geom_left_node)

174

175    next_id_right_node = doc.geometries.getlastkey(0) + 1
176    geom_right_node = MpcGeometry(next_id_right_node, '',
           right_node_vertex)
177    doc.addGeometry(geom_right_node)

178

179    # Connect these nodes to the corresponding arch nodes
180    left_arch_node = arch2_vertices[-int(len(arch2_vertices) /
           20) - 1]
181    right_arch_node = arch2_vertices[int(len(arch2_vertices) /
           20)]

182

183    left_link_edge = FxOccBuilder.makeEdge(left_node_vertex,
           left_arch_node)
184    next_id_left_link = doc.geometries.getlastkey(0) + 1
185    geom_left_link = MpcGeometry(next_id_left_link, '',
           left_link_edge)
186    doc.addGeometry(geom_left_link)

187

188    right_link_edge = FxOccBuilder.makeEdge(right_node_vertex,
           right_arch_node)
189    next_id_right_link = doc.geometries.getlastkey(0) + 1
```

143

```
190     geom_right_link = MpcGeometry ( next_id_right_link , '',
            right_link_edge )
191     doc.addGeometry ( geom_right_link )
192
193 # After the loop that creates piers and arches , before adding
        the final pier , we add the connection from the middle points
        on top of each pier to the top horizontal line
194
195 # Get the ID of the top horizontal line which connects the
        first and last piers
196 # Assuming it is the last geometry added before this step
197 id_top_horizontal_line = doc.geometries.getlastkey (0)
198
199 # Iterate over each pier and add the connection lines
200 for i in range (0 , NumberSpans +1):
201     pier_offset = i * ( ArchSpan + PierThickness )
202     # Calculate the middle point of the top horizontal side of
            the current pier
203     middle_point_x = pier_offset + ( PierThickness / 2.0)
204     middle_point_vertex = FxOccBuilder.makeVertex (
            middle_point_x , 0.0 , PierHeight )
205
206     # Add this vertex to the document
207     id_middle_point = doc.geometries.getlastkey (0) + 1
208     geom_middle_point = MpcGeometry ( id_middle_point , '',
            middle_point_vertex )
209     doc.addGeometry ( geom_middle_point )
210
211     # Create the edge connecting this middle point to the top
            horizontal line
212     # Assuming the top horizontal line is at the Z level of
            PierHeight + ArchRise + ArchThickness + Backfill_height
213     top_line_vertex = FxOccBuilder.makeVertex ( middle_point_x ,
            0.0 , PierHeight + ArchRise + ArchThickness +
            Backfill_height )
214
215     # Add the vertex for the connection to the top line
216     id_top_line_vertex = doc.geometries.getlastkey (0) + 1
217     geom_top_line_vertex = MpcGeometry ( id_top_line_vertex , '',
            top_line_vertex )
218     doc.addGeometry ( geom_top_line_vertex )
219
220     # Create and add the edge
221     connecting_edge = FxOccBuilder.makeEdge ( middle_point_vertex
            , top_line_vertex )
222     id_connecting_edge = doc.geometries.getlastkey (0) + 1
223     geom_connecting_edge = MpcGeometry ( id_connecting_edge , '',
            connecting_edge )
```

144

```
224        doc.addGeometry(geom_connecting_edge)
225
226 # Adding the final pier after the last arch
227 TotalOffset += ArchSpan + PierThickness
228 pier_final_vertices = [
229        FxOccBuilder.makeVertex(TotalOffset, 0.0, 0.0),
230        FxOccBuilder.makeVertex(TotalOffset, 0.0, PierHeight),
231        FxOccBuilder.makeVertex(TotalOffset + PierThickness, 0.0,
              0.0),
232        FxOccBuilder.makeVertex(TotalOffset + PierThickness, 0.0,
              PierHeight),
233 ]
234
235 for vertex in pier_final_vertices:
236        next_id = doc.geometries.getlastkey(0) + 1
237        geom = MpcGeometry(next_id, '', vertex)
238        doc.addGeometry(geom)
239
240 pier_final_edges = [
241        FxOccBuilder.makeEdge(pier_final_vertices[0],
              pier_final_vertices[1]),
242        FxOccBuilder.makeEdge(pier_final_vertices[0],
              pier_final_vertices[2]),
243        FxOccBuilder.makeEdge(pier_final_vertices[1],
              pier_final_vertices[3]),
244        FxOccBuilder.makeEdge(pier_final_vertices[2],
              pier_final_vertices[3]),
245 ]
246
247 for edge in pier_final_edges:
248        next_id = doc.geometries.getlastkey(0) + 1
249        geom = MpcGeometry(next_id, '', edge)
250        doc.addGeometry(geom)
251
252 # Adding additional vertices
253 x_first_pier_top = 0  # x of the top point of the very first
        Pier
254 x_last_pier_top = TotalOffset + PierThickness  # x of the top
        point of the last pier after the final loop
255
256 # Creating additional vertices
257 vertex_top_first_pier = FxOccBuilder.makeVertex(
        x_first_pier_top, 0.0, PierHeight + ArchRise + ArchThickness
        + Backfill_height)
258 vertex_top_last_pier = FxOccBuilder.makeVertex(x_last_pier_top,
        0.0, PierHeight + ArchRise + ArchThickness +
        Backfill_height)
259
```

```
260  # Adding vertices to the document
261  id_vertex_top_first_pier = doc.geometries.getlastkey(0) + 1
262  geom_vertex_top_first_pier = MpcGeometry(
         id_vertex_top_first_pier, '', vertex_top_first_pier)
263  doc.addGeometry(geom_vertex_top_first_pier)
264
265  id_vertex_top_last_pier = doc.geometries.getlastkey(0) + 1
266  geom_vertex_top_last_pier = MpcGeometry(id_vertex_top_last_pier
         , '', vertex_top_last_pier)
267  doc.addGeometry(geom_vertex_top_last_pier)
268
269  # Correcting the connection line for the first pier
270  connection_line_first_pier_corrected = FxOccBuilder.makeEdge(
         doc.getGeometry(2).shape, geom_vertex_top_first_pier.shape)
271  id_connection_line_first_pier_corrected = doc.geometries.
         getlastkey(0) + 1
272  geom_connection_line_first_pier_corrected = MpcGeometry(
         id_connection_line_first_pier_corrected, '',
         connection_line_first_pier_corrected)
273  doc.addGeometry(geom_connection_line_first_pier_corrected)
274
275  # Connect the top of the last pier to the last added vertex
276  connection_line_last_pier = FxOccBuilder.makeEdge(
         pier_final_vertices[3], vertex_top_last_pier)
277  id_connection_line_last_pier = doc.geometries.getlastkey(0) + 1
278  geom_connection_line_last_pier = MpcGeometry(
         id_connection_line_last_pier, '', connection_line_last_pier)
279  doc.addGeometry(geom_connection_line_last_pier)
280
281  # Connect the two added vertices
282  high_vertices_connection_line = FxOccBuilder.makeEdge(
         vertex_top_first_pier, vertex_top_last_pier)
283  id_high_vertices_connection_line = doc.geometries.getlastkey(0)
          + 1
284  geom_high_vertices_connection_line = MpcGeometry(
         id_high_vertices_connection_line, '',
         high_vertices_connection_line)
285  doc.addGeometry(geom_high_vertices_connection_line)
286
287
288
289  # ----- VISUALIZING GEOMETRIC MODEL ----- #
290
291  # Regenerate the view to visualize the new geometry
292  App.runCommand('Regenerate', str(2))
293
294  # Print completion message
295  print("Geometry creation completed!")
```

Listing 7.1.   Python Code to generate geometries of the model.

Chapter 8

Annex B - STKO items

The followings Figures 8.1; 8.2; 8.3; 8.4; 8.5; 8.6; 8.7; 8.8; 8.9; 8.10; 8.11; 8.12; 8.13; 8.14; 8.15; 8.16; 8.17; 8.18; 8.19 are the items used to assess the properties of the bridge and to run the analysis.
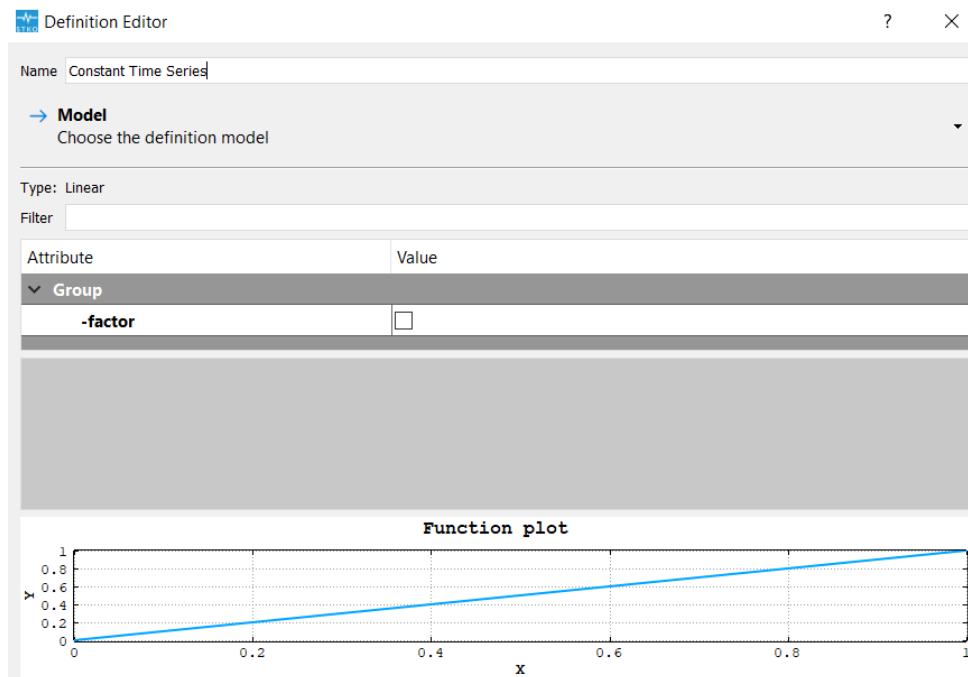
Figure 8.1.   Definitions: Constant Time Series.
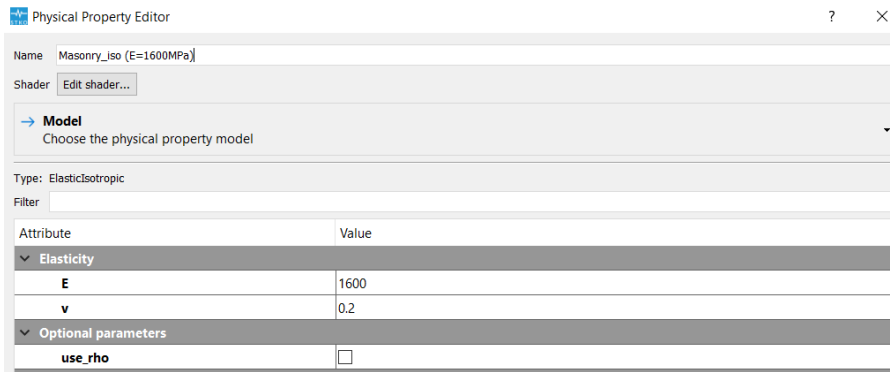
Figure 8.2.   Physical Properties: Masonry material.
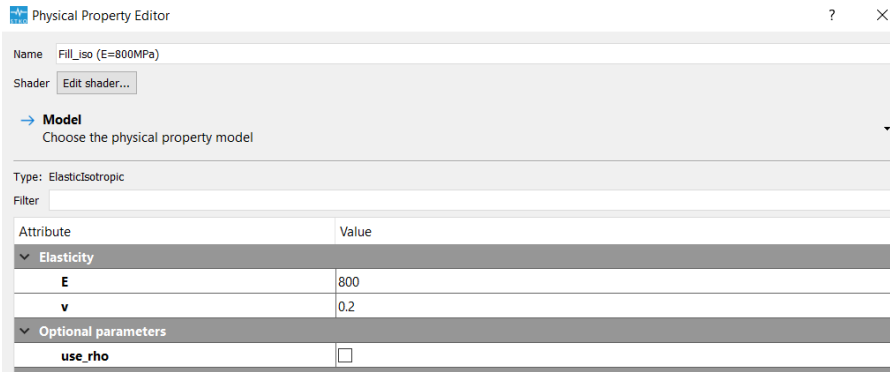
Figure 8.3.   Physical Properties: Fill material.
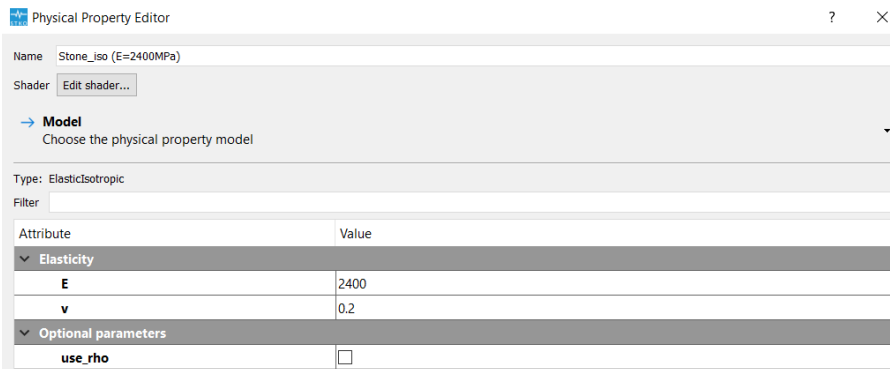
Figure 8.4.   Physical Properties: Stone material.
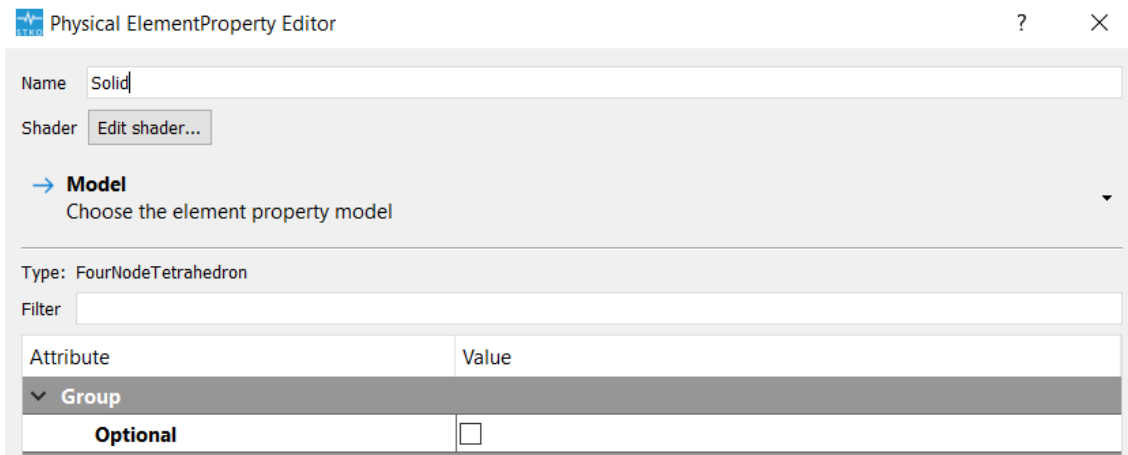
Figure 8.5.   Physical Properties: Discretization.
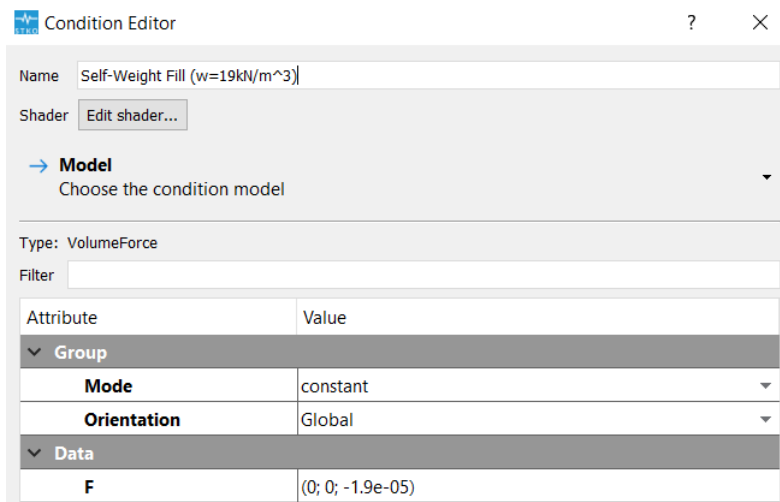
Figure 8.6.   Condition: Self-Weight of Fill material.
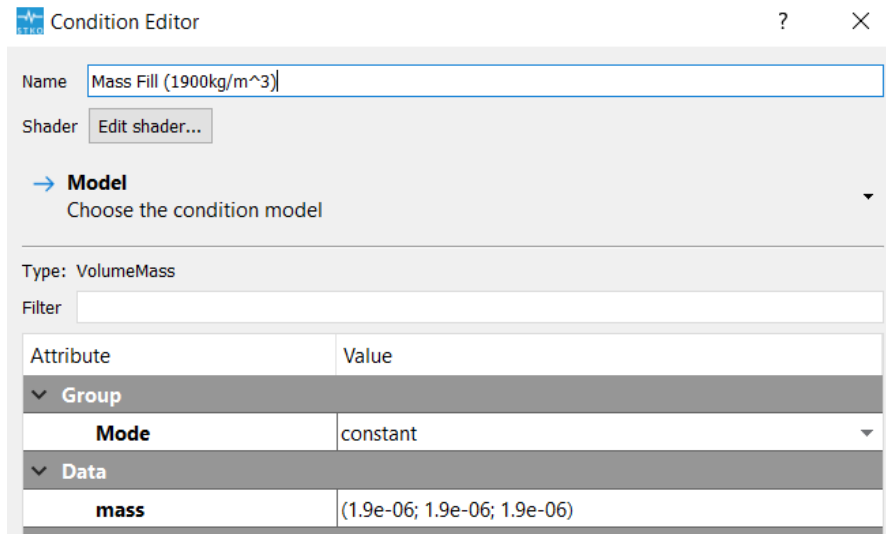
Figure 8.7.   Condition: Mass of Fill material.
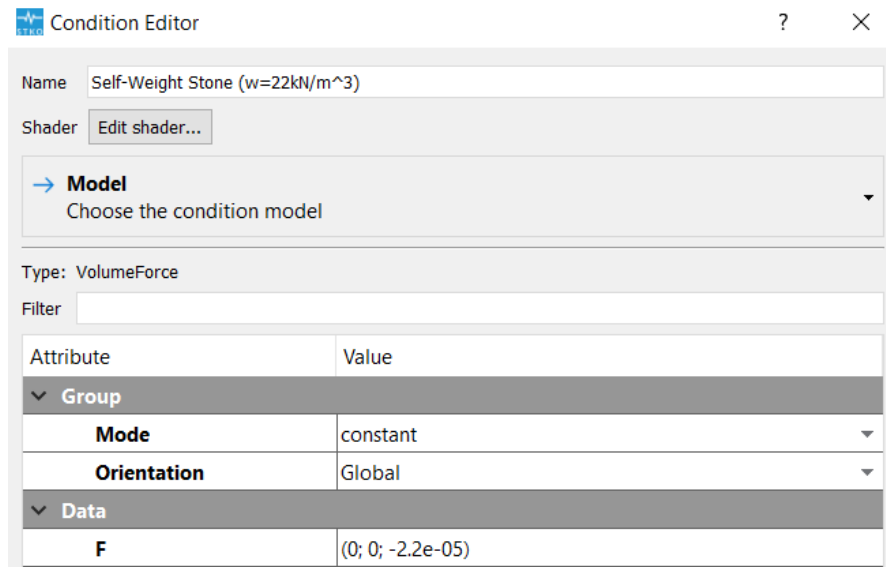
Figure 8.8.   Condition: Self-Weight of Stone material.

152
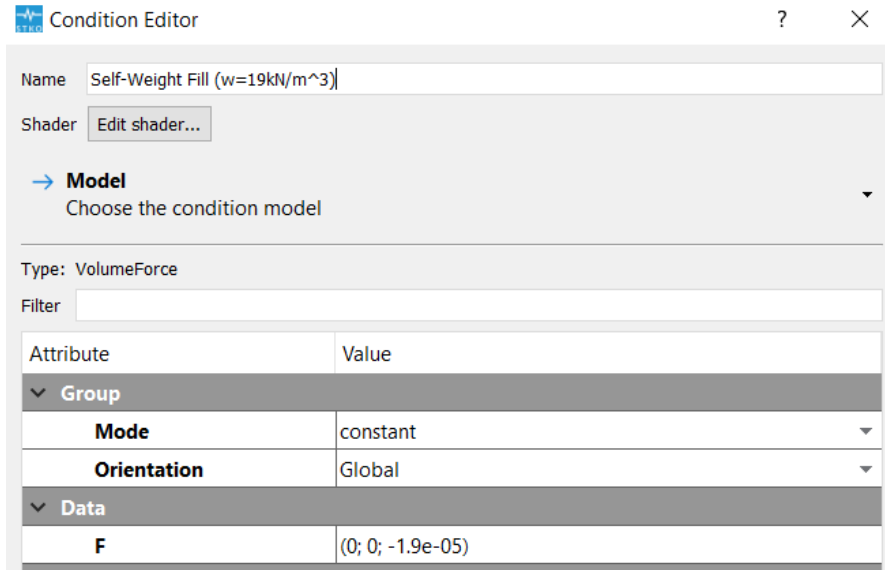
Figure 8.9.   Condition: Mass of Stone material.
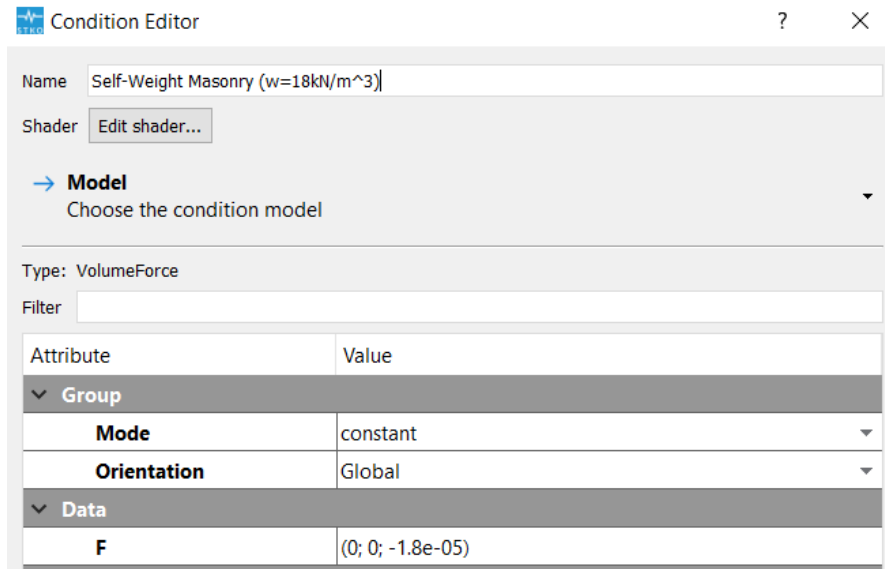
Figure 8.10.   Condition: Self-Weight of Masonry material.

153
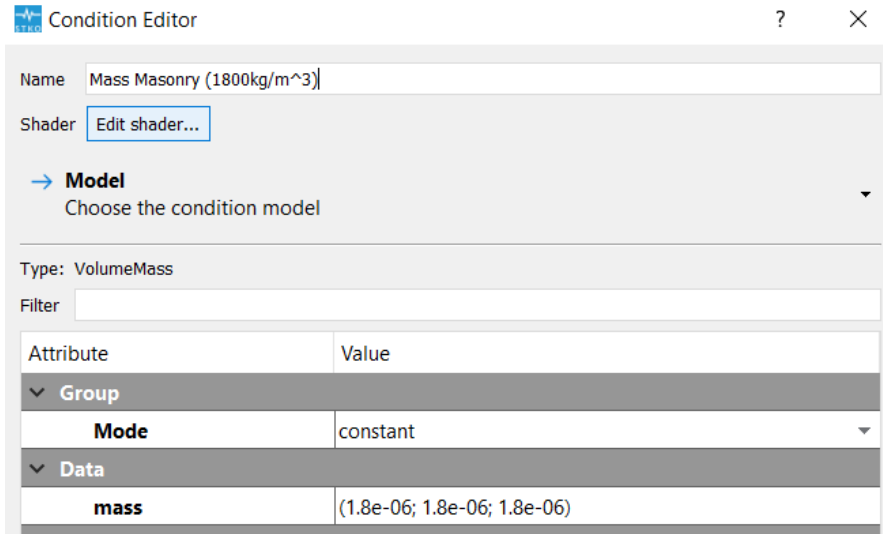
Figure 8.11.   Condition: Mass of Masonry material.
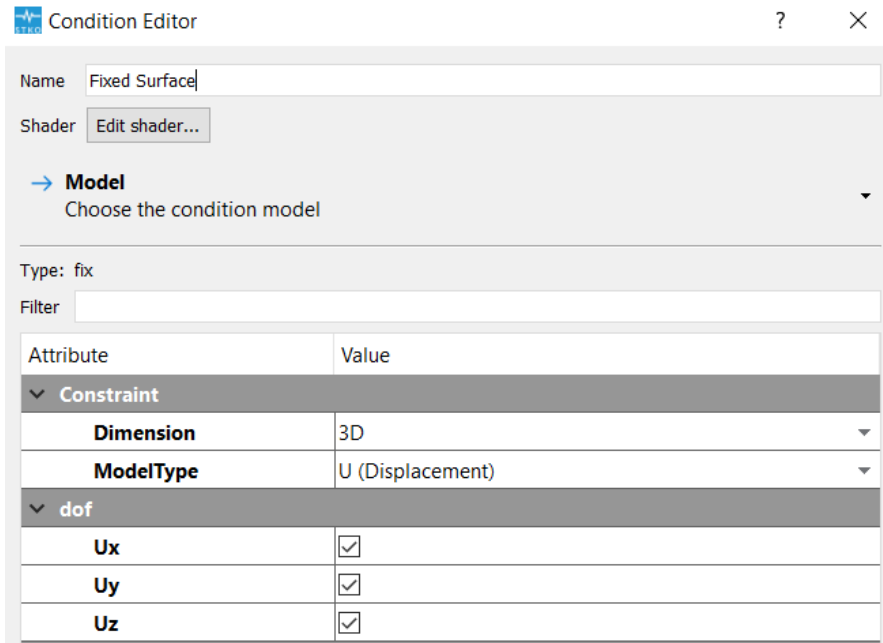
Figure 8.12.   Boundary condition: Fixed surface.

154
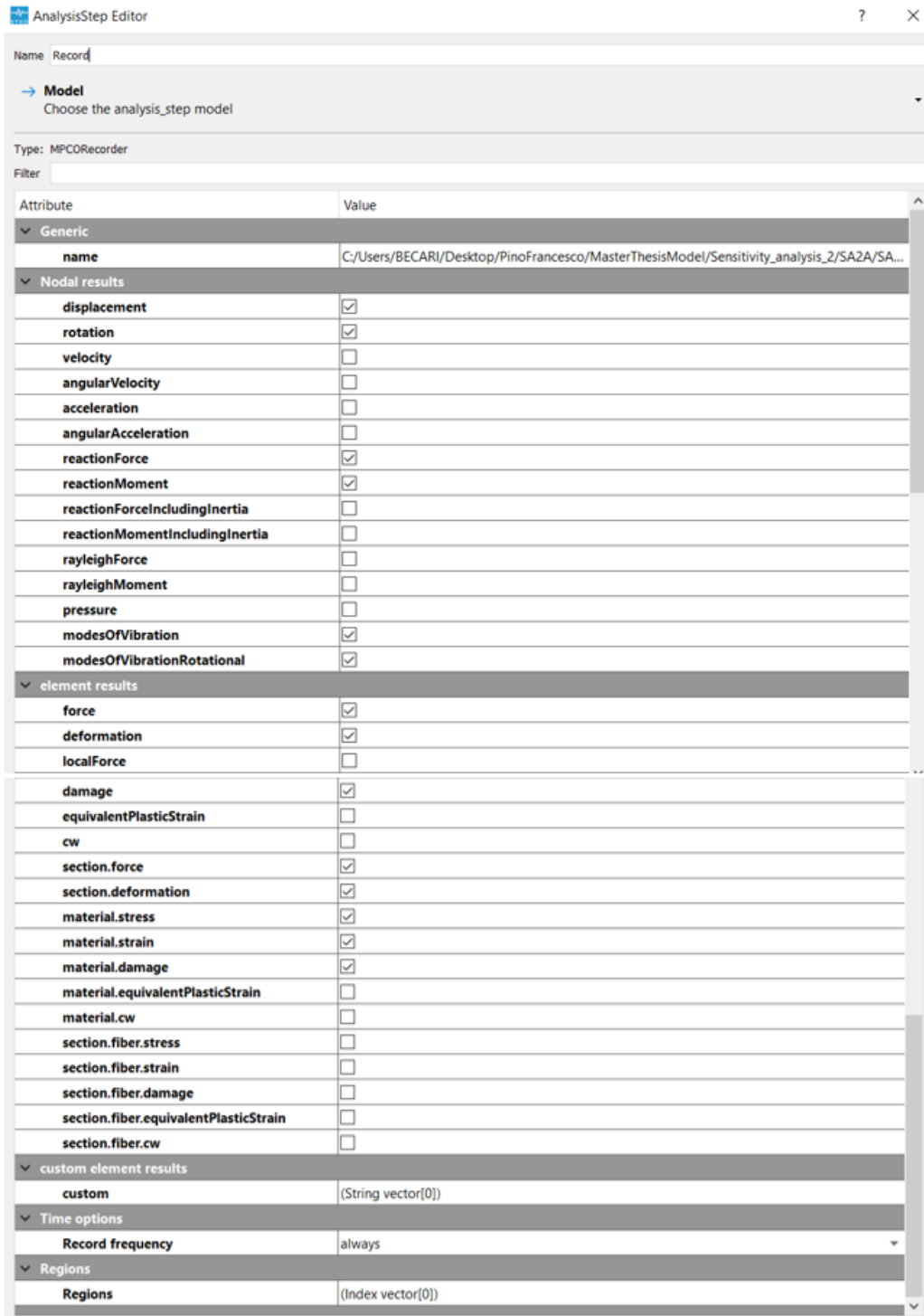
Figure 8.13.   Analysis Step: Record.
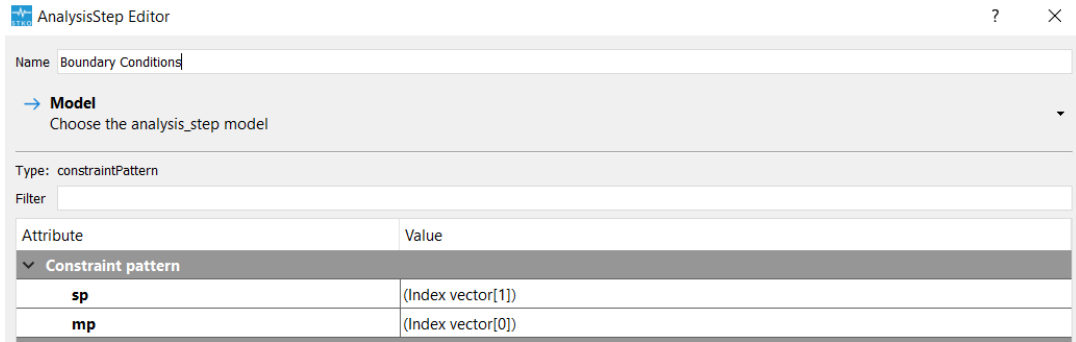
Figure 8.14.   Analysis Step: Boundary conditions.
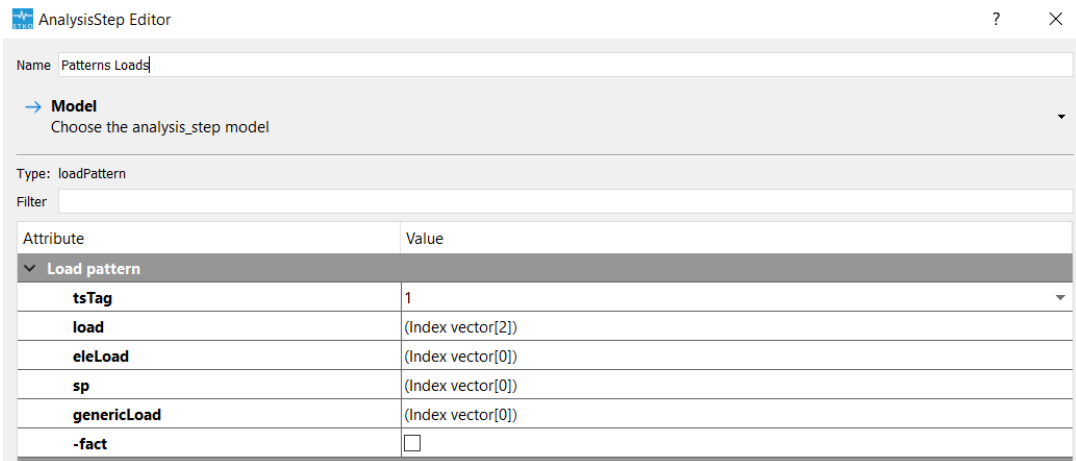
Figure 8.15.   Analysis Step: Patterns Loads.

156
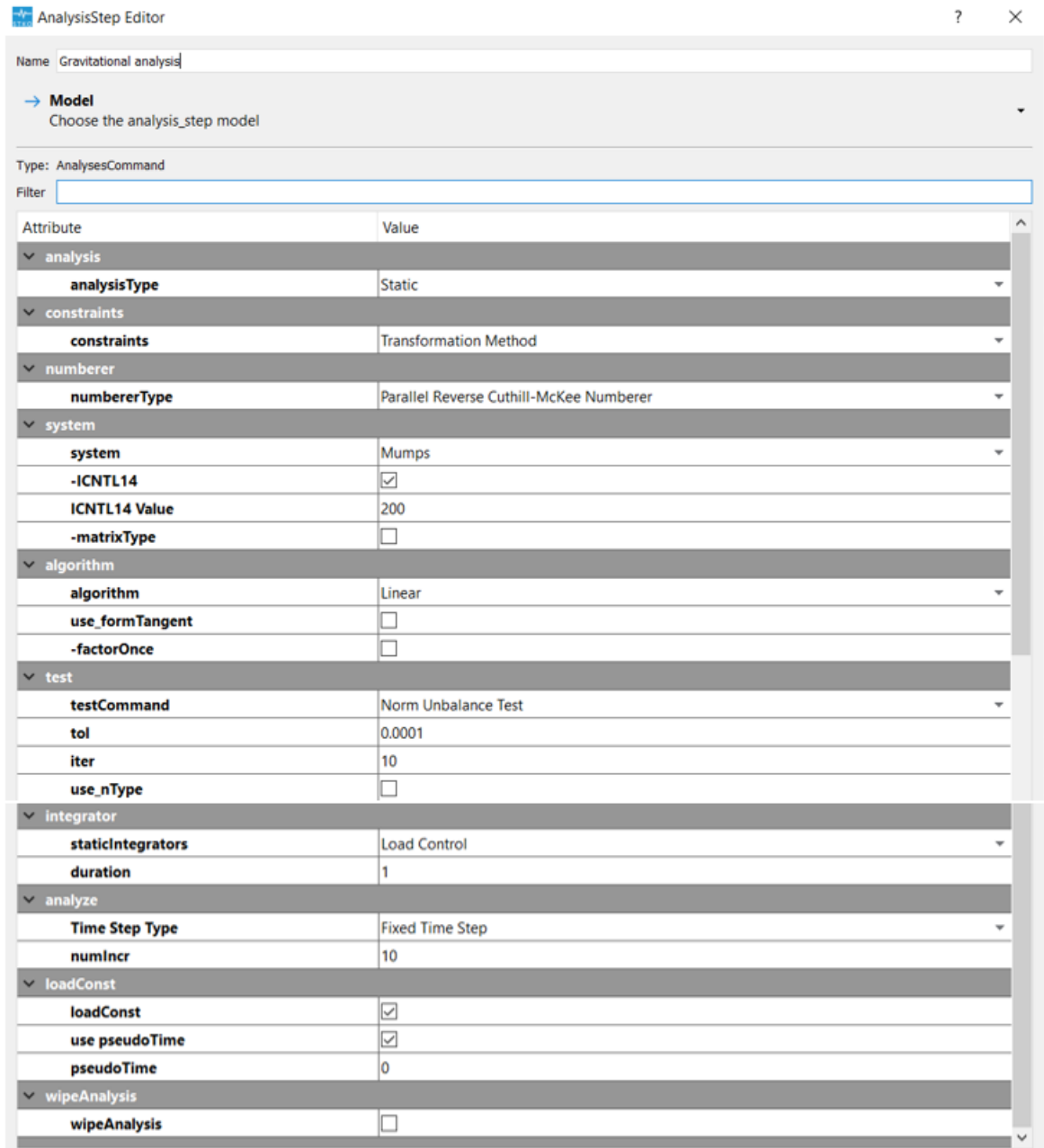
Figure 8.16.   Analysis Step: Gravitational analysis.
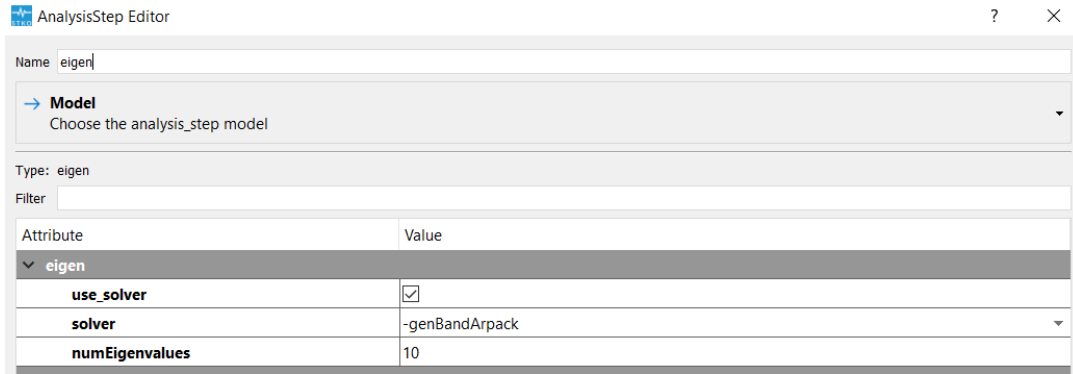
Figure 8.17.   Analysis Step: Eigenvalues.
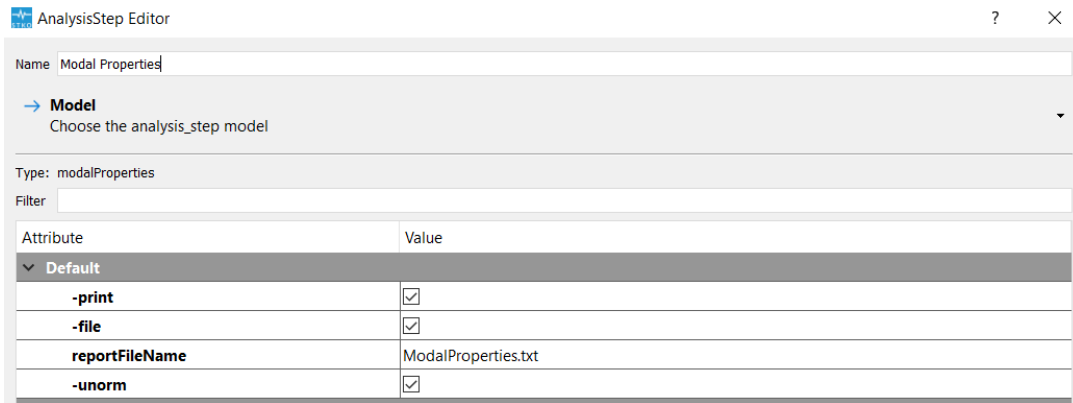
Figure 8.18.   Analysis Step: Modal properties.
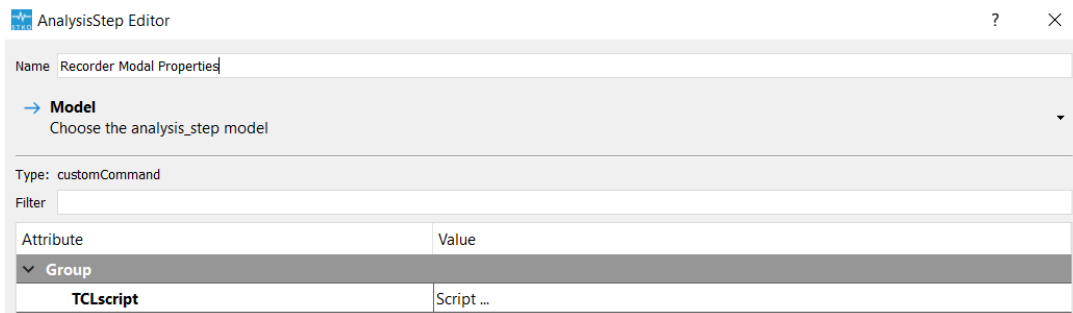
Figure 8.19.   Analysis Step: Recorder Modal properties.

Chapter 9

Annex C - Bridges data

Table 9.1 includes data related to the bridges in Spain and Portugal from Claudia Lemos's thesis [21].

Table 9.2 contains data related to the bridges in the Bragança region, Portugal, from João Jorge Carrazedo de Jesus's thesis [18].

Tables 9.3 and 9.4 encompasses data from the Monte Carlo analysis used for the parametric study and the obtained frequencies.

Table 9.1: Bridges data from Claudia Lemos's thesis [21].

#	Span [m]	Rise / Span Ratio [-]	Thickness / Span Ratio [-]	Bridge Width [m]	Pier Thick-ness [m]	Pier Height [m]
1	7.00	0.6214	0.0843	-	-	-
2	5.00	0.3900	0.0880	-	2.520	2.280
	8.03	0.3238	0.0635	-	2.730	2.550
	7.64	0.3298	0.0654	-	-	-
3	7.07	0.4144	0.0721	-	5.400	2.200
	8.49	0.5866	0.0624	-	5.450	2.440
	2.01	0.4279	0.2289	-	-	-
4	4.47	0.3445	0.0940	-	3.670	2.300
	5.92	0.2990	0.0709	-	3.020	2.900
	5.81	0.3029	0.0878	-	2.810	3.890

Continued on next page

Table 9.1 – continued from previous page

#	Span [m]	Rise / Span Ratio [-]	Thickness / Span Ratio [-]	Bridge Width [m]	Pier Thick- ness [m]	Pier Height [m]
	7.04	0.2401	0.0767	-	2.980	3.520
	5.40	0.2056	0.0926	-	2.230	2.950
	3.82	0.2749	0.0995	-	-	-
5	4.67	0.2677	0.2056	-	3.750	2.390
	5.67	0.3298	0.2363	-	4.210	3.090
	13.40	0.3485	0.0955	-	5.310	3.870
	6.00	0.3250	0.1917	-	-	-
6	5.51	0.2287	0.1143	4.000	3.920	6.640
	13.50	0.3770	0.0496	-	4.710	6.940
	5.31	0.2166	0.1149	-	-	-
7	2.20	0.3227	0.1727	-	2.120	1.070
	2.77	0.2924	0.1408	-	1.860	1.360
	3.99	0.3008	0.1128	-	2.120	1.430
	2.79	0.2724	0.1290	-	1.940	1.210
	1.89	0.1958	0.2063	-	-	-
8	5.81	0.4613	0.1136	3.400	5.040	5.040
	8.78	0.4191	0.0831	-	4.740	5.710
	15.00	0.3127	0.0667	-	3.170	6.430
	2.67	0.5393	0.2022	-	2.290	4.910
	3.59	0.5515	0.1560	-	-	-
9	8.70	0.2977	0.0736	4.200	3.470	2.110
	7.76	0.3518	0.1005	-	3.520	2.230
	5.80	0.2707	0.1052	-	-	-
10	5.59	0.3757	0.1002	-	2.390	1.960
	7.50	0.3680	0.0853	-	-	-

Table 9.1 – continued from previous page

#	Span [m]	Rise / Span Ratio [-]	Thickness / Span Ratio [-]	Bridge Width [m]	Pier Thick-ness [m]	Pier Height [m]
	2.10	0.3429	0.2571	-	-	-
11	5.00	0.3960	0.1360	4.000	-	-
12	5.00	0.7120	0.1220	-	-	-
13	15.00	0.3393	0.0873	-	3.340	10.540
	14.88	0.3468	0.0907	-	3.370	12.280
	14.39	0.3565	0.0896	-	3.400	12.280
	14.60	0.3514	0.0918	-	2.750	10.540
	14.65	0.3590	0.0846	-	-	-
14	11.99	0.2869	0.0575	-	4.390	7.950
	11.99	0.2819	0.0567	-	-	-
15	3.70	0.3838	0.0838	-	-	-
16	3.90	0.3615	0.0923	-	-	-
17	9.00	0.3856	0.0956	-	2.240	16.660
	9.00	0.3878	0.1011	-	2.400	16.660
	9.00	0.3644	0.1111	-	-	-
18	6.83	0.3280	0.1464	-	4.120	11.630
	7.06	0.3201	0.1303	-	4.060	13.250
	7.01	0.3210	0.1170	-	4.190	13.250
	7.05	0.3220	0.1149	-	4.300	13.250
	6.90	0.3304	0.1290	-	3.800	13.250
	6.94	0.3343	0.1282	-	4.290	11.630
	7.07	0.3296	0.1188	-	-	-
19	1.00	0.3400	0.1700	-	-	-
	5.00	0.3640	0.0660	-	-	-
20	7.50	0.4160	0.0480	-	-	-

Table 9.1 – continued from previous page

#	Span [m]	Rise / Span Ratio [-]	Thickness / Span Ratio [-]	Bridge Width [m]	Pier Thick-ness [m]	Pier Height [m]
21	3.01	0.1827	0.0797	-	-	-
22	0.86	0.3837	-	-	-	-
	4.90	0.1653	0.0510	-	-	-
23	8.00	0.3675	0.0488	-	-	-
24	9.00	0.3922	0.0478	-	-	-
25	-	-	-	-	-	-
26	10.08	0.1865	0.0913	-	2.37	7.03
	9.90	0.1899	0.0949	-	2.45	7.03
	9.98	0.1854	0.0942	-	-	-
27	4.01	0.3691	0.0948	-	-	-
28	4.00	0.3625	0.0975	-	-	-
29	4.00	0.4075	0.1650	3.00	-	-
30	7.10	0.4014	0.1070	-	2.44	9.39
	7.02	0.4074	0.1083	-	-	-
31	10.01	0.0549	0.1798	-	-	-
32	8.88	0.4989	0.1284	6.70	3.02	1.71
	8.82	0.5023	0.1134	-	3.09	3.71
	8.83	0.5017	0.1133	-	2.93	3.71
	8.97	0.4939	0.0959	-	2.92	3.14
	8.87	0.4994	0.0970	-	3.04	2.57
	8.73	0.5074	0.1145	-	-	-
33	6.17	0.3015	0.1313	6.74	-	-
	6.35	0.2929	0.1276	-	-	-
	6.34	0.2934	0.1278	-	-	-
	6.17	0.3776	0.1313	-	2.24	1.63

Table 9.1 – continued from previous page

#	Span [m]	Rise / Span Ratio [-]	Thickness / Span Ratio [-]	Bridge Width [m]	Pier Thick-ness [m]	Pier Height [m]
	6.35	0.3669	0.1465	-	2.20	1.63
	6.34	0.3675	0.1467	-	2.31	1.63
	6.09	0.3826	0.1527	-	2.30	1.63
	6.24	0.3734	0.1490	-	2.28	1.63
	6.24	0.3734	0.1298	-	2.33	1.63
	6.28	0.3710	0.1290	-	6.28	1.63
	6.27	0.3716	0.1292	-	3.75	1.63
	6.20	0.3371	0.1306	-	-	-
34	8.55	0.4971	0.0819	6.25	2.50	1.50
	9.14	0.4376	0.0766	-	2.50	0.88
	9.46	0.4757	0.0740	-	2.55	0.75
	8.89	0.5062	0.0787	-	2.85	1.00
	8.98	0.4176	0.0780	-	2.35	1.00
	8.64	0.4630	0.0810	-	-	-
35	3.42	0.4737	0.1316	7.10	-	-
	2.30	0.5087	0.1957	-	-	-
	3.40	0.4676	0.1471	-	-	-
	11.54	0.4723	0.0555	-	2.06	0.00
	9.85	0.4843	0.0650	-	1.80	0.00
	7.92	0.5164	0.0808	-	2.65	0.00
	7.30	0.5603	0.0877	-	2.55	0.00
	7.60	0.4605	0.0842	-	-	-
36	7.50	0.4667	0.1333	6.70	2.95	8.60
	7.80	0.5064	0.1282	-	3.00	10.70
	10.50	0.4876	0.0952	-	2.85	10.81

Table 9.1 – continued from previous page

#	Span [m]	Rise / Span Ratio [-]	Thickness / Span Ratio [-]	Bridge Width [m]	Pier Thick- ness [m]	Pier Height [m]
	8.30	0.4482	0.1205	-	2.85	6.98
	9.00	0.5167	0.1111	-	-	-
37	5.08	0.5079	0.1516	4.00	-	-
38	7.43	0.4428	0.0633	7.50	-	-
39	4.75	0.3684	0.1895	4.00	-	-
40	8.57	0.2964	0.0653	3.50	5.62	2.00
	11.42	0.3923	0.0525	-	6.60	1.96
	12.05	0.3967	0.0548	-	5.77	1.53
	15.01	0.3757	0.0460	-	5.42	2.40
	16.40	0.3037	0.0384	-	5.35	2.22
	12.07	0.3447	0.0530	-	-	-
41	7.03	0.4680	0.1138	3.50	3.81	2.66
	9.71	0.4974	0.0824	-	4.25	3.23
	13.35	0.4757	0.0599	-	6.09	3.15
	10.93	0.4172	0.0732	-	11.19	3.15
	9.15	0.4175	0.0874	-	6.37	2.99
	8.31	0.4777	0.0963	-	5.29	1.99
	7.87	0.5197	0.1017	-	8.30	1.76
	8.75	0.4194	0.0914	-	-	-
42	8.09	0.4536	0.0841	3.00	2.43	2.46
	6.36	0.5031	0.1006	-	2.57	2.38
	7.98	0.4586	0.0727	-	-	-
43	6.60	0.4985	0.0985	3.44	3.41	4.17
	11.80	0.3525	0.0703	-	3.69	2.65
	9.40	0.4064	0.0809	-	-	-

Table 9.1 – continued from previous page

#	Span [m]	Rise / Span Ratio [-]	Thickness / Span Ratio [-]	Bridge Width [m]	Pier Thick-ness [m]	Pier Height [m]
	2.70	0.6296	0.1889	-	-	-
44	5.00	0.6800	0.0900	7.00	-	-
45	7.18	0.3231	0.0682	-	2.40	-
	7.20	0.3208	0.0653	-	2.87	-
	7.50	0.3267	0.0533	-	2.61	-
	6.99	0.3777	0.0687	-	-	-
46	2.40	0.4125	0.1083	-	1.26	-
	4.40	0.3227	0.1000	-	-	-
47	3.25	0.5908	0.1108	-	5.06	2.29
	10.75	0.3553	0.0586	-	5.05	3.18
	8.50	0.3306	0.0706	-	-	-
48	5.24	0.3340	0.1107	-	5.38	-
	10.50	0.2552	0.0505	-	-	-
49	16.72	0.6830	0.0586	-	-	-
50	6.39	0.4194	0.0720	-	2.75	-
	6.07	0.3641	0.1186	-	4.74	-
	10.55	0.3422	0.0569	-	5.42	-
	9.68	0.3171	0.0692	-	-	-
51	18.00	0.2100	0.0561	-	-	-
52	16.00	0.1688	0.0469	6.70	-	-
53	4.90	0.5184	0.1204	4.90	-	-
54	4.90	0.5224	0.1204	4.90	-	-
55	2.92	0.4418	0.1849	5.20	2.97	0.86
	9.04	0.5000	0.0774	3.08	1.08	-
	3.59	0.4206	0.1950	1.51	1.29	-

Table 9.1 – continued from previous page

#	Span [m]	Rise / Span Ratio [-]	Thickness / Span Ratio [-]	Bridge Width [m]	Pier Thick-ness [m]	Pier Height [m]
	2.28	0.4737	0.1886	-	-	-
56	1.93	0.5078	0.5026	4.87	2.65	2.37
	4.55	0.3978	0.1758	2.45	2.09	-
	1.95	0.5026	0.4974	-	-	-
57	8.92	0.5157	0.0953	6.15	4.70	0.00
	8.92	0.5348	0.0953	-	-	-
58	4.10	0.5488	0.2171	6.00	-	-
59	14.50	-	0.0724	5.74	-	-
	3.12	-	0.3365	-	-	-
60	18.07	0.4776	0.0498	3.90	-	-
61	6.05	0.4529	0.0909	6.30	4.45	9.32
	18.76	0.3214	0.0362	4.12	8.63	-
	8.76	0.3596	0.0628	-	-	-
62	9.90	0.6313	0.1212	6.15	6.01	5.77
	10.75	0.6260	0.0670	4.30	6.25	-
	4.41	0.6531	0.2177	5.32	3.85	-
	20.29	0.4500	0.0473	6.28	5.29	-
	10.36	0.6033	0.0927	-	-	-
63	5.60	0.5125	0.1018	5.00	4.27	1.91
	6.70	0.5716	0.0955	4.60	2.23	-
	10.36	0.4315	0.0618	4.61	3.83	-
	10.40	0.4615	0.0615	4.76	3.19	-
	9.20	0.6587	0.0696	5.40	2.11	-
	9.72	0.6564	0.0658	5.10	2.55	-
	10.80	0.5315	0.0593	7.54	3.19	-

Table 9.1 – continued from previous page

#	Span [m]	Rise / Span Ratio [-]	Thickness / Span Ratio [-]	Bridge Width [m]	Pier Thickness [m]	Pier Height [m]
	7.83	0.4240	0.0817	-	-	-
64	5.34	0.4569	0.1367	7.10	3.32	0.49
	5.26	0.5095	0.1388	3.30	0.73	-
	5.29	0.4159	0.1153	2.91	0.73	-
	5.33	0.4034	0.1370	-	-	-
65	3.40	-	0.2941	6.75	3.10	-
	5.90	-	0.1695	3.10	-	-
	7.60	-	0.1316	3.20	-	-
	7.60	-	0.1316	3.10	-	-
	5.90	-	0.1695	3.10	-	-
	3.40	-	0.2941	-	-	-
66	2.69	0.5019	0.1413	7.25	-	-
	10.38	0.4817	0.0665	-	4.49	2.31
	10.00	0.4620	0.0770	-	-	-
	6.54	0.4235	0.0581	-	-	-
67	9.50	0.4842	0.1053	6.70	2.80	1.75
	9.75	0.5026	0.1026	-	2.80	2.00
	9.60	0.4792	0.1042	-	3.00	2.00
	9.80	0.4643	0.1020	-	2.80	2.00
	9.40	0.5213	0.1064	-	2.80	2.50
	10.10	0.4554	0.0990	-	2.60	2.60
	9.65	0.5181	0.1036	-	3.60	2.60
	9.80	0.4694	0.1020	-	3.50	2.50
	9.60	0.4792	0.1042	-	2.80	1.75
	9.80	0.5000	0.1020	-	2.90	1.50

Table 9.1 – continued from previous page

#	Span [m]	Rise / Span Ratio [-]	Thickness / Span Ratio [-]	Bridge Width [m]	Pier Thickness [m]	Pier Height [m]
	9.66	0.5072	0.1035	-	2.90	1.00
	9.48	0.4852	0.1055	-	3.00	0.75
	9.51	0.4732	0.1052	-	2.85	0.50
	9.68	0.4907	0.1033	-	3.00	0.00
	9.54	0.4979	0.1048	-	-	-
68	13.90	0.4683	0.1511	7.80	6.08	8.54
	22.53	0.4829	0.0932	-	6.70	18.14
	27.50	0.5044	0.0764	-	8.29	35.21
	28.80	0.5299	0.0729	-	8.00	35.21
	23.50	0.4996	0.0894	-	6.80	10.67
	13.50	0.5141	0.1556	-	-	-
69	4.73	0.4799	0.1163	4.60	2.83	5.32
	7.78	0.3997	0.0913	-	3.62	4.09
	7.70	0.3987	0.0922	-	2.80	4.91
	4.74	0.4662	0.1287	-	-	-
70	8.40	0.4500	0.0905	6.10	7.55	3.40
	18.85	0.5294	0.0403	-	7.91	3.02
	25.20	0.5702	0.0302	-	9.24	7.56
	37.98	0.4181	0.0237	-	9.95	7.56
	26.85	0.4507	0.0335	-	8.40	5.29
	18.59	0.5697	0.0446	-	9.07	3.02
	12.28	0.4308	0.0619	-	-	-
71	10.76	0.3699	0.0483	4.60	-	-
72	13.76	0.4331	0.0676	5.31	6.29	7.79
	19.55	0.3350	0.0460	-	5.48	7.52

Table 9.1 – continued from previous page

#	Span [m]	Rise / Span Ratio [-]	Thickness / Span Ratio [-]	Bridge Width [m]	Pier Thick- ness [m]	Pier Height [m]
	24.48	0.3031	0.0408	-	5.87	8.77
	14.51	0.2963	0.0586	-	5.41	2.14
	5.39	0.5436	0.1800	-	-	-
73	7.13	0.3885	0.1304	5.64	3.86	2.20
	11.15	0.4126	0.0879	-	4.44	2.75
	13.40	0.3537	0.0701	-	4.47	2.70
	16.50	0.3630	0.0570	-	6.48	2.59
	17.05	0.4123	0.0587	-	6.28	2.08
	16.70	0.4269	0.0533	-	6.17	2.24
	15.70	0.4115	0.0548	-	5.83	0.87
	12.11	0.4021	0.0677	-	4.58	0.99
	8.20	0.3817	0.1122	-	-	-

Table 9.2: Bridges data from João Jorge Carrazedo de Jesus's thesis [18].

#	Span [m]	Rise / Span Ratio [-]	Thickness / Span Ratio [-]	Backfill height above the arch crown [m]	Pier Thickness [m]	Pier Height [m]
1	10.00	0.50	0.06	0.84	2.00	13.15
2	4.00	0.50	0.13	1.01		
3	15.15	0.50	0.06	0.66		
4	6.90	0.51	0.08	0.77	1.80	6.80
5	4.00	0.50	0.13	0.68		
6	2.00	0.50	0.19	0.40		
7	5.30	0.49	0.10	0.75		
8	3.20	0.23	0.13	0.75		
9	6.00	0.50	0.13	1.25		
10	5.10	0.20	0.09	0.79		
11	4.00	0.50	0.13	1.60		
12	6.00	0.50	0.10	1.54		
13	13.20	0.50	0.06	4.45	4.40	5.85
14	4.00	0.50	0.10	0.50		
15	6.00	0.50	0.10	1.45		
16	5.80	0.52	0.10	1.43		
17	8.00	0.25	0.09	1.30		
18	10.85	0.46	0.06	1.20		
19	11.00	0.50	0.06	1.30		
20	4.25	0.47	0.11	0.90		
21	10.00	0.13	0.07	0.50	2.00	2.10

Table 9.2 – continued from previous page

#	Span [m]	Rise / Span Ratio [-]	Thickness / Span Ratio [-]	Backfill height above the arch crown [m]	Pier Thickness [m]	Pier Height [m]
22	4.00	0.50	0.13	0.82		
23	14.95	0.16	0.06	0.66	1.50	6.00
24	4.00	0.50	0.13	1.00		
25	3.90	0.51	0.14	0.65		
26	7.00	0.29	0.08	0.75	1.80	4.15
27	9.00	0.50	0.11	0.60	2.00	15.80
28	10.80	0.46	0.10	0.98		
29	4.00	0.31	0.14	0.67		
30	2.00	0.50	0.19	3.80	1.00	3.00
31	4.00	0.50	0.14	0.95		
32	3.00	0.50	0.17	0.81		
33	2.88	0.50	0.14	1.85		
34	3.00	0.50	0.13	0.60		
35	2.90	0.52	0.14	0.50		
36	4.00	0.50	0.11	0.95		
37	9.90	0.50	0.07	1.05	2.20	4.25
38	3.97	0.31	0.10	1.04		
39	12.20	0.49	0.06	0.60		
40	3.90	0.50	0.10	0.75		
41	9.00	0.49	0.08	0.95		
42	8.00	0.50	0.07	0.75		
43	7.90	0.60	0.08	0.50		

Table 9.2 – continued from previous page

#	Span [m]	Rise / Span Ratio [-]	Thickness / Span Ratio [-]	Backfill height above the arch crown [m]	Pier Thick-ness [m]	Pier Height [m]
44	2.00	0.50	0.25	2.50		
45	5.00	0.52	0.10	0.75		
46	3.00	0.16	0.13	0.95		
47	5.00	0.13	0.12	0.50		
48	10.00	0.20	0.06	1.10		
49	8.15	0.49	0.07	0.65		
50	10.30	0.50	0.06	0.65		
51	13.30	0.49	0.06	3.25	3.35	2.15
52	4.00	0.50	0.13	1.65		
53	4.10	0.11	0.13	0.26		
54	4.00	0.50	0.18	6.25		
55	10.45	0.48	0.06	0.85		
56	7.00	0.14	0.10	1.63		
57	6.00	0.50	0.10	1.26		
58	2.60	0.42	0.19	1.00		
59	8.95	0.45	0.08	0.45	2.50	1.80
60	5.00	0.50	0.10	0.65		
61	10.00	0.49	0.06	0.70	3.20	2.00
62	6.00	0.50	0.10	0.63		
63	7.00	0.11	0.10	1.50		
64	2.90	0.50	0.19	0.45		
65	6.55	0.53	0.09	2.35		

Table 9.2 – continued from previous page

#	Span [m]	Rise / Span Ratio [-]	Thickness / Span Ratio [-]	Backfill height above the arch crown [m]	Pier Thickness [m]	Pier Height [m]
66	7.00	0.48	0.10	0.75		
67	6.55	0.50	0.11	1.10		
68	1.95	0.41	0.26	3.00		
69	12.00	0.33	0.08	0.55	3.25	1.65
70	7.50	0.47	0.17	0.05	3.80	2.50
71	10.50	0.51	0.07	1.20	4.30	2.63

Table 9.3: Bridges data for Parametric Analysis.

#	Span [m]	Rise / Span Ratio [-]	Thickness / Span Ratio [-]	Width [m]	Backfill height above the arch crown [m]	Bridge Mass [kg]
1	24.867	0.396	0.033	4.910	1.274	5.51E+06
2	23.800	0.453	0.042	6.271	1.886	6.93E+06
3	23.267	0.404	0.069	6.796	0.870	7.23E+06
4	21.667	0.497	0.118	4.264	1.632	5.23E+06
5	15.533	0.156	0.143	6.103	1.789	3.25E+06
6	12.867	0.269	0.144	7.414	0.415	2.83E+06
7	7.533	0.314	0.219	4.858	1.215	1.07E+06
8	17.933	0.224	0.118	5.056	2.256	3.61E+06
9	23.000	0.123	0.038	7.443	0.538	4.15E+06
10	9.400	0.492	0.201	5.289	1.254	1.81E+06
11	22.467	0.383	0.051	4.635	1.678	4.69E+06
12	6.733	0.180	0.224	4.770	0.801	7.71E+05
13	11.533	0.173	0.222	6.513	2.466	2.82E+06
14	9.133	0.371	0.191	5.794	1.887	1.86E+06
15	8.333	0.265	0.149	4.907	0.561	9.99E+05
16	17.133	0.134	0.169	6.571	1.795	4.15E+06
17	10.467	0.280	0.224	6.710	2.363	2.71E+06
18	24.333	0.164	0.035	5.453	1.492	4.12E+06
19	14.733	0.423	0.114	5.298	2.020	3.33E+06
20	19.533	0.470	0.125	5.440	2.372	5.86E+06
21	5.133	0.103	0.244	6.726	2.118	9.17E+05

Table 9.3 – continued from previous page

#	Span [m]	Rise / Span Ratio [-]	Thickness / Span Ratio [-]	Width [m]	Backfill height above the arch crown [m]	Bridge Mass [kg]
22	16.600	0.353	0.125	4.487	0.532	2.78E+06
23	16.067	0.364	0.147	7.618	1.022	4.97E+06
24	21.933	0.212	0.043	5.241	0.506	3.35E+06
25	18.200	0.449	0.148	5.798	0.481	4.83E+06
26	23.533	0.238	0.091	7.349	0.476	6.34E+06
27	24.067	0.113	0.033	6.734	1.539	4.49E+06
28	8.067	0.147	0.223	4.579	1.548	1.04E+06
29	8.600	0.419	0.234	6.402	2.435	2.16E+06
30	20.867	0.373	0.042	4.329	1.634	3.75E+06
31	5.933	0.415	0.236	7.771	1.336	1.34E+06
32	11.800	0.349	0.186	7.350	1.620	3.29E+06
33	9.933	0.429	0.178	5.519	0.870	1.83E+06
34	19.267	0.118	0.097	6.733	2.022	4.32E+06
35	7.267	0.276	0.228	7.968	0.880	1.57E+06
36	21.133	0.207	0.076	4.444	1.932	3.49E+06
37	20.333	0.303	0.093	6.895	2.238	6.22E+06
38	15.000	0.460	0.118	6.980	2.120	4.74E+06
39	8.867	0.233	0.218	6.900	1.266	1.84E+06
40	7.000	0.341	0.215	4.558	1.411	9.44E+05
41	16.867	0.108	0.113	5.970	1.225	2.92E+06
42	5.400	0.192	0.246	4.016	0.367	4.55E+05
43	6.200	0.441	0.220	4.851	2.022	9.75E+05

Table 9.3 – continued from previous page

#	Span [m]	Rise / Span Ratio [-]	Thickness / Span Ratio [-]	Width [m]	Backfill height above the arch crown [m]	Bridge Mass [kg]
44	7.800	0.201	0.198	4.367	1.569	9.62E+05
45	13.133	0.434	0.163	5.493	0.973	2.82E+06
46	18.467	0.251	0.094	6.207	2.460	4.66E+06
47	22.733	0.356	0.040	7.039	0.727	6.20E+06
48	14.467	0.129	0.152	5.803	1.010	2.48E+06
49	5.667	0.395	0.209	5.317	0.892	7.72E+05
50	10.200	0.318	0.178	7.716	1.054	2.49E+06
51	17.400	0.481	0.075	7.303	0.851	5.31E+06
52	20.600	0.234	0.172	6.484	2.231	6.42E+06
53	9.667	0.259	0.186	7.499	0.799	2.08E+06
54	14.200	0.161	0.190	4.184	1.351	2.04E+06
55	22.200	0.486	0.061	6.990	1.223	7.71E+06
56	16.333	0.289	0.166	5.500	1.400	3.66E+06
57	15.267	0.140	0.093	4.867	2.296	2.39E+06
58	10.733	0.381	0.219	7.100	1.137	2.79E+06
59	12.600	0.322	0.203	5.454	0.316	2.33E+06
60	21.400	0.244	0.061	4.822	2.276	4.08E+06
61	11.000	0.397	0.188	4.056	1.581	1.69E+06
62	13.400	0.444	0.163	7.901	1.843	4.61E+06
63	11.267	0.221	0.208	6.583	1.650	2.56E+06
64	18.733	0.325	0.069	7.255	0.542	4.69E+06
65	15.800	0.294	0.056	7.753	2.485	4.54E+06

Table 9.3 – continued from previous page

#	Span [m]	Rise / Span Ratio [-]	Thickness / Span Ratio [-]	Width [m]	Backfill height above the arch crown [m]	Bridge Mass [kg]
66	17.667	0.193	0.142	6.683	1.313	4.26E+06
67	13.933	0.343	0.111	7.588	1.832	3.98E+06
68	12.067	0.476	0.141	4.684	0.992	2.11E+06
69	13.667	0.151	0.154	7.438	0.353	2.74E+06
70	6.467	0.467	0.219	7.476	1.703	1.55E+06
71	12.333	0.333	0.190	5.225	1.437	2.44E+06
72	24.600	0.279	0.047	4.339	0.891	3.98E+06
73	20.067	0.181	0.160	7.192	0.626	5.33E+06
74	19.000	0.203	0.079	4.270	1.975	2.89E+06
75	19.800	0.298	0.113	6.873	0.566	5.21E+06

Table 9.4: Obtained frequencies from Parametric Analysis.

#	Transversal MS		Vertical MS		Longitudinal MS	
	n.	Freq [Hz]	n.	Freq [Hz]	n.	Freq [Hz]
1	1	0.099637	3	0.218263	4	0.284982
2	1	0.119945	3	0.236409	4	0.311067
3	1	0.133733	2	0.242052	4	0.314097
4	1	0.094648	3	0.263512	5	0.353451
5	1	0.215230	2	0.310797	5	0.510055
6	1	0.322764	2	0.405803	4	0.594071
7	1	0.504478	2	0.691165	5	1.056460
8	1	0.151227	2	0.279440	4	0.437119
9	2	0.191476	1	0.145210	3	0.267457
10	1	0.384707	2	0.579975	4	0.801719
11	1	0.106072	3	0.240313	4	0.328177
12	1	0.600954	2	0.739588	5	1.180020
13	1	0.311129	2	0.434929	5	0.699181
14	1	0.407482	2	0.573891	5	0.867274
15	1	0.479814	2	0.617858	4	0.919132
16	1	0.194074	2	0.282085	5	0.468961
17	1	0.354441	2	0.492693	5	0.766907
18	1	0.128148	2	0.166133	4	0.287481
19	1	0.203628	2	0.366688	4	0.523837
20	1	0.130883	3	0.283774	5	0.397667
21	1	0.836489	2	0.94268	4	1.52229
22	1	0.166456	3	0.331476	4	0.457299
23	1	0.226571	2	0.340796	4	0.482004

178

Table 9.4 – continued from previous page

#	Transversal MS		Vertical MS		Longitudinal MS	
	n.	Freq [Hz]	n.	Freq [Hz]	n.	Freq [Hz]
24	1	0.153261	2	0.196995	4	0.305199
25	1	0.162943	2	0.317041	4	0.420959
26	1	0.150202	2	0.209633	4	0.313857
27	2	0.153910	1	0.148883	3	0.283221
28	1	0.449522	2	0.609959	5	0.993882
29	1	0.474253	2	0.652928	5	0.959453
30	1	0.115364	3	0.254824	4	0.350373
31	1	0.751787	2	0.883977	4	1.334770
32	1	0.323344	2	0.450175	5	0.669712
33	1	0.375887	2	0.551718	4	0.784383
34	1	0.176976	2	0.231353	4	0.404627
35	1	0.620081	2	0.713776	4	1.091440
36	1	0.117072	2	0.226654	4	0.361871
37	1	0.153137	2	0.257248	4	0.379947
38	1	0.227399	2	0.363057	4	0.514531
39	1	0.463081	2	0.575596	5	0.899475
40	1	0.538603	2	0.742888	5	1.136640
41	1	0.206370	2	0.257760	4	0.459032
42	1	0.783174	2	0.939259	5	1.475060
43	1	0.620735	2	0.841620	5	1.295425
44	1	0.460816	2	0.639128	5	1.019430
45	1	0.251298	2	0.422101	4	0.590578
46	1	0.165974	2	0.274343	4	0.421587
47	1	0.154342	2	0.234135	4	0.307199
48	1	0.242771	2	0.321588	5	0.543747

Table 9.4 – continued from previous page

#	Transversal MS		Vertical MS		Longitudinal MS	
	n.	Freq [Hz]	n.	Freq [Hz]	n.	Freq [Hz]
49	1	0.753263	2	0.935014	4	1.390880
50	1	0.409359	2	0.517635	4	0.754846
51	1	0.207314	2	0.330940	4	0.419842
52	1	0.153339	2	0.257291	5	0.409634
53	1	0.442440	2	0.535907	5	0.811008
54	1	0.193993	2	0.347688	5	0.565364
55	1	0.139903	3	0.259526	4	0.328318
56	1	0.182620	2	0.324035	4	0.484480
57	1	0.196175	2	0.304194	4	0.511148
58	1	0.364494	2	0.502778	5	0.740354
59	1	0.285116	2	0.437621	4	0.628863
60	1	0.118828	2	0.230017	4	0.355562
61	1	0.267332	2	0.486736	5	0.719371
62	1	0.278177	2	0.405354	5	0.583143
63	1	0.331663	2	0.452592	5	0.711011
64	1	0.202836	2	0.283478	4	0.386093
65	1	0.232433	2	0.319567	4	0.479661
66	1	0.192544	2	0.280029	4	0.445561
67	1	0.268997	2	0.378043	4	0.552118
68	1	0.262653	2	0.461621	4	0.635040
69	1	0.308469	2	0.344469	5	0.566617
70	1	0.663435	2	0.809240	4	1.217530
71	1	0.262883	2	0.431287	5	0.643363
72	1	0.100280	3	0.198878	4	0.286479
73	1	0.173027	2	0.245978	4	0.393329

Table 9.4 – continued from previous page

#	Transversal MS		Vertical MS		Longitudinal MS	
	n.	Freq [Hz]	n.	Freq [Hz]	n.	Freq [Hz]
74	1	0.132714	2	0.252586	4	0.404355
75	1	0.172228	2	0.268846	4	0.382674